2009

DEVELOPMENT OF RAPID DIE WEAR TEST METHOD FOR ASSESSMENT OF DIE LIFE AND PERFORMANCE IN STAMPING OF ADVANCED/ULTRA HIGH STRENGTH STEEL (A/UHSS) SHEET MATERIALS

Omer Necati Cora
Virginia Commonwealth University

School of Engineering
Virginia Commonwealth University

This is to certify that the dissertation prepared by Ömer Necati Cora entitled
DEVELOPMENT OF RAPID DIE WEAR TEST METHOD FOR ASSESSMENT OF
DIE LIFE AND PERFORMANCE IN STAMPING OF ADVANCED/ULTRA HIGH
STRENGTH STEEL (A/UHSS) SHEET MATERIALS
has been approved by his committee as satisfactory completion of the dissertation
requirement for the degree of Doctor of Philosophy

Muammer Koç, Ph.D, Committee Chair, School of Engineering

Karla M. Mossi, Ph.D, Committee Member, School of Engineering

---

Ramana M. Pidaparti, Ph.D, Committee Member, School of Engineering

---

Hooman V. Tafreshi, Ph.D, Committee Member, School of Engineering

---

Kenneth J. Wynne, Ph.D, Committee Member, School of Engineering

---

Russel D. Jamison, Dean, School of Engineering

Dr. F. Douglas Boudinot, Dean of the Graduate School

November, 2009

DEVELOPMENT OF RAPID DIE WEAR TEST METHOD FOR ASSESSMENT OF

DIE LIFE AND PERFORMANCE IN STAMPING OF ADVANCED/ULTRA HIGH

STRENGTH STEEL (A/UHSS) SHEET MATERIALS

A Dissertation submitted in partial fulfillment of the requirements for the degree of
Doctor of Philosophy at Virginia Commonwealth University.

by

ÖMER NECATİ CORA
M.S.M.E, Middle East Technical University, Ankara, TURKEY, 2004
B.S.M.E, Karadeniz Technical University, Trabzon, TURKEY, 2000

Director: MUAMMER KOÇ
ASSOCIATE PROFESSOR, DEPARTMENT OF MECHANICAL ENGINEERING

Virginia Commonwealth University
Richmond, Virginia
November 2009

Acknowledgement

Above and more important than all, I am grateful to Allah the Almighty who gave me endurance and let me complete this study at last.

"Say: My Lord! Increase my knowledge" (The Holy Quran, 20:114)

Table of Contents

ix

<h1>List of Tables</h1>

xii

List of Figures

xvii

List of Abbreviations

AFM   : Atomic force microscopy

AHSS   : Advanced High Strength Steel

AISI   : American Iron and Steel Institute

AKDQ   : Aluminum-Killed Drawing Quality steel

ANOVA   : Analysis of Variance

ASTM   : American Society for Testing and Materials

CAFE   : Corporate Average Fuel Economy

CNC   : Computer Numerical Control machine

CVD   : Chemical Vapour Deposition

CP   : Complex-Phase steel

DP   : Dual-Phase steel

FB   : Ferritic-Bainitic steel

FRP   : Fiber-Reinforced Polymer

HDGA   : Hot-Dip GalvaAnnealed

HF   : Hot Formed steel

HSLA   : High-Strength Low-Alloy steel

MART   : Martensitic Steel

PFHT   : Post-Formed Heat Treatable steel

PVD   : Physical Vapour Deposition

SEM   : Scanning Electron Microscope

TD   : Thermal Diffusion

TRIP   : Transformation Induced Plasticity steel

TWIP   : Twinning-Induced Plasticity steel

ULSAB-AVC : UltraLight Steel Autobody – Advanced Vehicle Concept

UHSS   : Ultra High Strength Steel

USCAR   : United States Council for Automotive Research

Abstract

DEVELOPMENT OF RAPID DIE WEAR TEST METHOD FOR ASSESSMENT OF
DIE LIFE AND PERFORMANCE IN STAMPING OF ADVANCED/ULTRA HIGH
STRENGTH STEEL (A/UHSS) SHEET MATERIALS

By Ömer Necati Cora, Ph.D

A Dissertation submitted in partial fulfillment of the requirements for the degree of
Doctor of Philosophy at Virginia Commonwealth University.

Virginia Commonwealth University, 2009

Major Director: Muammer Koç, Ph.D
Associate Professor, Department of Mechanical Engineering

Automotive companies are actively pursuing to increase the use of high-strength-
lightweight alloys such as aluminum, magnesium, and advanced/ultra high-strength steels
(A/UHSS) in body panel and structural part applications to achieve fuel efficiency while
satisfying several environmental and safety concerns. A/UHSS sheet materials with higher
strength and crashworthiness capabilities, in comparison to mild steel alloys, are
considered as a near-term (i.e., ~5 years) choice of material for body and structural
components due to their relatively low cost when compared with other lightweight
materials such as aluminum and magnesium. However, A/UHSS materials present an

increased level of die wear and springback in stamping operations when compared to the currently used mild steel alloys due to their higher surface hardness and high yield strength levels. In order to prevent the excessive wear effect in stamping dies, various countermeasures have been proposed such as alternative coatings, modified surface enhancements in addition to the use of newer die materials including cast, cold work tool, and powder metallurgical tool steels.

In this study, a new die wear test method was developed and tested to provide a cost-effective solution for evaluating various combinations of newly developed die materials, coatings and surfaces accurately and rapidly. A new slider type of test system was developed to replicate the actual stamping conditions including the contact pressure state, sliding velocity level and continuous and fresh contact pairs (blank-die surfaces). Several alternative die materials in coated or uncoated conditions were tested against different AHSS sheet blanks under varying load, sliding velocity circumstances. Prior to and after wear tests, several measurements and tribological examinations were performed to obtain a quantified performance evaluation using commonly adapted wear models.

Analyses showed that (1) the rapid wear method is feasible and results in reasonable wear assessments, (2) uncoated die materials are prone to expose severe form wear (galling, scoring, etc.) problems; (3) coated samples are unlikely to experience such excessive wear problems, as expected; (4) almost all of the recently developed die materials (DC 53, Vancron 40, Vanadis 4) performed better when compared to conventional tool steel material AISI D2, and (5) in terms of coating type, die materials coated with thermal diffusion (TD) and chemical vapor deposition (CVD) coatings

performed relatively better compared to other tested coating types; (6) It was seen that wear resistance correlated with substrate hardness.

CHAPTER 1

Introduction

Advanced or Ultra High Strength Steels (AHSS or UHSS, hereafter) refer to a class of steel developed recently to have increased levels of ductility, yield strength, hardness, and crash energy absorption properties with relative low cost and commercial availability. They are shown to have less formability problems compared to their lightweight competitors such as aluminum and magnesium. Therefore, they are seen as the promising near-future solutions to realize the lightweight vehicles in automotive industry.

Weight reduction in vehicles offers reduced fuel consumption, tailpipe emissions and improved vehicle performance. Use of AHSS is continuously growing mainly in auto-body panels and structural parts. However; there are problems yet to be addressed for their widespread implementation for many other candidate parts and products. For instance, their increased yield strength and hardness typically result in amplified springback and die wear issues during stamping operations. Die wear, in particular, leads to surface quality, and geometrical deviation problems for the stamped part; and necessitates the frequent replacement of the expensive die sets subsequently leading to unacceptable levels of down-time and production losses.

This study focuses on the development and validation of a new die wear test method to rapidly and accurately evaluate several possible combinations of recently suggested alternative, die materials (substrate), coatings, and surface conditioning techniques for stamping of AHSS sheet blanks.

The rest of this chapter intends to provide background information on common issues and trends in the automotive industry and links these problems to weight reduction of vehicles (lightweight vehicle concept), and consequently to AHSS use. Furthermore, alternative material options, their challenges particularly, benefit of AHSS use, and its processing, current and projected use will be discussed. In the end, description of basic stamping process and its important parameters and characteristics will be reviewed.

Second chapter will cover the commonly used terminology in tribology area; and then a review of existing die wear test systems will be presented. This chapter concludes with necessary specifications for a reliable test system that mimics the actual stamping conditions.

First generation "robot-based" die wear test system and preliminary proof-of-concept tests will be explained in third chapter. This chapter also includes the results of wear test and analysis of 7 different uncoated die material using 1st generation test system.

Description of second generation "CNC-based" test system and test results for several coated die samples are presented in fourth chapter.

Finally, the chapter V is devoted to overall discussions, conclusion and recommended future work.

1.1 Automotive in Numbers

According to the Bureau of Transportation Statistics, the number of registered vehicles in United States has been steadily increasing over the past 40 years and roughly 251 million registered vehicles are on United States highways by 2006 [National Transportation Statistics, 2009]. Likewise, the world vehicle population is estimated as 820 million in 2008 and it is expected to exceed 1 billion by 2020, and 3.5 billion cars by 2050 [Singh, 2009; Carpenter, 2004; Daniels 2003]. Moreover, the roadway-vehicle-miles traveled (VMT) are also incessantly escalating. Meanwhile, fuel economy has been always an utmost concern due to its several consequences including, but not limited to, limited fossil fuel sources, growing dependency on imported oil (hence, political issues) and environmental pollution and health impact issues because of CO_2 and greenhouse gas (GHG) emissions. Solutions for an improved fuel economy of vehicles have been under investigation including lightweighting via use of lightweight materials and green power generation via electric batteries, fuel cells and/or hybrid cars.

The rest of this chapter will be presenting brief information about the current situation of the petroleum dependency related problems in automotive industry, environmental concerns, and lightweight vehicle concepts utilizing alternative material choices.

1.2 Oil Dependency Problem, and Improved Fuel Efficiency Regulations

Until 1950's, the United States produced nearly all the petroleum it needed. Towards the end of the decade, the gap between production and consumption began to

widen and imported petroleum became a major component of the U.S. petroleum supply. Beginning in 1994, the nation imported more petroleum than it produced. Imported oil percentage was 52% in 2000 and rose up to 66% in 2006, which approximately equals to 20.6 millions of barrels per day [Energy Information Administration, 2006]. Global petroleum usage in transportation, on the other hand, is reported as 85 millions of barrels per day [Singh, 2009].

In order to lessen dependency on imported oil and increase fuel efficiency of the vehicles, several measures are adopted by different organizations. The National Highway Traffic Safety Administration has been regulating the Corporate Average Fuel Economy (CAFE) standards for passenger cars and light trucks that would enhance energy security by improving fuel economy since 1975. The current Energy Independence and Security Act of 2007 (EISA), which Congress passed in December 2007, mandates the setting of separate maximum feasible standards for passenger cars and for light trucks at levels sufficient to ensure that the average fuel economy of the combined fleet of all passenger cars and light trucks sold by all manufacturers in the U.S. in model year 2020 equals or exceeds 35 miles per gallon. That is a 40 percent increase above the average of approximately 25 miles per gallon for the current combined fleet [National Highway Traffic Safety Administration, 2008].

In addition to lightweighting approach, which has been continuously improved and adopted at different levels, another prominent approach to decrease the oil dependency is the utilization of new and green power generation technologies; such as hybrid, or fuel cell

4

cars, however; there are still certain challenges to be overcome for their prevalent use. For example, in spite of its proven benefits such as high efficiency, smooth and quiet operations, and near-zero emissions, fuel cells are not yet cost competitive when compared to the existing power generation technologies, particularly in the transportation applications. The cost of fuel cell is ~10 times more expensive than the internal combustion engines, ($200–300 kW^{-1} vs. $30–50 kW^{-1}) in its current condition. Extensive research and development efforts are necessary to address the materials and manufacturing related technical issues to bring the cost of fuel cells down to competitive levels since around 60–70% of the fuel cell cost is in materials and manufacturing [Koç, et. al, 2007].

1.3   Environmental Concerns

In addition to diminishing of fossil fuel sources, the exhaust gases released by cars are always major concerns. Carbon monoxide and carbon dioxide (CO, CO_2), nitrogen dioxide (NO_2), sulphur dioxide (SO_2), suspended particles, PM-10 (particles less than 10 micron), benzene, formaldehyde, and polycyclic hydrocarbons are just some of the health-hazard substances emitted from motor vehicles. In particular, CO_2 is one of the main greenhouse gases that cause global warming, and consequently climate change. Global atmospheric concentration of CO_2 level was 280 ppm (part per million) in 1870's while it went up to 370 ppm in 2000 and it is still going on to increase. Solely transportation emissions are responsible from 42% of total CO_2 emissions [Daniels, 2003].   As precautions, European Union targets the average of 120 g of CO_2 per kilometer driven for passenger car by 2010. Similarly, California state Assembly Bill 1493's goal is to achieve

an average of 205 g of CO_2 equivalent per mile (~ 127 g/km) driven for passenger cars by 2016 [Geyer, 2006]. Another preventive, global act is Kyoto protocol that it aims to stabilize greenhouse gas concentrations in atmosphere and has been ratified by 188 countries by August 2009 [United Nations Framework Convention on Climate Change, 2009].

1.4 Lessening Oil Addiction and Lightweight Vehicle Concept

To overcome the limited availability of fossil fuels, increasing environmental pollution matters, several healer mechanisms have been put forward, including improved fuel efficiency, alternative energy use (hybrid cars, fuel cell vehicles, etc.) for power related matters, and increased use of lightweight materials for lessening the total weight of auto-body structures. Prevalent use of lightweight materials itself will have a great contribution in solving those problem since light vehicles account for 40% of U.S oil consumption which is mainly imported. Moreover, light vehicle operation contributes approximately 20% of all U.S. CO_2 emissions [Schultz, 2007]. To this end, in 1993, Partnership for a New Generation of Vehicles (PNGV) has been established between the U.S. government agencies and "Big Three" automakers. The partnership targets the high-fuel efficiency autos through the use of alternate power plants (mainly diesel-electric hybrids), advanced design and lightweighting materials. In 2002, the PNGV morphed to FreedomCAR (Cooperative Automotive Research) with more emphases on fuel-cell vehicles and all sorts of light-duty vehicles. 2010 specific goals include the 50% percent reduction in vehicle weight. FreedomCAR has been formed by two partners; Department

of Energy and U.S Council for Automotive Research (USCAR) [Geyer, 2006]. In 2003, FredomCAR expanded to include the Hydrogen Fuel Initiative to discover technologies for generating and delivering hydrogen for transportation and other uses such as energy-supply. Federal government committed to provide ~ $ 1.7 billion for hydrogen fuel initiative and FreedomCAR joint research acts during 2004-2008 period. [Carpenter, 2004].

The 2010 Technology-specific Research Goals for "Materials" in FreedomCAR and Fuel Partnership Plan is based on "Material and manufacturing technologies for high-volume production vehicles which enable/support the simultaneous attainment of:

- 50% reduction in the weight of the vehicle structure and subsystems
- Affordability
- Increased use of recyclable/renewable materials" [FreedomCAR & Fuel Partnership Materials Technical Team, 2006].

Another attempt to achieve lightweight vehicles target is the UltraLight Steel Auto Body –Advanced Vehicle Concept (ULSAB-AVC) project that has been supported by 33 steel companies from 18 countries around the world. The ULSAB-AVC program, presents advanced vehicle concepts that help automakers use steel more efficiently and provide a structural platform for achieving: a) Anticipated crash safety requirements for 2004, b) Significantly improved fuel efficiency, c) Optimized environmental performance regarding emissions, source reduction and recycling, and d) High volume manufacturability at affordable costs. The current ULSAB structure weighs merely 203 kg,

7

comprised more than 80 percent AHSS and remaining 20 percent HSS, and satisfies the mandated crash requirements, even at speeds exceeding the requirements. In addition to weight and superior performance, ULSAB costs no more to build than typical auto body structures in its class and can even yield potential cost savings, according to economic analysis [ULSAB-AVC Overview Report, 2002].

1.5   Lightweight Materials and Challenges

Important materials that offer weight reduction in vehicles are listed in Table 1.1 with their weight savings capacities, and costs compared to their replaced materials. In this table cost of mild steel was taken as a base material. Similarly, from materials strength point of view, increased strength results in weight savings. Specifically, the use of AHSS with 400 MPa yield strength provides 15-25 % weight reduction, while this values can go up to 50-55% when AHSSs with 1100 MPa yield strength are employed [Johansson, and Olsson; 2005]. Contrary to strength increase, total elongation, nominal strain at fracture, consequently formability is lowered as can be seen from the Figure 1.1. The same tendency is valid for other alternative material choices [Kleiner et al., 2002].

Table 1.2 provides estimated cost information for some specific metals including some AHSS that are used in automotive industry along with their some mechanical properties. Low-density is an important criteria in utilization of lightweight materials, however; several other factors should be taken into account, as well. For example, aluminum has a one-third density value of that steel has, which provides 67% reduction in weight theoretically, however; it's strength, and elastic modulus are around one third value

of that steel that limits its formability and consequently widespread use when high-strength, and critical applications are considered. Therefore, specific material properties are considered more appropriate as design criteria. Specific stiffness, for instance, is required to be as high as possible for structural automotive applications; and as can be seen from Table 1.2 that all the steel types listed have higher specific stiffness than that of other alternative materials. Contrarily, dent resistance and shell stiffness values for steels are considerably lower than the ones for aluminum, titanium, and magnesium [Kleiner et al., 2002].

Table 1.1 Weight savings and cost for alternative lightweight materials (*: including both materials and manufacturing) [*Powers, 2000*]

Lightweight material	Material Replaced	Mass Reduction (%)	Relative Cost (per part) *
High Strength Steel	Mild Steel	10	1
Aluminum (Al)	Steel, Cast Iron	40-60	1.3-2
Magnesium	Steel or Cast Iron	60-75	1.5-2.5
Magnesium	Aluminum	25-35	1-1.5
Glass FRP Composites	Steel	25-35	1-1.5
Graphite FRP	Steel	50-60	2-10 +
Al Matrix Composites	Steel or Cast Iron	50-65	1.5-3+
Titanium	Alloy Steel	40-55	1.5-10 +
Stainless Steel	Carbon Steel	20-45	1.2-1.7

From material strength point of view, increased strength results in weight savings. Specifically, the use of AHSS with 400 MPa yield strength provides 15-25% weight reduction, while this value can go up to 50-55% when AHSSs with 1100 MPa yield strength are employed [Johansson, and Olsson; 2005]. Contrary to strength increase, total

9

elongation, nominal strain at fracture, consequently formability is lowered as can be seen

from the Figure 1.1. The same tendency is valid for other alternative material choices

[Kleiner et al., 2002].

Table 1.2 Estimated Cost Comparisons for Some Automotive Materials [*After Sohmshetty, 2009; Rivard et al., 2005; Kleiner et al., 2003*]

Grade	Tensile Strength (MPa)	Modulus of Elasticity (GPa)	Density (g/cc)	Specific Strength (10^6N.mm/kg)	Specific Stiffness (10^9N.mm/kg)	Cost ($/lb)
Al 5082-O	250	68	2.7	93	25.2	1.4
Al 5754-O	205	68	2.7	76	25.2	1.47
Al 6111-T4	295	68	2.7	109	25.2	1.51
Mg AM60B	220	45	1.8	122	25.0	2.1
Titanium	910-1190	110	4.5	202-264	24.4	8-50
Steel BH210	360	210	7.9	46	26.6	0.37
Steel BH250	384	210	7.9	49	26.6	0.37
Steel BH280	395	210	7.8	51	26.9	0.4
Steel DP 500	560	210	7.8	72	26.9	0.38
Steel DP 600	610	210	7.8	78	26.9	0.4
Steel DP 780	790	210	7.8	101	26.9	0.42
Steel DP 980	990	210	7.8	127	26.9	0.44
Steel DR210	360	210	7.9	46	26.6	0.39
Steel HSLA340	440	210	7.8	56	26.9	0.37
Steel Mild	300	210	7.9	38	26.6	0.35
Steel MS1250	1520	210	7.9	192	26.6	0.51
Steel TRIP600	610	210	7.8	78	26.9	0.54

1.6   AHSS, UHSS and their Advantages, and Challenges

The Advanced/ Ultra High Strength Steels refer to recently developed and structurally improved class of steels. Their unique characteristics are obtained by a continuous heat treating process that creates martensite in the steel microstructure. The amount of martensite, together with the amount of carbon, determines the strength level of the steel. They exhibit a superior combination of high strength with good formability and high strain hardening capacity [Demeri, 2006]. AHSS and UHSS can be differentiated in terms of their yield strength values. Usually, the steels with yield strength values higher than 210 MPa (30 ksi) are regarded as high strength steels; while ultra-high strength steels have yield strength levels of 550 MPa and above. Figure 1.1 shows different type of A/UHSS along with their elongation and yield strength values as well as conventional high strength steel ones.

Designation of advanced/ ultra high strength steels are usually done by their ultimate tensile strength values as can be seen in Table 1.2. For example, DP 600 refers to dual-phase AHSS which has 600 MPa ultimate strength value. In some cases both yield and ultimate strength values are also used such as MART 1250/1520 (Martensitic steel; yield strength: 1250 MPa, ultimate tensile strength: 1520 MPa).

Dual-phase (DP) steels are a mixture of ferrite (soft phase of iron offer ductility) matrix and martensite islands (hard, offers strength) decorating grain boundaries with possible addition of bainite. Formable DP steels contain approximately 5-15% martensite.

11

In a typical microstructure of DP steels shown in Figure , light colored sections is ferrite matrix while dark points on grain boundaries are martensite.

Transformation Induced Plasticity (TRIP) steels, on the other hand, have ferrite-bainite-austenite in their compositions and exhibit better ductility at a given strength level. This enhanced formability comes from the transformation of retained austenite (ductile, high temperature phase of iron) to martensite (tough, non-equilibrium phase) during plastic deformation [U.S. Steel Corp., 2009].

CP (Complex-phase) steels, are characterized by a very fine microstructure of ferrite and a higher volume fraction of hard phases (martensite and bainite), strengthened further by fine carbon or nitrogen precipitates of niobium, titanium, or vanadium. These steel grades have been used for parts that require high energy-absorption capacity, such as bumpers and B-pillar reinforcements.

Martensitic steels (MART) have a microstructure that is 100 percent martensite. Minimum tensile strengths of this family of steels are typically between 900 and 1,500 MPa (130 and 220 ksi). These grades can be made directly at the steel mill (quenching after annealing) or via post-forming heat treatment. Because of its limited elongation, mill-produced martensite typically is roll-formed. More complex shapes can be fabricated by hot forming and quenching a lower carbon grade [Schaeffler, 2005].

On the other hand, HSLA (High-strength low-alloy) steels have been used as primary high-strength steels for the last 30-35 years. Other conventional steels are, CMn

(Carbon-Manganese), BH (bake hardenable), IF (Interstitial-free), high-strength IF steels, mild steels, IS (isotropic) steels etc.
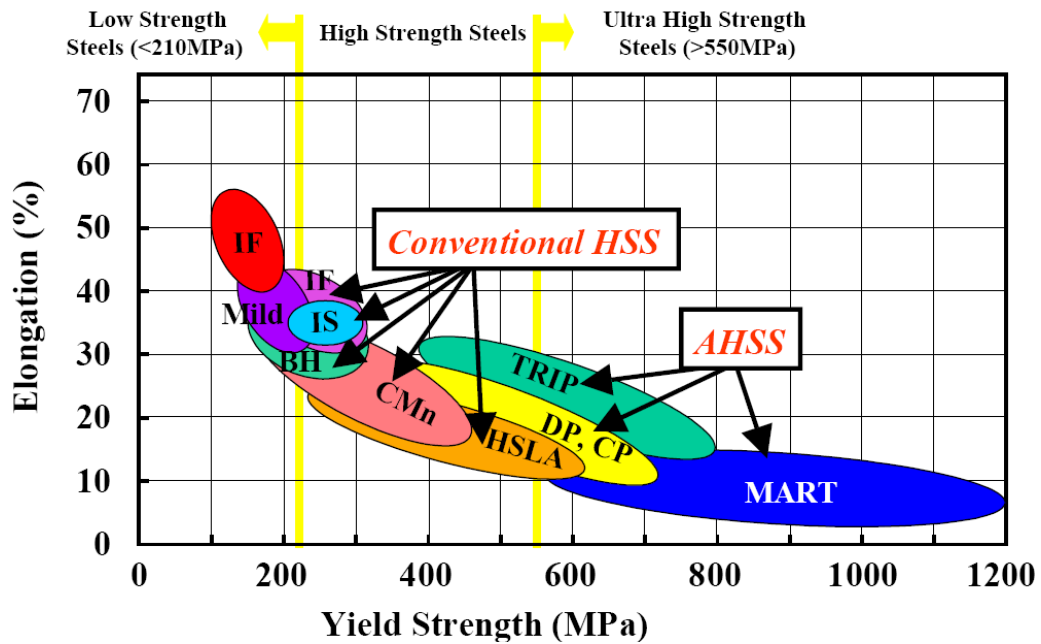
Figure 1.1 Elongation vs. yield strength values for automotive steels [*Wohlecker et. al, 2006*]
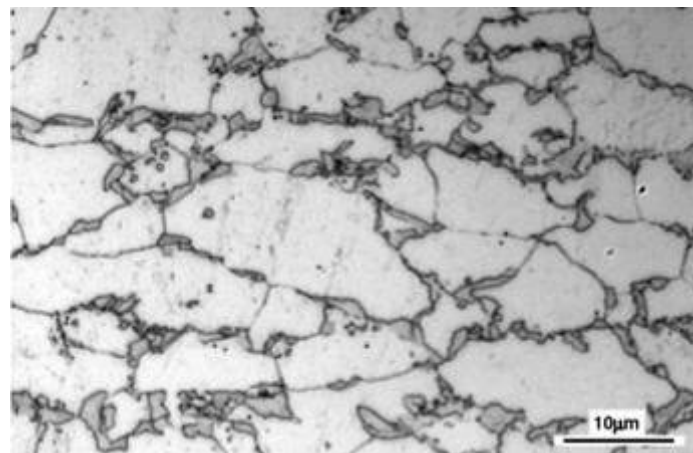
Figure 1.2 Microstructure of DP steel [*Oliver et. al, 2007*]

Although it is not included in Figure 1.1, Ferritic-Bainitic (FB) steels, Twinning-Induced Plasticity (TWIP) steels, Hot-Formed (HF), Post-Forming Heat-Treatable steels are also considered as other AHSS types.

FB steels, microstructurally consisted of fine ferrite and bainite, are preferred to improve stretch flangeability and high hole expansion capabilities; and available as hot-rolled products. Strengthening is realized by grain refinement and second phase hardening with bainite.

TWIP steels, classified as one of second generation AHSS types, have a 17-24 % manganese content that makes them fully austenitic at room temperatures. This type of steels gets their name from the formation of "deformation twins" during their deformation. This deformation mechanisms causes a high value of the instantaneous hardening rate (n value) as the microstructure becomes finer and finer. The resultant twin boundaries act like grain boundaries and strengthen the steel. TWIP steels combine extremely high strength (UTS is around 1000 MPa) with very high stretchability (around 60% total elongation).

For optimized part geometries with complex shapes, implementation of press-hardening applications and use of hardenable steels are preferred. For example, boron-based HF steels (including 0.002-0.005% boron) are heated up to 850°C prior to forming process. Forming process (austenization) is followed by a cooling with a fast rate such as 50°C/s to achieve the desired mechanical properties.

One of the major problems that holds back the widespread implementation of high strength steels is to maintain the part geometry during and after heat treatment process.

Post-forming heat treatment is a general method to develop an alternative higher strength steel. Fixturing the part and then heating by means of furnace of induction, and immediate quenching appear to be a solution with production applications. Post-formed heat-treatable (PFHT) steels can be produced with different combination of forming strength levels and quenching types [AHSS Application Guidelines, 2009].

Main benefits of utilization of lightweight materials, in particular AHSS, provide the following categorized improvements;

- Fuel economy and reduction of toxic emissions

- Performance related issues (static axle load distribution enhancement, faster acceleration and driving comfort, reduced braking distance, increased payload, etc.)

- Safety (increased crash energy absorption capability)

In addition to abovementioned advantages, environmental impact of AHSS is considerably less compared to aluminum considering the GHG emissions during production. Moreover, AHSS has higher recyclability rate over aluminum [Geyer, 2006].

Nevertheless, in terms of challenging situations of AHSS use, as discussed before, increased yield strength aggravates the elongation and this phenomenon is represented with "Banana curve" seen in Figure 1.1. Numerically speaking, DP 350/600 has 24-30 % elongation, while DP 700/1000 has considerably lower elongation as 12-17 %. MART type steels have the smallest elongations among the advanced high strength steels as 4-6 % for MART 1250/1520 which requires hot forming process to be formed. Moreover, increasingly pronounced die wear and springback are the other matters.

1.7 Current and Projected AHSS Use

Advanced High Strength Steels are thought to be one of major contributions of ULSAB (UltraLight Steel Auto Body) program that started almost a decade ago. Since then, it is being increasingly used in automotive industry because of several advantages such as better performance in crash energy management that allows lessening the sheet thickness, higher strength and enhanced formability. First AHSS use, DP 600 type steels, was implemented by Volvo and Ford Europe in 1990's, and today every car manufacturer use U/AHSS in their models with varying percentages [Lee; 2005]. While ULSAB-Advanced Vehicle Concept (AVC) is the utmost use example of AHSS, advanced high strength steels stands for more than 80% in its steel structure and achieving 25 % mass reduction in BIW (Body-in-white) mass, AHSS implementation in commercially marketed cars is in averagely 9.5 % levels in North America [Schultz, 2007; Hall, 2008].

AHSS is used in selective applications, where conventional steel could not meet the crash energy absorption targets and formability requirements such as in roof structures (roof bow, roof rail etc.) , front and rear bumpers, A, B, C-pillars, side door beams, fuel tank guard, cross members, seat tracks, longitudinal members, rear chassis, etc. Figure 1.3 shows main AHSS use locations in a passenger car with some examples from commercially marketed models and FGPV (Future Generation Passenger Vehicle) concept also, while Table 1.3 lists some examples for AHSS use in commercially available vehicles.
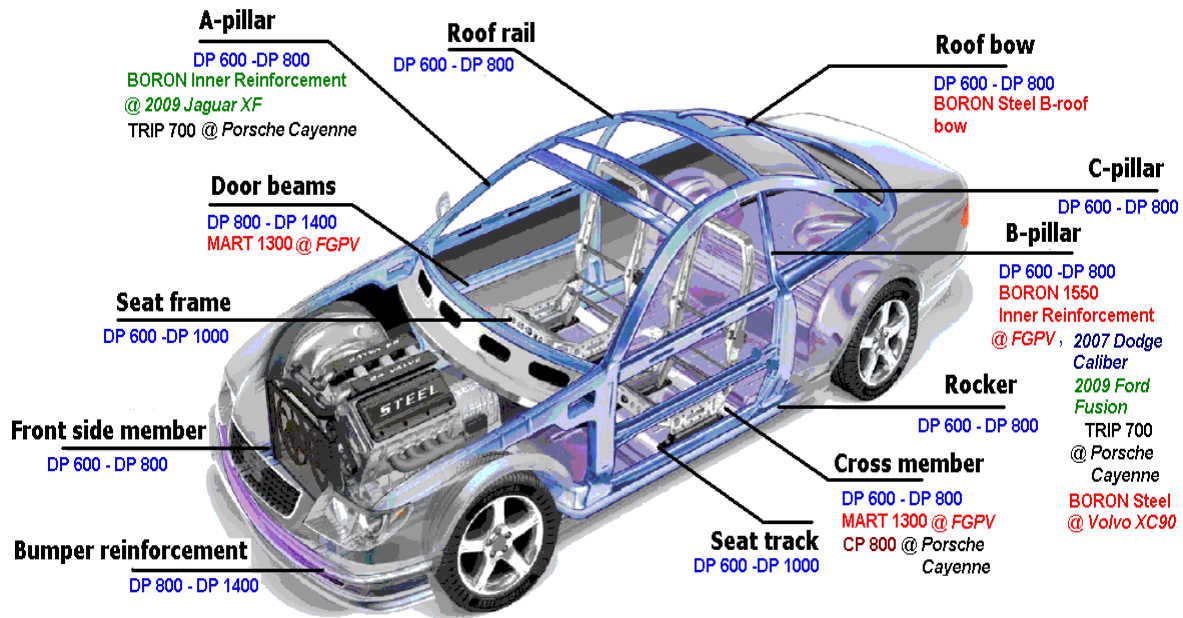
Figure 1.3 Main AHSS exploitation locations in a car and some examples [*After Johansson, and Olsson 2005; Farahani, 2007; Bernquist, 2004; Porsche Engineering, 2004; http://www.boronextrication.com/, 2009*]

AHSS use is expected to reach 35-40 % levels (equivalent of 403 pounds) by 2015 [Hall, 2008; Horvath, 2004]. By the same date, European cars will have more AHSS implementations as in nowadays. On the other hand, based on Ducker Worldwide report, aluminum and magnesium will only increase from 7 pounds per vehicle in the body and closures today to 20 pound levels by 2015 [Schultz, 2007]. Currently, research laboratories in both academia and industry are trying to come up with solutions that will offer improved formability (total elongation) for a given strength level while reducing the cost and welding problems caused by high austenite content [AHSS Application Guidelines, 2009].

Outcome of these studies will enable the utilization of new types of AHSS which are dubbed as 3rd generation AHSS types [Hall, 2008].

Table 1.3 AHSS use examples from marketed cars [*After Shaw, 2009; Mallen, and Tarr, 2008; Pafumi, 2007; Anderson, 2008; Schultz, 2007*]

Make/ Model	U/AHSS Use (%)	Remarks
Honda Acura MDX, 2007	28.8	DP 590 (21.6%), TRIP 780 (5.8%), DP 980 (1.4%)
Audi Q7	32	AHSS, UHSS
Honda Civic,2006	38	DP 590 (38 %)
Nissan Altima, 2007	17	DP 590 (10%), other AHSS (5%)
Toyota Tundra, 2007	20	DP 590 (15%), others (5%)
Mercedes M Class, 2007	17	DP (15%), other AHSS (2%)
Ford Expedition, 2007	16	DP (15%), other AHSS (1%)
Honda CR-V, 2007	35	DP (28%), other AHSS (7%)
GMC Acadia, 2007	22	DP (13%), other AHSS (9%)
Dodge Caliber, 2007	12	DP (11%), MART (~1 %)

1.8   Processing of AHSS

Advanced High Strength Steel types are produced by controlling the cooling rate from the austenite or austenite+ferrite phase to the room temperature, either on the run out table of the hot mill (for hot rolled products) or in the cooling section of the continuous annealing furnace (continuously annealed or hot dip coated products). AHSS cooling patterns and resultant microstructures are illustrated on the continuous cooling-transformation diagram given in Figure 1.4.
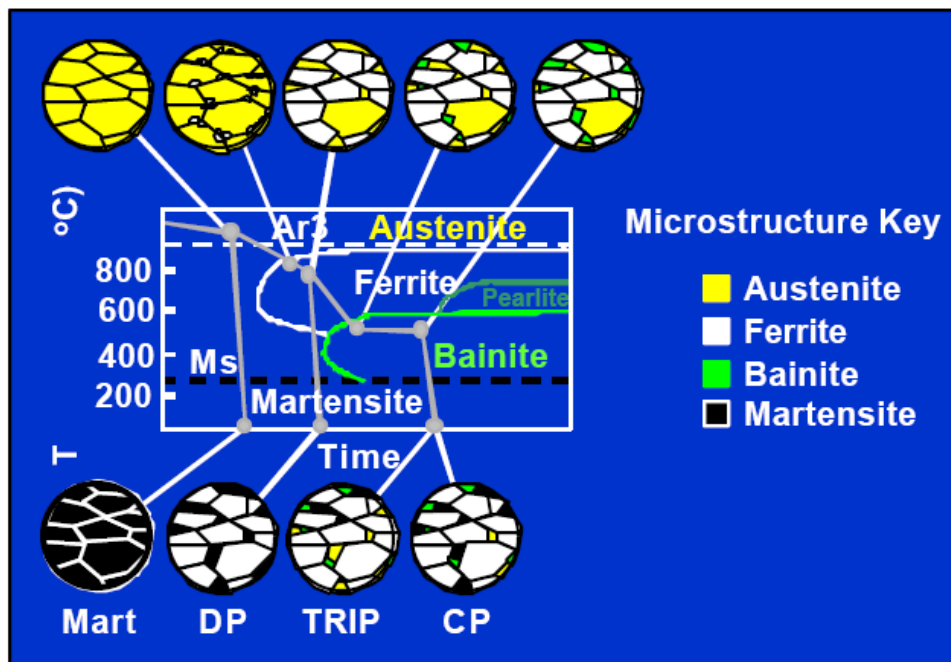
Figure 1.4 Cooling patterns and microstructure formation in production of AHSS [*ULSAB-AVC, TTD #6, 2001*]

Martensitic steels are produced from the austenite phase by rapid quenching to transform most of the austenite to martensite. Dual phase ferrite + martensite steels are produced by controlled cooling from the austenite phase (in hot rolled products) or

from the two-phase ferrite + austenite phase (in hot rolled products) or from the two-phase ferrite + austenite phase (for continuously annealed and hot dip coated products) to transform some austenite to ferrite before rapid cooling to transform the remaining austenite to martensite. TRIP steels typically require the use of an isothermal hold at an intermediate temperature, which produces some bainite. The higher silicon and carbon content of TRIP steels also results in significant volume fractions of retained austenite in the final microstructure. Complex phase steels also follow a similar cooling pattern, but here, the chemistry is adjusted to produce less retained austenite and fine form precipitates to strengthen the martensite and bainite phases [ULSAB-AVC, TTD #6, 2001].

1.9   Forming of AHSS Sheet Blanks

As it was mentioned above, AHSS sheet blanks are primarily used in auto-body sheet panels and structural parts. Main sheet metal forming techniques are bending, flanging, blanking, deep drawing, stamping, hydroforming etc. A typical stamping/deep drawing equipment usually consists of following main parts; moving die (male die or punch), stationary lower die (or female die) that sheet blank or plate is formed into its cavity, die rings that support the sheet blank, and pressure plates that apply blank holder force the sheet blank from its edges that helps to control the material flow during sheet forming. Figure 1.5 depicts these parts as well as different contact situation regions in typical deep-drawing operation. In region 1 and 2, the sheet blank is compressed between pressure plates (blank holder) and lower die under the applied blank holder force. Under

20

this compressive load limited radial flow of blank material occurs in this region, and mean contact pressure varies between 1-10 MPa levels. Zone 3 experiences bending and stretching heavily, and contact pressure levels are in the order 100 MPa. In zone 4, punch flank is in contact with the sheet blank and increased stretching effects take place. Punch corner - sheet blank interaction occurs in region 5 with high level strains as in zone 3. In region 6, punch bottom expose drawing force against the thinned sheet blank with stretching effect [Westeneng, 2002]. The most critical zones regarding with die wear issues are regions numbered with 4, 5 and 6. For the dies used in stamping and blanking operations; abrasive and adhesive wear effects are experienced in region 4, while surface fatigue and cratering type of wear are observed for the zones 5, and 6 respectively.

a)   b)
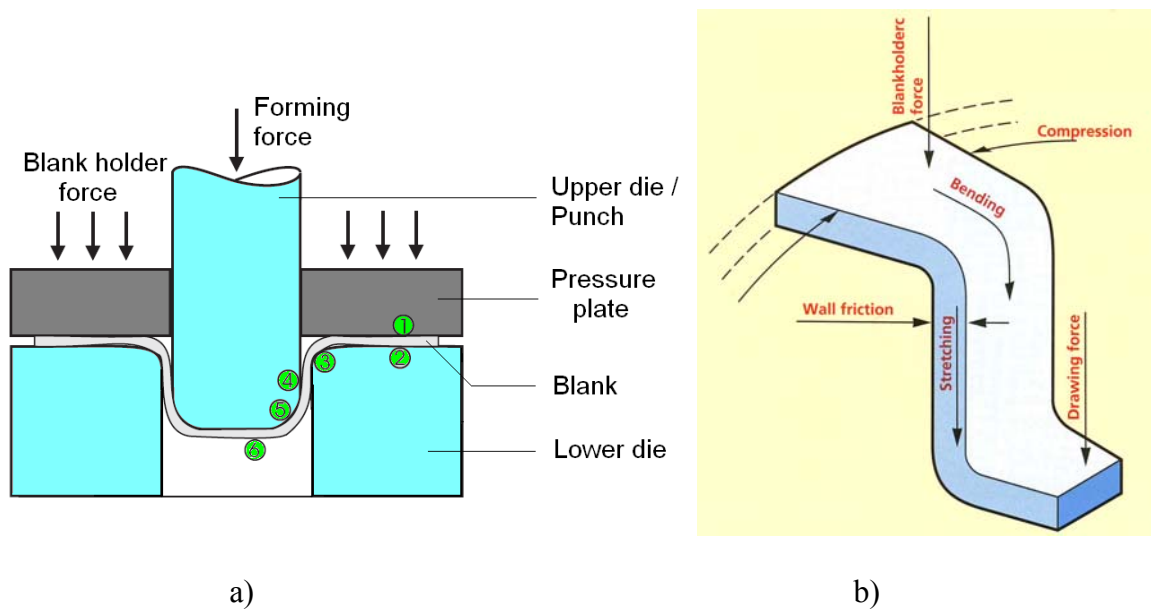
Figure 1.5 a) Description of typical stamping (deep-drawing) operation and different contact mode locations [*After Westeneng, 2002*], b) Forces acting on sheet blank during deep-drawing [*SSAB Sheet Steel Forming Handbook, 1998*]

In a nutshell, forming of lightweight materials, in particular AHSS requires not only higher forming loads in forming processes but also more rigid forming tools which result in more pronounced die wear and springback issues. One of the main challenges, namely die wear, will be discussed in following chapters.

CHAPTER 2

State-of-the Art Review for Die Wear Tests

Wear is a fairly complex phenomenon and affected by a wide range of parameters including contact pressure, surface finish of contact pair, sliding velocity, type of motion, temperature, mating surfaces' structures, coating conditions, lubrication and/or debris formation at the interface, etc. From manufacturing point of view, die wear is a disliked situation that affects surface quality leading to interrupted operation and unexpected cost increases.

In order to assess the tribological performance of mating surfaces with the numerous combinations of above parameters, numerous methods and test systems have been developed and used. Before conducting a wear test, it is crucially important to identify the type of wear that may potentially occur, and select proper test method and test conditions. Main wear mechanisms seen in sheet metal forming operations are (1) Adhesive wear, (2) Abrasive wear, (3) Fatigue wear, and (4) Thermal fatigue. Adhesive and abrasive wear are mainly observed on forming die tip and side surfaces due to high contact pressure and frictional forces generated by relative motion between punch and sheet blank. Fatigue wear is experienced close to the corners of the dies as a result of high temperatures and cyclic loadings. Thermal fatigue is observed in sheet metal forming dies in which heating and

cooling cycles are applied to the dies. Depending on the wear type or types to be investigated, specific different testers or a unique test system, if available, that replicates all possible wear types should be preferred.

This chapter, firstly, presents some important wear related definitions that will be mentioned frequently in this study, then, it reviews prominent friction and wear test systems, the ones used in sheet metal forming area, and lists the specifications of a rapid, reliable, accurate and inexpensive wear method and system for stamping dies.

2.1 Definitions

Tribology: ASTM G 40 defines tribology as "the science and technology concerned with interacting surfaces in relative motion, including friction, lubrication, wear, and erosion".

Wear: ASTM defines wear as "Damage to a solid surface, generally involving progressive loss of material, due to relative motion between that surface and a contacting substance or substances" [ASTM, G40]. Correspondingly, wear in general is defined as "The progressive loss of substance from the surface of a solid body caused by mechanical action, i.e. contact and relative motion of a solid, liquid, or gaseous counterbody" [DIN 50320, 1979]. Particularly, mechanical wear processes can be categorized into 4 main groups: abrasion, erosion, adhesion, and surface fatigue [Williams, 1999].

Abrasive wear: Wear due to presence of particles or hard protuberances forced against and moving along a solid surface.

Adhesive wear: Wear due to localized bonding (cold welding effect) between contacting solid surfaces leading to material transfer between the two surfaces or loss from either surface.

Apparent area of contact: The area of contact between two solid surfaces defined by the boundaries of their macroscopic interface.

Asperity: A protuberance in the small-scale topographical irregularities of a solid surface.

Catastrophic wear: Rapidly occurring or accelerating surface damage, deterioration, or change of shape caused by wear to such a degree that the service life of a part is appreciably shortened or its function destroyed.

Coefficient of friction (μ): The dimensionless ratio of friction force (F) between two bodies to the normal force (N) pressing these bodies together.

Coefficient of Wear (K_w): Non-dimensional wear quantification parameter obtained by multiplying specific wear rate with room temperature hardness value of softer contact pair.

$$K_W = \frac{V \cdot H_{soft}}{s \cdot F_N} \qquad \qquad \textbf{\textit{(Eq.1)}}$$

where; K_w is coefficient of wear, V is wear volume, H_{soft} is hardness of the softer contact pair, s is sliding distance, and F_N denotes applied normal load.

Fatigue wear: Wear of solid surface caused by fracture arising from material fatigue

Galling: A form of surface damage arising between sliding solids, distinguished by macroscopic, usually localized, roughening and creation of protrusions above the original surface; it often includes plastic flow or material transfer or both.

A condition whereby excessive friction between high spots results in localized welding with subsequent splitting and a further roughening of rubbing surfaces of one or both of two mating parts. [ASM Handbook, v.17]

Hertzian contact pressure: The magnitude of the pressure at any specified location in a Hertzian contact area, as calculated from Hertz' equations of elastic deformation.

Lubricant: Any substance interposed between two surfaces for the purpose of reducing the friction or wear between them.

Pitting: A form of wear characterized by the presence of surface cavities the formation of which is attributed to processes such as fatigue, local adhesion, or cavitation.

Plowing: The formation of grooves by plastic deformation of the softer of two surfaces in relative motion.

Real area of contact: The sum of local areas of contact between two solid surfaces, formed by contacting asperities that transmit the interfacial force between the two surfaces.

Scoring: A severe form of wear characterized by the formation of extensive grooves and scratches in the direction of sliding.

Scratching: The mechanical removal or displacement, or both, of material from a surface by the action of abrasive particles or protuberances sliding across the surfaces.

Scuffing: A form of wear occurring in inadequately lubricated tribosystems which characterized by macroscopically-observable changes in surface texture, with features related to the direction of relative motion.

Sliding wear: Wear due to the relative motion in tangential plane of contact between two solid bodies.

Specific wear rate (k): The rate of material removal (volume loss) from contact surface due to wear per unit sliding distance per unit load applied, given by following formula;

$$k = \frac{V}{s \cdot F_N} \qquad \left(\frac{mm^3}{N \cdot m} \right) \qquad\qquad \textbf{\textit{(Eq.2)}}$$

where; k is specific wear rate, V is volume loss, s is sliding distance, F_N is applied normal load.

Surface fatigue: Wear resulted from high contact stresses because of point or line-contact loading. These high stresses and repeated contact generate subsurface micro-cracks that subsequently leads to propagation of cracks and removal of particles from the surface.

Surface topography: The geometrical detail of a solid surface, relating particularly to microscopic variations in height.

Tribosurface: Any surface (of a solid body) that is in moving contact with another surface or is subjected to impingement or cavitation.

Tribosystem: Any system that contains one or more triboelements, including all mechanical, chemical, and environmental factors relevant to tribological behavior.

Wear rate: The rate of material removal or dimensional change due to wear per unit of exposure parameter, for example, quantity of material removed (mass, volume, thickness) in unit distance of sliding or unit time.

2.2 Review of Friction and Wear Test Systems

There are numerous friction and wear test systems available in literature ranging from easy to conduct, automated, and lab-scale/desktop ones to relatively complex ones requiring auxiliary units, larger spaces, human intervention. Overall cost of the test systems and their reliability and repeatability shows variations. Moreover, there are several classifications for the test systems used in the literature. For example, Bay et al. categorized the tribological tests as process tests and simulative tests [Bay et al., 2008]. In process tests, metal forming operations are applied without changing the basic process kinematics; whereas in simulative tests tribological conditions are attempted to be modeled to study friction and/or lubrication in controlled way. It was concluded that simulative tests are often characterized with substantial deviations from the forming operations applied in industry in terms of process kinematics.

In this study, the available tests systems are classified into three (3) groups as follows;

a) Repeated contact, low-cost test systems
b) Mid-size, non-repeated contact, moderate cost test systems
c) Large-scale, non-repeated contact, high-cost test systems

2.2.1 Repeated contact, low-cost test systems

This group of test systems is the most commonly used ones as much as gathered and learned from a wide literature and industrial survey. Their operations are relatively easy when compared to other test systems, however; results may not be conforming with industrial practice all the time.

The pin-on-disk test systems are the most conventional and widely used tools by researchers in academia. In test system, a small pin (die material of interest) is pressed against a rotating or reciprocating disc (sheet metal of interest) with a specific normal load. The pins used in these systems are in 1-10 mm in diameter and normal force can be applied ranges between 1- 2000 N in most systems. Although spiral wear track are possible, the same contact area scanned throughout these tests. This leads to misrepresentation of the actual stamping operation circumstances, since at every stamping stroke the die material gets in contact with new sheet metal surfaces (i.e., fresh/untouched surface conditions). Conversely, these type of test systems are quite conforming when the actual process to be simulated has a repeated contact in its nature as in the linear slides with reciprocating action, magnetic storage devices in which its magnetic medium and head comes into contact during starting and stopping of data recording resulted in wear of magnetic medium [Bhushan, 1996], door hinges, brake pads etc. Pin-on-disk tester has several configurations such as ball-on-plate [Antunes and Ramalho, 2005], ball-on-disk [Carlsson and Olsson; 2006], disc-on-disc, and crossed cylinder contact [Ramalho and Miranda, 2006] etc. as seen in Figure 2.1.

a)   b)   c)   d)   e)
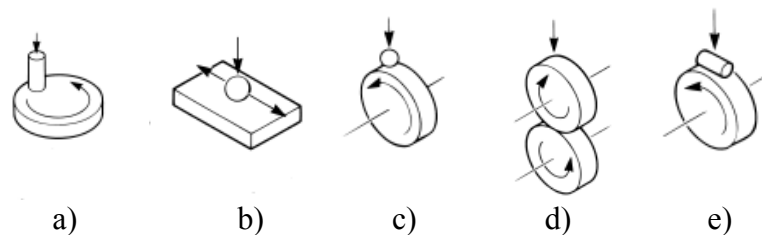
Figure 2.1 Several configurations of pin-on-disk apparatuses; a) Pin-on-disk b) Ball-on-plate   c) Ball-on-disk   d) Disk-on-disk   e) Crossed-cylinder-contact [*Source: http://www.phoenix-tribology.com/cat/at2/index/prodlistcontact.htm*]

Similar to pin-on-disk system; in a SRV (Schwingung Reibung Verschlei: reciprocating friction and wear) tester, the upper specimen is oscillated against the stationary lower specimen with an electromagnetic drive as shown in Figure 2.2. A prominent feature of SRV is to ability to test materials at elevated temperatures up to 900 ºC [Hardell, 2007; Wan et al., 1995].
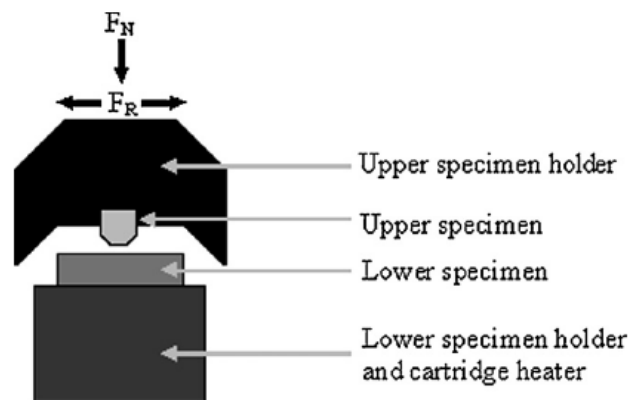
Figure 2.2 Schematic of SRV tester configuration used in high-temperature wear tests [*Hardell et. al, 2008*]

Twist-compression test (TCT) is also based on the repeated contact tracks on the same contact surface. An annular sample is pressed against a sheet sample with a certain normal load and twisted while load and torque are measured as seen in Figure 2.3. TCT is found to be appropriate tool for investigating severe wear conditions leading to lubricant breakdown, galling, adhesion of dissimilar material pairs, and the effects of tool surface finish and surface coatings on friction and metal transfer. [Lenard et al., 1996; Costello and Riff, 2005]. Primary use of this test system is to compare the effect test variables such as

30

pressure, torque, lubricant on wear, have rather than obtaining an absolute measure of it. Besides, it is not well-suited in terms of mimicking stamping conditions.
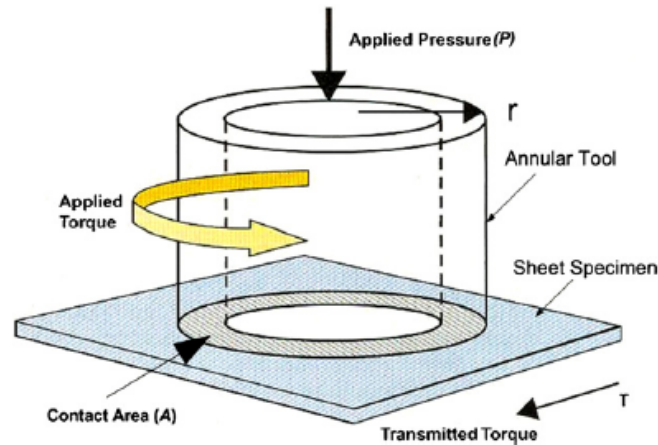
Figure 2.3 Schematic representation of twist-compression test [*Kim et al., 2008*]

The load-scanner (or cylinder-on-cylinder) test is reported to be good instrument for determining galling threshold load levels of materials. A stationary test cylinder is used as a tool sample, and it is in contact with another rotating cylinder which is sheet material of interest under certain loading conditions and constant speed. The normal load is gradually elevated during forward strokes and correspondingly reduced in reversed strokes. Hence, every point at the contact interface of both samples experiences a unique loading and shows tribological history after the test is completed. Thus, the number of test specimens needed for galling resistance investigation can be limited to only one pair, which can be rotated around their axes for subsequent testing. Figure 2.4 depicts the test

system mechanism and its load-position plot. Yet again, the repeated contact action confronts with the stamping's nature.
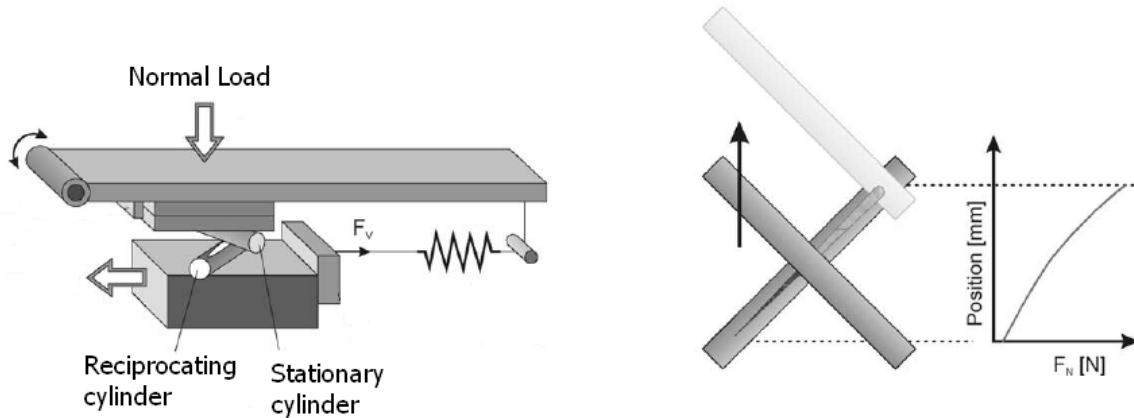
Figure 2.4 Load-scanner test system and typical load-position history [*Podgornik et. al, 2004*]

2.2.2 Non-repeated contact, moderate cost test systems

The TNO tribometer and its close replication slider-on-flat surface (SOFS), and the test system designed in this study can be given as examples to this class. Their common features can be listed as

a) non-repeated contact

b) ability to achieve high contact pressures

c) easy to conduct and faster tests

TNO slider-on-sheet tribometer was developed by researchers in Netherlands to provide always fresh, well-defined reproducible contact between die - sheet metal surface,

using sheet blanks without special preparations for longer test tracks [van der Heide, 2002]. The non-rotating, double-curved slider (die material of interest) shown in Figure 2.5 pressed against the sheet metal forces with normal load of F_N and it is dragged in x-direction with a sliding speed of v. When the slider reaches the end of the track on the sheet, it is raised above the sheet and moved over 1 mm in y-axis, then it goes back to x= 0 position. The slider moved down against the sheet with the same normal load again and sliding action is repeated till the whole sheet surface covered. 1 km test can be realized by 1m x 1 m sheet surface size. Test system also enables the measure of the friction forces independent from normal load applied. Several tests can be performed using one slider just rotating the slider slightly in its mounted position. After the tests slider is taken out and roughness measurements and wear calculations are performed.

a)   b)
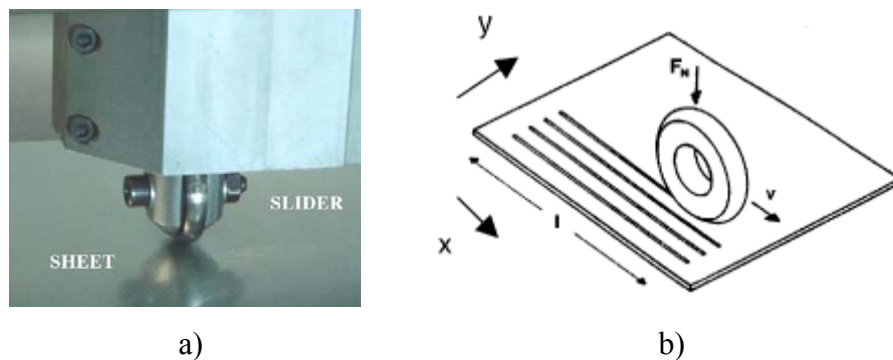
Figure 2.5 a) TNO tribometer and b) its slider movement on the sheet [*van der Heide et al., 2006; 2003*]

As a very close replication of TNO tribometer, slider-on-flat-surface (SOFS) uses double-curved tool geometry slider as a die sample, too. The travels in x and y-direction

33

are realized by a linear guidance systems driven by two separate serve motors. Likewise, the normal load is also exerted by another servo motor which is capable of applying different load curves such constant or time-dependent etc. within the 30-1000 N load range. Hence, determination of galling initiation contact stress type of studies is also made possible [Gåård et al., 2007, 2008].

Based on the continuously fresh contact area principle Cao et al.; proposed strip-on-cylinder test system in which the strip is made of the sheet metal of interest and the cylinder is made of tooling material representing a die or a drawbead as shown in Figure 2.6. The sheet strip is pulled by a small motor through a control box and the cylinder is driven in the opposite direction by an electric motor. In their study, researchers investigated the wear conditions of AISI D2 tool steel, against DP 600 sheet metal strips under 25 cm/s relative sliding speed and 260 MPa average contact pressure conditions. The tests completed after 300 m sliding distance which was measured on the cylinder. Die wear volume was measured with a white light interferometer.
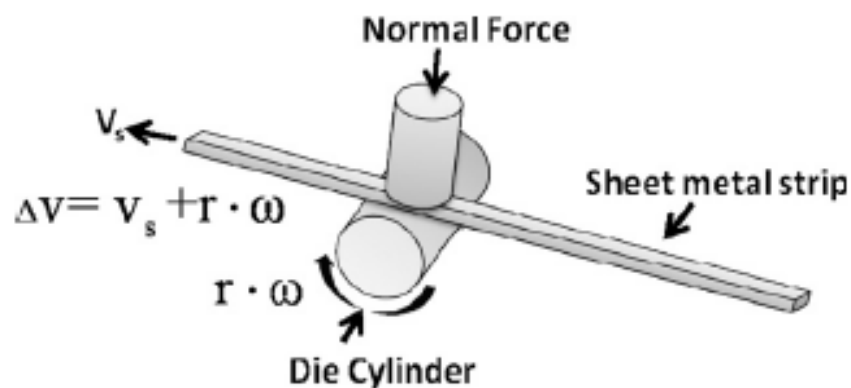
Figure 2.6 Illustration of the strip-on-cylinder test apparatus [*Cao et al., 2009*]

Scratch tester, on the other hand, is another tool that offers non-repeated contact. It is mainly used for characterizing the mechanical properties of thin films and coatings such as adhesion strength, and substrate-coatings compatibility. A stylus with a rounded diamond cone (200 μm in diameter), depicted in Figure 2.7.a, is pressed against the coated surface and moved along the surface under gradually increasing normal load. Normal load values can be selected as in mN range, and scratch length, and scratching speed are considerably low with respect to other test systems leading to faster tests. The load on the diamond stylus, at certain point, causes to delamination of coating as the test progressed. The load level that coating failed is called as the critical load. Figure 2.7.b shows a typical after scratch test surface. Coating failure can be detected either by observing instantaneous increase in friction coefficient obtained by load cells or acoustic emission techniques. Although this test provides very reliable and quick information about the strength of coatings, it is not appropriate for testing of die materials against AHSS sheet blanks since, sheet blank of interest is not available in the test system.

a)

b)
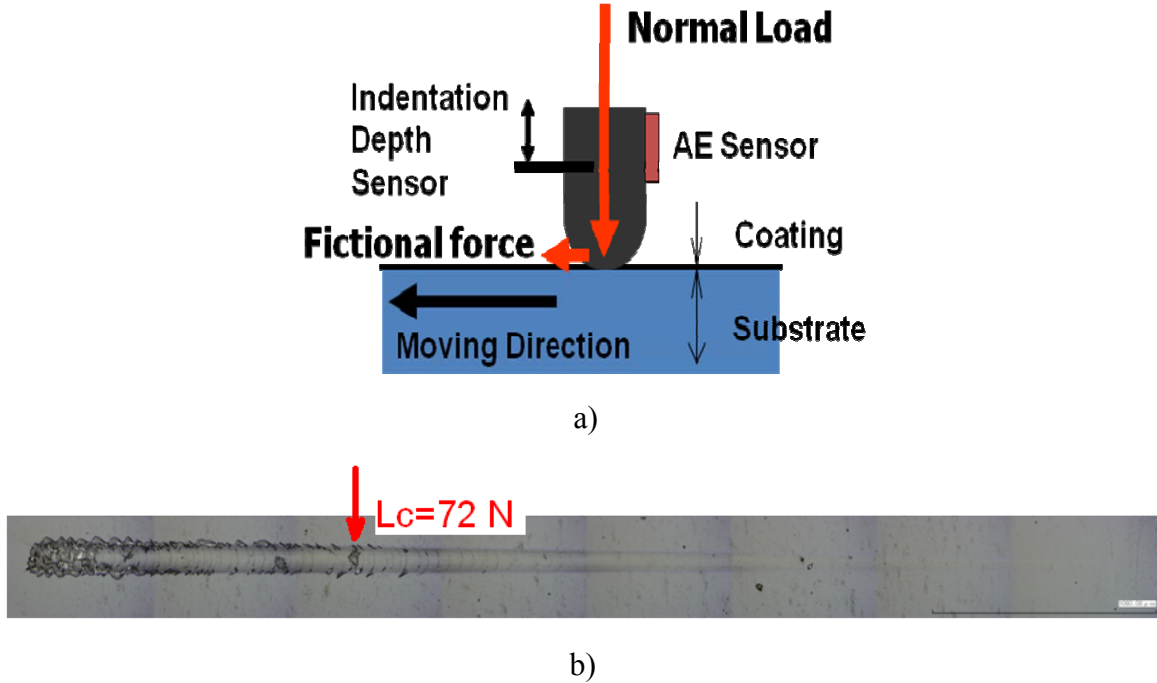
Figure 2.7 a) Schematic of scratch tester b) typical coated surface failure after scratch test [*Tsuchiya et al., 2007*]

2.2.3   Non-repeated contact, high-cost test systems

In terms of mimicking the actual forming conditions the third type of systems give conformant results with the industrial practice, however, this type of test systems require extensive pre-test preparations, relatively complex and expensive test equipments, and longer test durations. In addition, these wear testers are usually not standardized and there is no consensus in designating the tests systems.   Therefore, in this study, working principles of test systems will be emphasized rather than their names.

American Deep Drawing Research Group (ADDRG) and International Deep Drawing Research Group (IDDRG) also encouraged the development of several sliding friction tests

for investigating the galling of steel sheets. These can be classified into the following three groups [Bernick et al., 1978].

1) Drawing in plane strain tests: the sample is drawn between two dies

2) Draw bead simulation tests: the sample goes through a series of bending and unbending operations over a set of draw beads

3) Draw cup tests

A very good way of categorization for frequently used simulative tests in sheet metal forming operations was done by Bay [Bay et al.; 2008] as seen in Figure 2.8. According to his categorization, the first three tests, (1) strip drawing with flat dies, (2) draw bead testing, (3) drawing with tangential compression tests, are suitable for representing the contact conditions in flange region of sheet forming process. The conditions on die radius can be modeled with bending under tension (4); while bending with tangential compression (5) is appropriate tool for combined flange and die curvature like conditions. Ironing in a conical die can be simulated with strip reduction testing (6), whilst the situations like stretching over the punch radius of curvature and under the punch nose like conditions can be imitated via strip-tension(7) and hemispherical stretching tests (8).
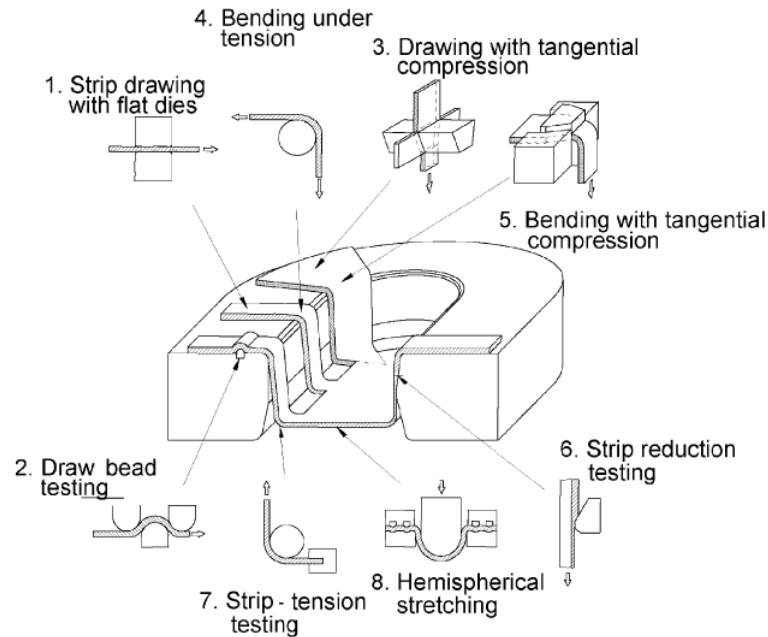
Figure 2.8 Schematic descriptions of simulative tests for sheet metal forming according to Bay [*Bay et al., 2008*]

Strip pulling tester is one of the widely used test systems in which sheet metal slides through two clamped flat-dies. It was originally developed by Wojtowicz to test the metalworking lubricants and dubbed as sliding friction test [Wojtowicz, 1955]. The main purpose of these tests is to simulate contact conditions at blank holder region where deformation is small and sliding length is relatively long. It is mostly used for steel sheet friction/galling studies rather than die wear analyses. It has been modified and named by several researchers differently such as strip drawing [Kim et al., 2009], plane-drawing, Inland test [Boher et al., 2005], drawing in plane strain, flat-platen [Bernick et al., 1978], strip drawing with flat dies [Bay et al.; 2008], flat-die type friction tester [Wichern, and Van Tyne; 1999], etc. Jonasson et al., replaced one of the flat dies with a cylinder and pulled the sheet strip through these clamped dies calling their system as strip-drawing

simulator [Jonasson et al., 1997]. Even though these test systems do not represent real deep-drawing conditions, they enable the study of the sheet-lower die (or blank holder) part interaction. Bernick et al., modified strip pulling tester in 2 different ways; (a) replacing one of the dies with rounded one and used it against flat die, (b) using a rounded die against recessed bottom die [Bernick et al., 1978]. The latter configuration resembles what is known as draw-bead test which will be discussed in next paragraphs.

Wear issues at die radius (Zone 3 in Figure 1.5, Test #4 in Figure 2.8) can be analyzed by a slightly modified version of strip pulling test system in which one of the dies that clamp the sheet has a curvature at its corner instead of flat surface and sheet is bent over the die radius with a certain angle (Figure 2.9). Boher et al. used this system, called as deep drawing process simulator (DDPS), in their studies to investigate the degradation of the die radius. The steel grade for the material was X160CrMoV12 (AISI D2 or DIN 1.2379); while the strip sheets was made of low skin-passed steel used in cold forming DC04 grade steel (DIN 1.0338). The strip was covered with a thin, protective oil film prior to blank holder region. It was reported that the metal strip is 50 mm wide and 1 mm thick and the coil length is 150 m long. Test parameters such as sliding speed, blankholder pressure, sliding distance are selected to obtain a degradation of the die radius after only 1200 cycles (one coil) [Boher et al., 2005].
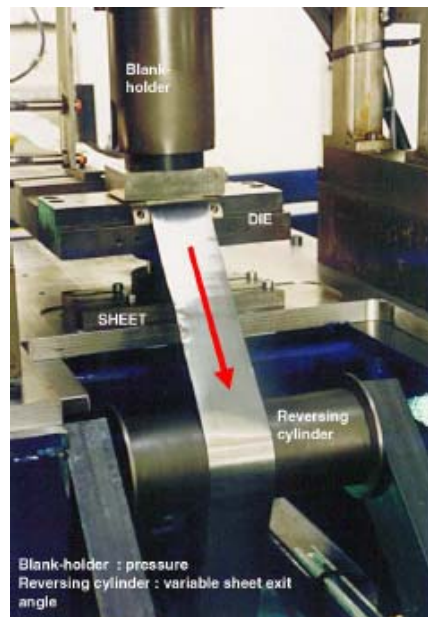
a)
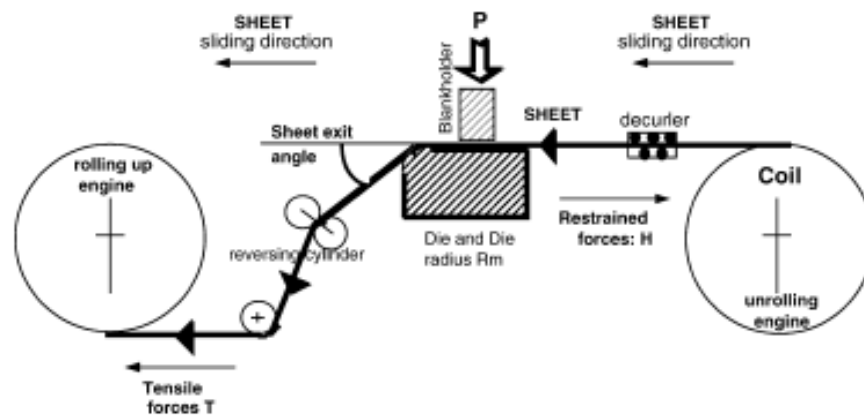
b)

Figure 2.9 a) Active part of the process simulator, b) Complete description of DDPS [*Boher et al., 2005*]

In strip-drawing with bending test, developed in Institute of Production Technology and

Metal Forming Machines (Institut für Produktionstechnik und Umformmaschinen: PtU) of

Technical University of Darmstadt and also known as PtU test [Schmoeckel, and Frontzek,

1986], a sheet metal strip is drawn through a model-tool consisting of blank holder and draw die and then bent over the draw die radius for 90º as seen in Figure 2.10. This system is capable of simulating the conditions both in flange (blank holder), and die corner areas and is named also as "bending with tangential compression test" [Bay et al., 2008].
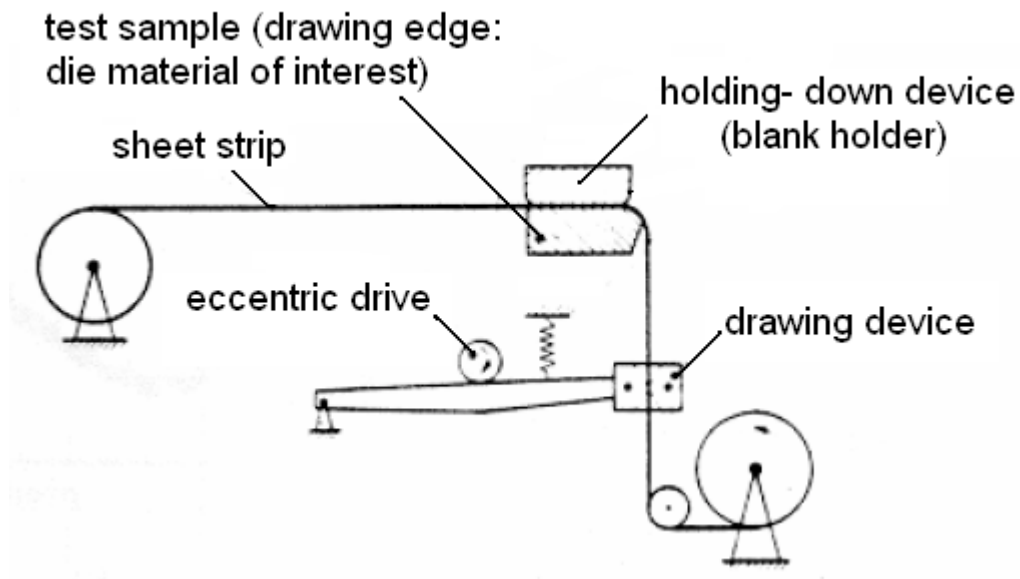
Figure 2.10 Strip drawing with bending (PtU) test [*After Matthes et al., 1991*]

Hortig and Schmoeckel used FEA to identify the characteristics distribution of local loads on the draw die surface. Major influence parameters such as sheet thickness, draw die radius, coefficient of friction, material differences are analyzed. Then, FEA results were verified with strip drawing with bending test results. It was concluded that the contact pressure shows a very uneven distribution with a characteristic local maxima. The sheet

thickness and the dimension of the draw die radius show a high impact on the load maxima [Hortig, and Schmoeckel, 2001].

Although Eriksen denoted the system he used as "modified bending-under-tension tester" seen in Figure 2.11, this tester also can be categorized in strip drawing with bending testers group [Eriksen, 1997]. Basically strip sheet (1) is pulled by hydraulic cylinder (6) with a clamping system (5) through lubrication system (2) and into the wedge die. After the wedge die the strip is bent 90º over a cylindrical die. Before the wedge dies, the strip is 25.2 mm and after the wedge dies it is 20 mm wide. To avoid the wrinkles between the wedge dies, a blank holder force of 3000 N applied, resulting in surface pressure of 1 N/mm^2. After the clamping, test sample (7) is transferred to cutting machine (8). He studied the effect of die geometry on tool wear in deep drawing with 150 m long St 1403 sheet strip on cast iron GG25 tool materials (wedge dies) both experimentally and numerically [Eriksen, 1997].
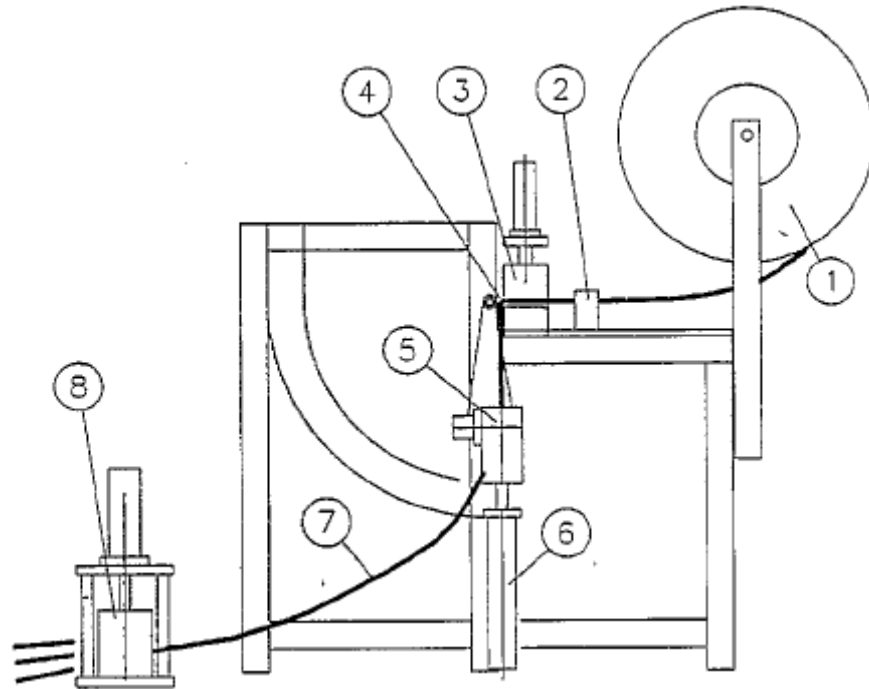
1-Wound sheet strip, 2-Lubrication system, 3-Wedge die, 4-Cylindrical die, 5-Clamping system, 6-Hydraulic cylinder for pulling the strip, 7-Test material, 8-Cutting machine

Figure 2.11 Modified bending under tension tester [*Eriksen, 1997*]

Schedin, used very similar arrangement of test device with an addition of a draw bead, "strip drawing with draw bead test", which consisted of hydraulic system to clamp, uncoil and draw the strip through a model draw bead. The strip is then bent over the die shoulder as seen in Figure 2.12. Draw beads are frequently used in sheet forming to control the material flow, especially in stretch forming. This setup was used to find out the galling mechanisms in sheet forming systems. The blank holder pressure was reported as 3 MPa and more than 2000 parts with 70 mm sliding length were required to be drawn for galling

to be experienced [Schedin and Lehtinen, 1993; Schedin, 1994]. Michler et al., applied computer controlling to combined strip-drawing with bending and draw-bead test to monitor and adjust the blank holder force and drawbead penetration [Michler et al., 1994].
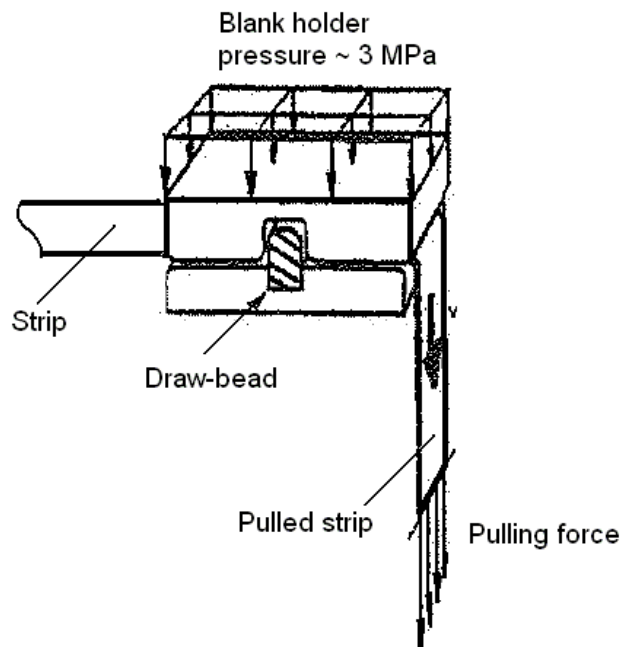
Figure 2.12 Strip drawing through draw-bead test [*After Schedin, 1994*]

One of the most widely used other test system in which the sheet strip is stretched 90° over a fixed or rotating cylinder is called as "bending under tension" (BUT) as illustrated in Figure 2.13. In this way, tribological conditions in the die entry zone in deep drawing operation can be simulated. The two actuators are used in the system to provide a constant restraining force (back tension force) and to displace the sheet from other end at constant speed. Two force readings, pulling force, and back tension force, are obtained between the

actuators and the strip grips individually. Bay et al.. categorized this test as representing mild tribological conditions with normal pressure, low sliding length and no surface expansion test. Different versions of this tester have been reported in literature, and it is used to study the large number parameters on friction and lubrication, and mainly to determine the friction coefficient in sheet metal forming operation [Jonasson et al., 1997; Coughbrough et al., 2002; Alinger and Van Tyne, 2003; Andreasen et al., 2006; Shih, and Shi, 2006; Bay et al., 2008]. It is also known as "radial strip-drawing test" [Sniekers, and Smits, 1997]. A slightly modified version of this tester is recognized as "tensile strip test", originally developed by Duncan, in which a strip specimen of sheet metal is pulled over the cylindrical pins to replicate the stretching and drawing operation. Pulling and strip forces on sheet strips are measured along with the strain on the strip using extensometer and calculated from the measured strain using stress-strain characteristics of the test material, respectively. Coefficient of friction is assumed to be constant over the pin surface, and the strip tensions are used in capstan friction model to calculate the coefficient of friction (Figure 2.14). It is also called as "strip friction" [Hao et al.; 1999], and "strip tension test" [Bay et al., 2008].
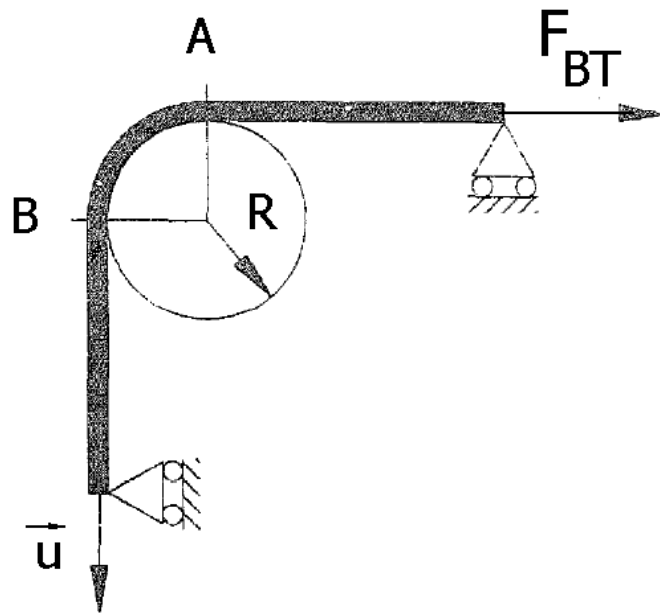
Figure 2.13 Bending under tension (BUT) test [*After Sniekers, and Smits, 1997*]
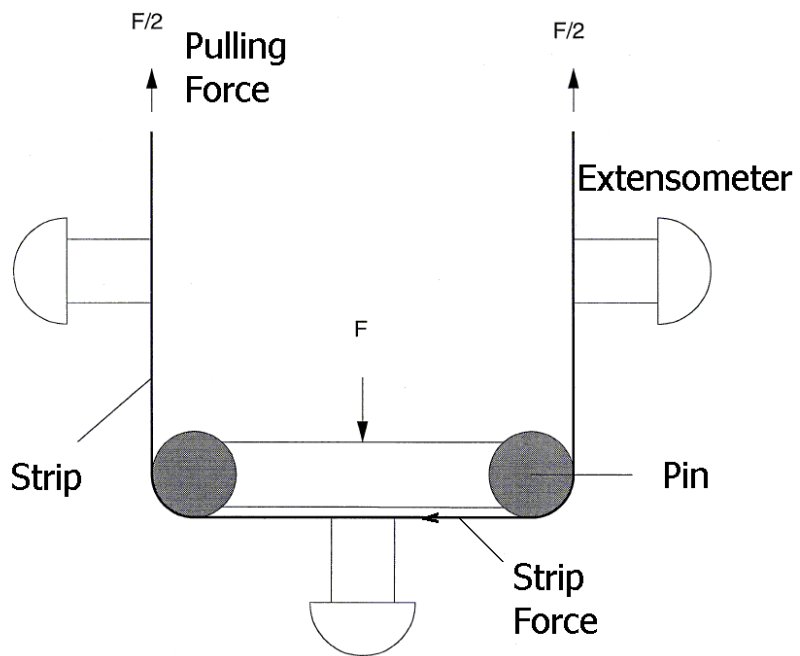
Figure 2.14 Tensile strip or strip friction test [*After Hao et al.; 1999*]

U-Bending or deep-drawing test, on the other hand, is based on the drawing of the sheet strips as in the deep-drawing process as described in Figure 2.15. Sheet blank is, firstly, clamped between blank holders, punch and die tool specimens. Then, punch is move upward in stage (Figure 2.15, stage 3) and forming of u-shaped sheet is completed. Nilsson et al., used u-bending test to experiment three different zinc alloys as tool materials in short-run sheet metal forming processes. Zinc alloys, e.g Kirksite, are from alternative tool materials that those are still under research and mainly used for prototype productions mainly by automotive industry [Nilsson et al., 2002].
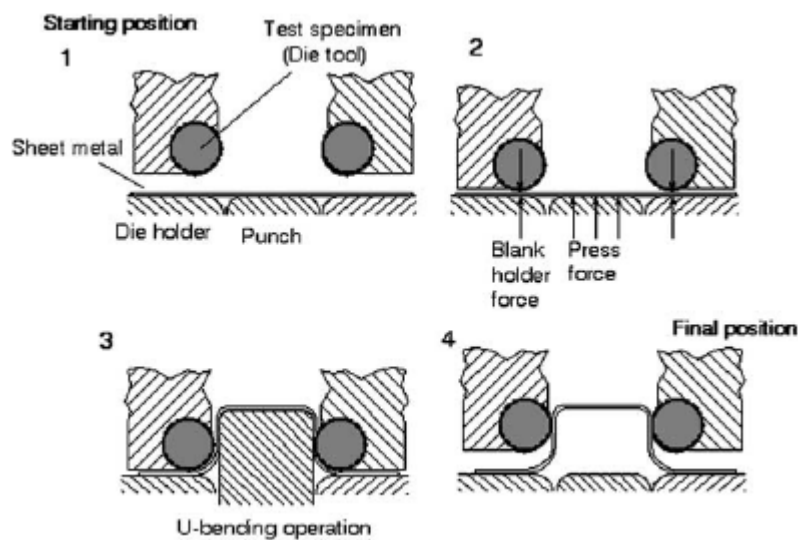
Figure 2.15 Outline of U-bending test [*Nilsson et al., 2002*]

Schedin and Lehtinen used slightly different U-bending tester, in which blank holder package moves downward, while punch head is stationary [Schedin and Lehtinen, 1993].

47

They demonstrated the influence of the tool surface roughness on the galling mechanisms. Schedin also investigated the galling mechanisms in sheet metal forming operations with various combinations of tool and sheet materials under lubricated and non-lubricated conditions. The total sliding length for each strip was 110 mm and sliding speed 25 mm/s and galling was observed after less than 50 strips under non-lubricated conditions. He concluded that build up of large lumps transferred from sheet blanks to tool surface is faster for non-lubricated tests [Schedin, 1994].

Sato and Besshi conducted anti-galling tests for some uncoated and coated die materials against aluminum alloy sheets using U-bending test. As discussed in chapter 1, aluminum is one of the alternative lightweight material choices with its inherited challenges. For example, limiting drawing ration of aluminum is lower than that of steel, and it is more prone to adhere to forming tools. Their study revealed that coated tools (TiC, TiN, CrN) have higher anti-galling performance than bare SKD 11 material, however; their performances are low compared to cemented carbide tool [Sato and Besshi, 1998]. Apart from the tool wear studies, similar test system that use cylindrical tool and sheet blanks can be used for limiting drawing ratio (LDR) experiments for the sheet materials as Shih and Shi performed LDR tests for aluminum sheet materials [Shih and Shi; 2006].

The draw bead test, originally developed by Nine [Nine, 1978], has a general acceptance in automotive industry especially in North America. Basically, the sheet metal is pulled to flow between three cylindrical pins of equal radii. F_{CR} and F_R are the clamping force and pulling forces respectively. Pulling force is the tension force required to pull the sheet

48

through the drawbead element, and it is also called as "Restraining Force". Figure 2.16 shows the working principle of draw-bead tester. Initially, sheet metal strip deforms in pure bending mode as F_{CR} is applied, then the strip undergoes a combined bending and drawing deformations as it goes through the drawbead under stretching-drawing effect. To determine the friction, 2 specimens need to be tested. In one of them, the sheet strip is pulled between cylindrical pins supported by ball or roller bearings. Friction on the bearings is negligible small and the pulling and clamping forces measure the bending and unbending resistance of the sheet strip under frictionless conditions. Second sheet strip is pulled between pins of radii equal to the rollers, yet tightly secured to the tools (not-rotating). Thus, frictional forces encountered during the sliding of the sheet over the fixed tools. The pulling and clamping forces measure the combined loads required to slide, and bend and unbend the sheet as it goes through the fixed pins/beads. Then, the measured values from two tests are inserted into an equation yielding friction coefficient [Sanchez, 1999]. North American Deep Drawing Research Group (NADDRG) undertook a systematic work from 1989 to 1998 to establish a test procedure that may lead to reliable comparisons between the friction results obtained by participating laboratories. In this study, pin material (die material of interest) was selected as AISI D2 tool steel (9.5 mm in diameter), hardened to 55-60 HRC (Rockwell Hardness Scale C) and finished longitudinally to 0.09-0.13 μm R_a. The sheet specimens to be pulled are 150 mm long and 50.8 mm wide. Test speed was selected as 85 mm/s. All the test supplies such as cylindrical pins, lubricants and sheet materials were each supplied to all participating labs from a same source. The friction coefficient data obtained from all the labs was pretty

49

scattered, ranging from 0.07 to 0.16, and it was considered that friction was useful only as an indicator of relative performance within the same laboratory.
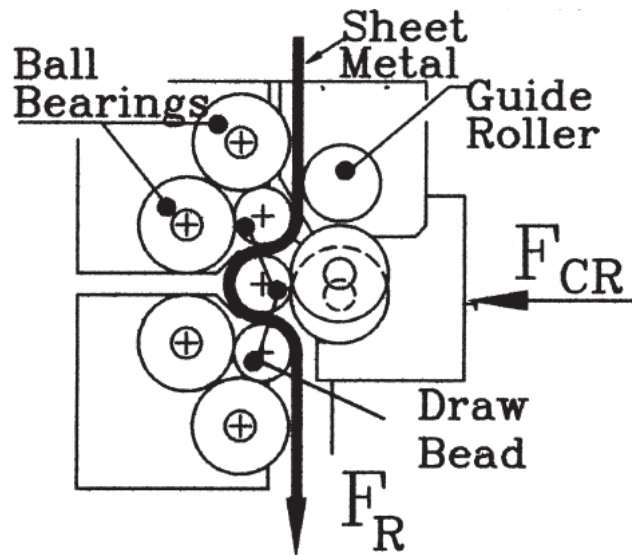
Figure 2.16 Schematic view of draw-bead test [*Sanchez, 1999*]

Firat used square, and fixed type of beads to establish an analytical model for the sectional deformation analysis of automotive sheets passing through a drawbead element [Firat, 2008]. Another study on friction behavior of automotive steels in different forming modes utilizing different test systems were performed by Shih and Shi [Shih, and Shi; 2006]. In their study, they developed a stretch forming simulator and evaluated the friction behavior of seven different zinc coated sheet steels. Test results obtained from these tests were compared with the ones obtained from bending under tension as well as draw-bead simulator tests.

50

One of the most comprehensive and remarkable studies using draw-bead tester was performed by Dalton [Dalton; 2002, 2003, 2004]. Prepared for the Auto/Steel Partnership, this project aimed to understand the effect of tribological factors such as bead penetration, stroke length, sliding speed, temperature, restraining force etc. on stamping die wear in forming of advanced high strength steels. Their study examined the effect of lubricant and die material on formability and die life with coated and uncoated advanced high strength steels. In first phase, the effect of lubricant on friction, springback, and wear with advanced high strength steels was examined using draw-bead simulator and twist compression test. More than 700 tests were performed and analyzed in first phase. [Dalton, 2002]. Figure 2.17 depicts the schematic view of modified drawbead tester. Phase 1 findings revealed that temperature and pull force became important factors for HSLA and DP 600 AHSS sheets. It was also found that sheet coatings had a significant effect on friction. In the second phase of this study, the effects of bead penetration (positioning of bead relative to the pins) and stroke length on die wear were studied. Six coils of material (each 800 m long) were run through draw-bead tester using three bead penetrations and two stroke lengths. Depending on the stroke lengths (long stroke: 100 mm; short stroke: 50 mm) 8000 and 16000 strokes were performed on sheet strips [Dalton, 2003].Third phase studies focused on die life. In order to understand how die life will be affected with advanced high strength steels, die wear of three different sheet materials (DP 600, HSLA, AKDQ galvaannealed sheet steels) on three die surface treatments (flame hardened, ion nitrided, chromium nitride) were tested. For each test, one coil, or the equivalent of 9,000 parts, was processed [Dalton, 2004].

51
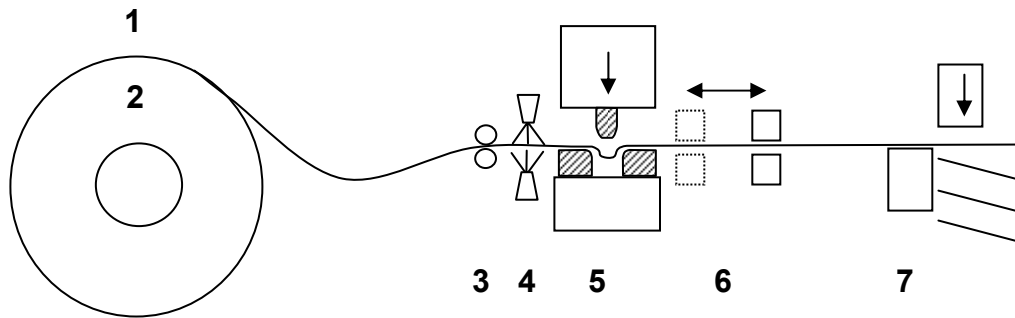
No.	Name	Description
1	Decoiler/Leveler	42" OD, 12 ID x 4" wide
2	Coil	2 " coil - 0.040" thick, 2200' , 1000 lb
3	Guide Rollers	Vertical and horizontal guiding
4	Lubricator	Air brush spray top and bottom
5	Die Set and Inserts	Guided die set with bead inserts (3/set)
6	Feeder - 0-6" stroke	6000 lb hydraulic with hydraulic clamps
7	Cut-off	Synchronized with feeder

Figure 2.17 Schematic of modified drawbead tester and its main section descriptions [*Dalton, 2003*]

Dalton's study is probably the most detailed wear test study on the stamping die wear of advanced high strength steel sheet blanks. 48,000 parts with 16 different conditions, in total 768,000 parts were tested during the whole test spec [Pearson, and Dalton; 2007]. It is recognized as the most reliable means of determining the coefficient of friction for a sheet or lubricant, however; it requires special arrangements such as strip form of sheet metal, coiling / decoiling of strips, large space and relatively longer test durations.

2.3 Overall Evaluation of Die Wear Test Systems

Although the literature on wear test systems is abundant, limited number of those could be reviewed above. As discussed, testers show differences in terms of geometries of the mating surfaces, deformation types, contact pressures etc. Best test results, in terms of reliability and conformity to production results can be obtained by applying real manufacturing conditions, or simply from production itself. However, cost is an important concern that restricts the number of experiments to be performed. Therefore, an ideal test system can compromise from the real manufacturing conditions within certain limits as long as it replicates the main process conditions such as deformation mode, contact stress levels, temperature etc. reasonably well. Group 1 test systems enable easy-to-perform tests, however; those do not seem to be appropriate for sheet metal forming dies. In contrast, group 3 testers are the production-like testers, and the most conformant results are obtained with these process type of high-cost test systems. Figure 2.18 depicts the estimated cost-reliability relation of the test systems.
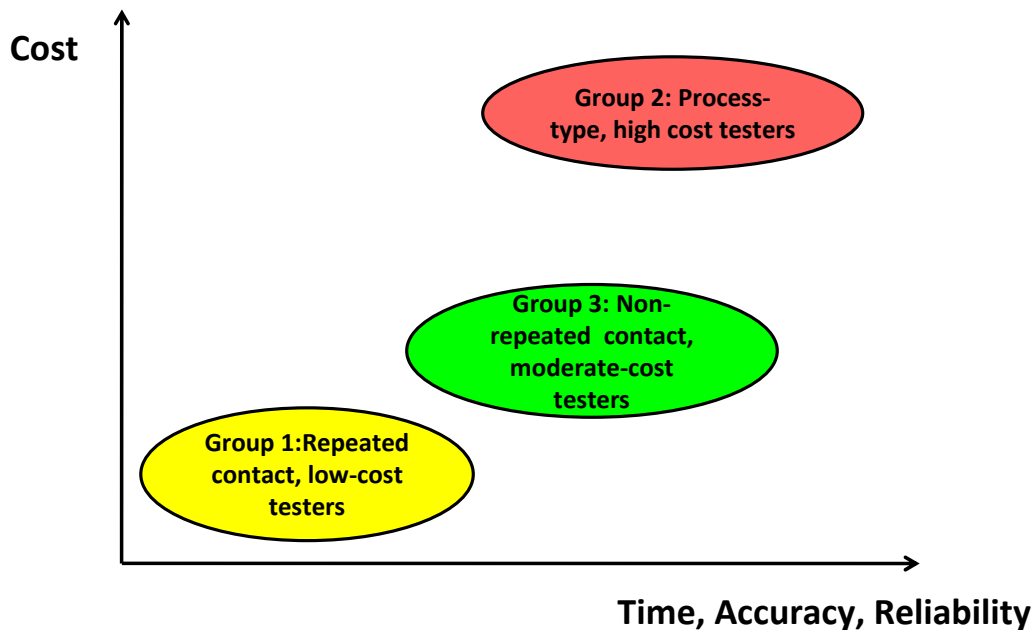
Figure 2.18 Estimated cost and reliability of the wear testers reviewed

This study intended to establish a test system that offer following specifications;

   a) It truly represents the contact conditions in a typical stamping (non-repeated contact)

   b) Test conditions (sliding velocity, contact force, temperature) can all be adjusted and

   controlled as opposed to existing test systems

   c) It can take regular sheet metal blanks – No special preparations (stripping, coiling,

   decoiling), automated system

   d) Friction and wear testing at elevated temperature is possible,

   e) Reducing human intervention

   f) Rapid and cost-effective,

The designed test system that falls into category 2 in Figure 2.18, its specifications and the

experiments performed with these test systems will be discussed in next chapters.

CHAPTER 3

Die Wear Test Development – Phase I

Based on the conclusions of the chapter 2, this study aims to establish a novel, rapid, cost-effective die wear test method and an apparatus that reflects stamping-like conditions. In the next section, the methodology and 1st generation device design of the wear test is discussed followed by a description of experimental conditions and procedures. Experimental results with uncoated die samples and a discussion of the experimental findings in comparison with data from literature will also be presented.

3.1 First Generation Die Wear Test Setup

First, a robot-based die wear test system was developed as depicted in Figure 3.1 and Figure 3.2. A die sample held by a robot arm (Adept Cobra 600, Adept Tech. Inc., CA) via a specimen holder is compressed against the surface of a sheet blank of interest under a controlled normal load, and moved along the untouched sheet surface over multiple tracks. When the entire sheet blank surface area (330x330 mm) is scanned, a new sheet blank is introduced under the die sample either manually or automatically for longer wear lengths. The resulting compressive force is measured with strain-gage type of load cell (Honeywell

Sensotec Model 41, Honeywell Sensors, Columbus, OH) installed above the specimen holder. This data is accumulated in a PC through load cell, in-line amplifier, data-acquisition system to calculate the resultant average normal contact load during the test. This arrangement offers a great flexibility in terms of adjusting various test parameters such as magnitude of compressive load, sliding speed, and direction. Furthermore, optional heating/cooling elements can be embedded to change the testing conditions as close to the real working conditions as possible or for the purposes of speeding up the tests. Optionally, non-contact optical measurement systems such as CCD cameras or lasers can be added to examine the surface of the die specimens at certain intervals to characterize the progress of the wear.

Under the circumstances of 1st generation test system, there were two options in choosing die specimen shape and dimensions to achieve different contact stress levels. As the first option, a die sample with a small contact surface area (around 1 mm^2, a bullet form as shown in Figure 3.2.a or a slim disc as shown Figure 3.2.b that the contact area is either a point or a line at the start of test could be used. As a second option, specimens with larger contact area (75 mm^2 or greater) could be selected Figure 3.2.c. With a bullet-type sample configuration, high contact stress levels up to 1-2 GPa levels can be achieved while the cylindrical (flat end) samples would offer up to 50 MPa contact pressure levels. The latter necessitates applying relatively high forces to achieve the specific contact stress level with respect to the first option. In this initial study, a die specimen which is closer to the second option is used to simulate the conditions in the blank holder region of stamping operations.
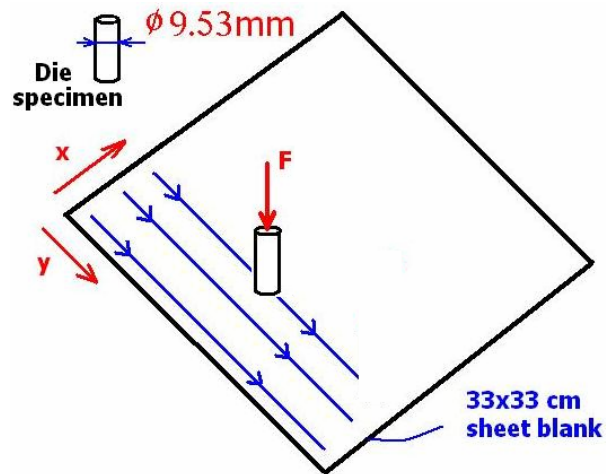
Figure 3.1 Schematic description of the proposed test method
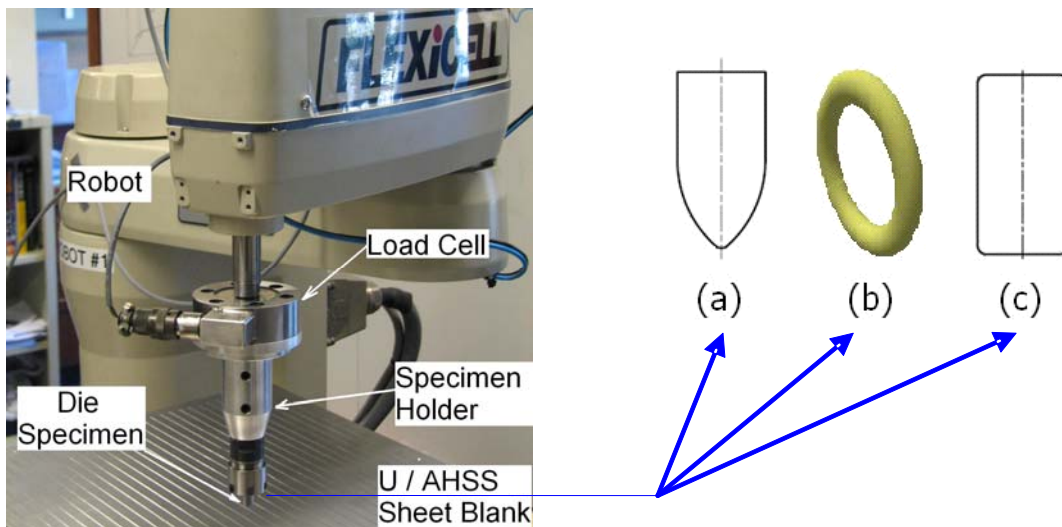
Figure 3.2 Robot based die-wear test setup and die specimen configurations (a, b, c)

3.1.1 Proof of concept tests

In order to test the capabilities of the proposed wear testing method and robot-based device, two preliminary experiments were conducted with two different die samples on different type of sheet blanks. In the first case, relatively hard die and sheet materials, namely heat treated AISI D2 tool steel and AHSS sheet metal blanks, were used while in the second case, non-heat treated AISI A2 die sample and ordinary AISI 1008 low-carbon cold rolled steel sheet blanks were used. Cylindrical shape die specimens as shown in Figure 3.2.c were machined to 9.53 mm in diameter. Then, the heat-treatment applied for the first specimen (AISI D2) only to attain higher hardness value compared to second specimen AISI A2. The reason in choosing in these die materials is that these are historically used tool steels for stamping and other forming operations. Typical chemical compositions for die samples and sheet blanks used in tests are given in Table 3.1 and Table 3.2 respectively. Experimental conditions, specific material properties, hardness values with different testers (HRC: Rockwell Hardness Scale C, BHN: Brinell Hardness Number, HRB: Rockwell Hardness Scale B), length of contact, etc. for both Case 1 and 2 experiments are given in Table 3.3.

Table 3.1 Chemical composition for sheet blanks used in Case 1 and Case 2 [Cuddy et al., 2005; Material Spec. for AISI 1008 B]

Material	C	Si	Mn	P	S	N	Cr	Ni	Cu	Al	Nb
DP 600	0.106	0.310	0.800	0.010	0.005	0.004	0.022	0.037	0.009	0.044	< 0.01
DP 800	0.113	0.440	1.560	0.012	0.004	0.029	0.026	0.038	0.008	0.043	0.019
DP 1000	0.144	0.540	1.520	0.010	0.001	0.003	0.040	0.050	0.010	0.043	0.017
AISI 1008	0.050	0.016	0.280	0.011	0.010					0.055	

Table 3.2 Chemical composition for die samples used in Case 1 and Case 2

Material	C	Si	Mn	Mo	Cr	V
AISI D2	1.55	0.3	0.4	0.8	11.8	0.8
AISI A2	1	0.3	0.75	1	5	0.25

Table 3.3 Test specs for Case1, and Case 2

	Case Study I	Case Study II
Die Specimen	Heat Treated AISI D2 tool Steel	Non-Heat Treated AISI A2 tool steel
Hardness	58-60 HRC (615-654 BHN)	18 HRC (214 BHN)
Dimensions	Ø 9.53 mm (3/8"), Height: 16 mm	Ø 9.53 mm (3/8"), Height: 14 mm
Average Surface Roughness (Ra) Before/After Test	0.216 µm / 0.27 µm	0.064 µm / 0.722 µm
Sheet Blank Materials	DP 600 (330x330x1.2 mm), DP 800 (330x330x1.45 mm), DP 1000 (330x330x1.5 mm)	CS AISI 1008 Type B (330x330x1.4mm)
Hardness Values for Sheet Blanks	DP 600 (10-13 HRC/190-200 BHN) DP 800 (222BHN/20HRC) DP1000 (327 BHN/35HRC)	95 BHN (60 HRB)
Total Test Length	2.3 km	1 km

The compressive load applied at the die sample-sheet blank interface was 300 N (Figure 3.3) on average and sliding speed of the robot's end-effector was about 0.35 m/s. Before each test, sheet surfaces were cleaned by means of acetone. Die samples were weighted before and after each test. The volume loss of the materials was calculated using density values of materials and mass losses. Finally, coefficient of wear and specific wear rate values were obtained using the volume loss and some other experimental data as it will be discussed later.
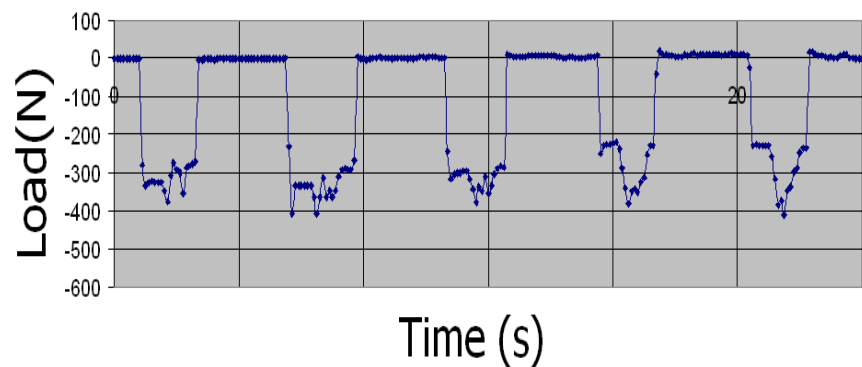
Figure 3.3 Typical contact normal load profile experienced at the die sample – sheet blank interface

3.1.2 Surface topography and roughness measurements

Several equipments and measurement devices were used to obtain surface profile and roughness information during the initial phase of die wear test studies such as surface profilometer, laser measurement, AFM (Atomic force microscopy), 3-D image photogrammetry etc. KEYENCE LK-G37 (Keyence Corp. of America, Woodcliff Lake, NJ) laser measurement systems were used to get the contact surface profile for the die

samples over the contact surface, normal to the sliding direction before and after tests. Since the laser measurement is based on the reflected light from the measured surface, there were some peak and valley points that reflected light was out of the laser sensor range and data could not be read at. Atomic force microscopy (AFM) measurements (with Nanosurf® EasyScan 2, Phoenix, AZ) were also taken from the die contact surfaces as seen in Figure 3.4. It is capable of performing not only line measurements but also area measurements in a very precise manner, however; the area can be scanned in one measurement as small as 3.8 nm^2 (62 µmx62 µm) which requires multiple measurements to cover the whole contact surface. Another disadvantage of AFM used for our case was its inability to detect surface height differences higher or deeper than 7 µm. 3-D image correlation photogrammetry was employed to get the surface profile, specimen dimensions and worn volume information after wear tests as depicted in Figure 3.5 with ARAMIS 3-D optical measurement system (GOM mbH, Braunschweig, Germany). This technique requires spraying black and white paints over the contact surface to form fine black dots on the white paint contour as reference points which causes filling in the valley points and changing the original surface texture. Surface roughness and topography information were also obtained using AMBIOS XP-1 contact type profilometer (Ambios Technology Inc., Santa Cruz, CA) which can detect surface profile changes up to 400 µm. Equally spaced line measurements were performed to have surface profile and average surface roughness information as described in Figure 3.6. Measurements are analyzed with TrueMap (TrueGage^{TM} Surface Metrology, North Huntingdon, PA) as shown in Figure 3.7. After

the analyses, profilometer was found to be the most appropriate technique among the equipments used to get the surface roughness data.
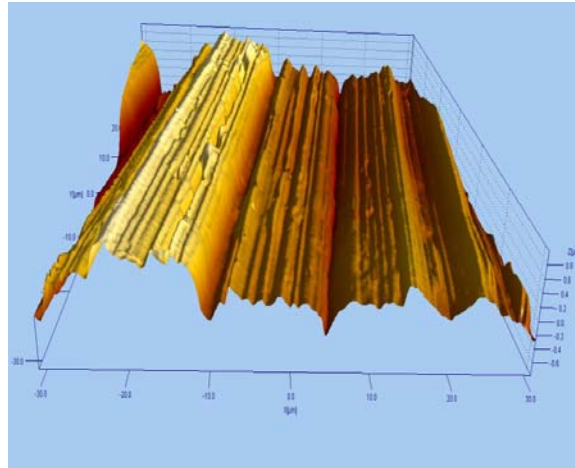
Figure 3.4 Surface topography of Case Study I die sample contact surface obtained by AFM after the tests (Area 62 µm x 62 µm)
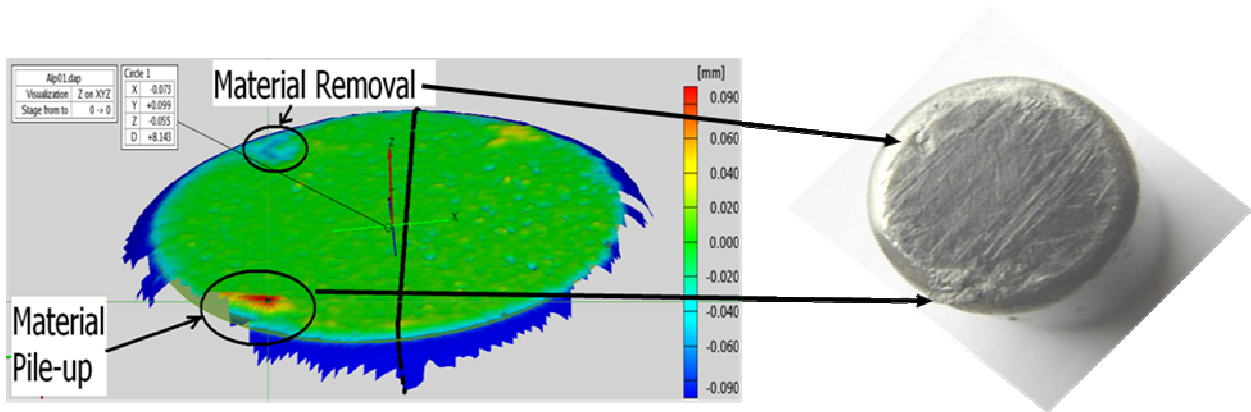
Figure 3.5 3-D image correlation photogrammetry picture of the Case Study II die sample AISI A2 after test
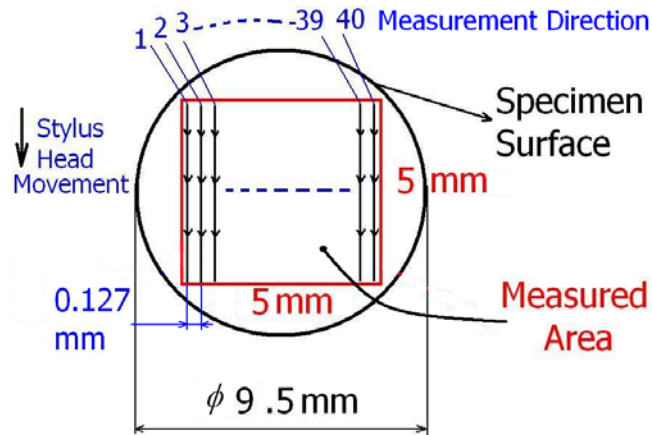
Figure 3.6 Stylus measurement procedure on worn die surface. At least 40 line measurements are taken normal to the sliding direction
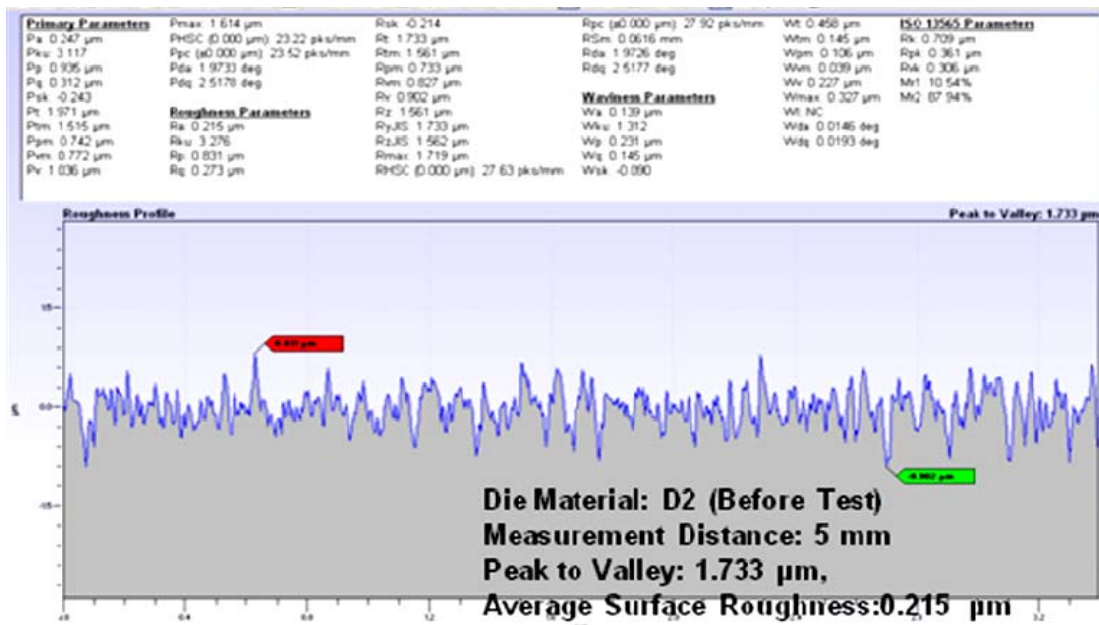
Figure 3.7 Contact type profilometer surface roughness measurement output from TrueMap software for Case Study I die sample (before test)

3.1.3 Test results

3.1.3.1 Results for Case Study I

In the first case, the heat treated D2 tool steel die sample (58 HRC) was tested on three different grades of AHSS sheet blanks; DP 600, DP800, and DP1000, respectively. The goal of these tests were to reveal the capabilities of the test system, hence the same contact pair use was disregarded due to limited sheet blank sources. Total test length was calculated as 2.3 km. The change in surface roughness before and after the tests over the die sample contact surface was relatively small compared to Case II as given in Table 3.4. During Case I tests, no galling was observed on the die sample surface. A 3-dimensional surface plot obtained by the stylus line measurements before and after tests is presented in Figure 3.8. The machining/polishing traces prior to wear test were still present on the contact surface after the test, in addition to sliding wear tracks as could be seen in SEM (Scanning Electron Microscope) picture of AISI D2 die sample given in Figure 3.9.

(a)   (b)
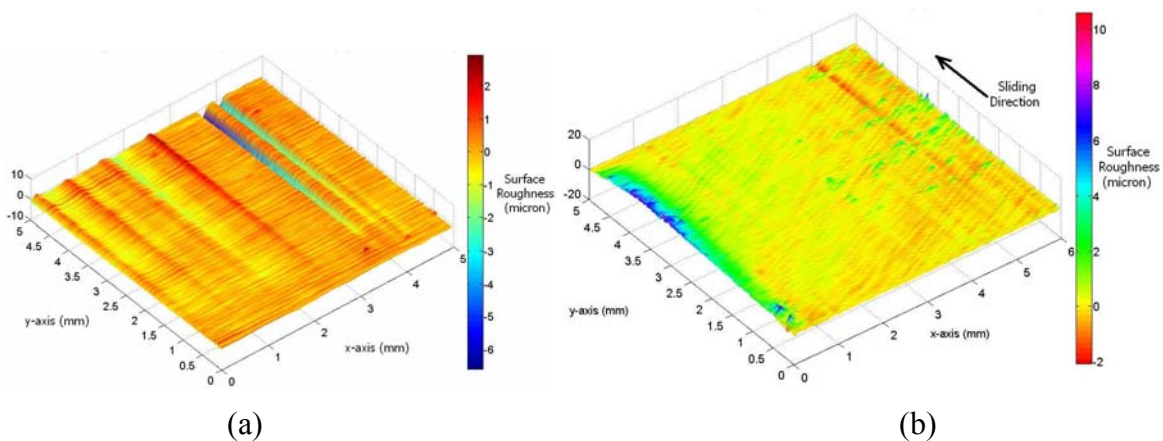
Figure 3.8 Surface topography for heat treated D2 die sample surface (a) before test with an R_a of 0.216 μm, (b) after test with an Ra of 0.270 μm (note to the differences in scales)

64
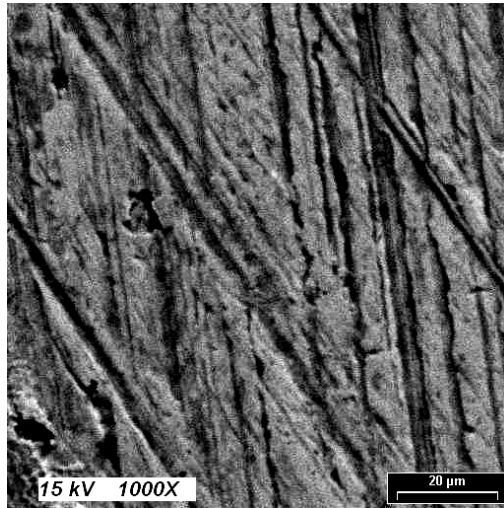
Figure 3.9 SEM picture of AISI D2 specimen after 2.3 km test

3.1.3.2 Results for Case Study II

In order to validate the proposed test method, another extreme contact condition; soft die-soft sheet metal contact pair was tested. Die material was made of non-heat treated A2 tool steel with a relatively low hardness of 18 HRC. After 1 km of testing, some galling marks on the contact surface were observed and the test was stopped. As usually observed, it started with the material transfer from the sheet blank to the die sample surface during the test. The material transfer mechanism that occurred is believed to be cold welding. The lumps are grown with the time and start to scratch the sheet blank/workpiece. Strong weld sometimes causes the lumps to be broken off from the die sample surface as well as continuous pile-up of sheet material. The surface roughness measurements showed that surface topography changed significantly when Figure 3.10 is examined carefully. Material transfer from sheet blank to die sample can be clearly seen in SEM picture of the die sample in Figure 3.11.

65

(a)   *(b)*
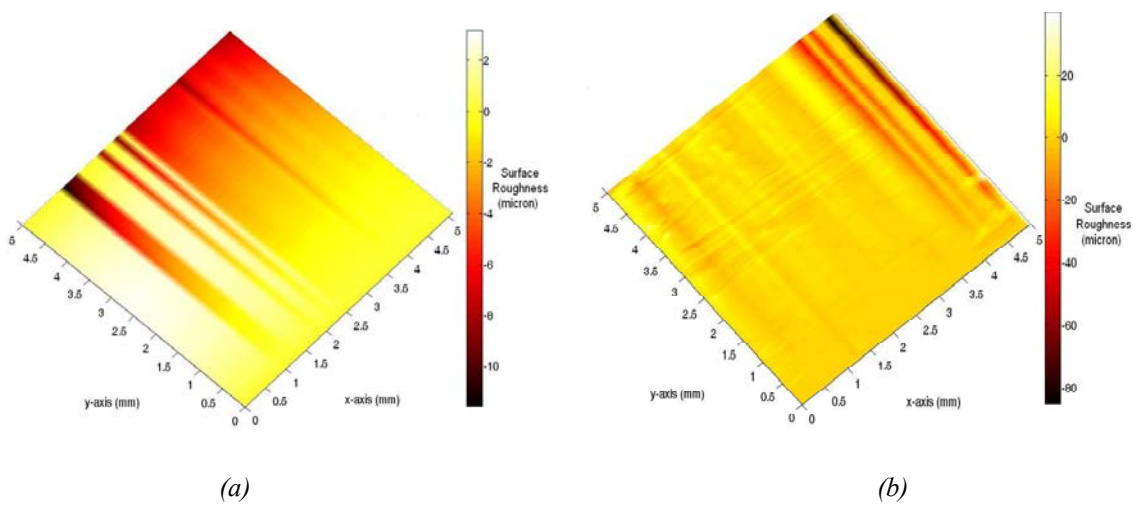
Figure 3.10 Surface topography for non-heat treated A2 die sample surface (a) before test where Ra is around 0.064 μm , (b) after test where Ra is around 0.722 μm (note to the differences in the scales)
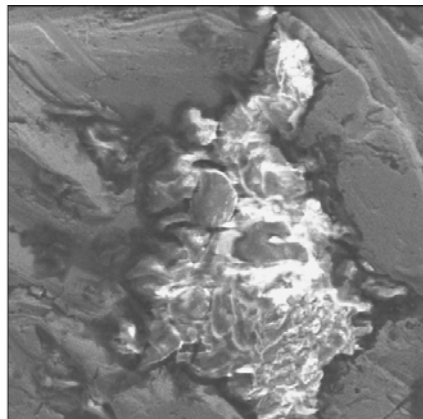
Figure 3.11 Piled-up sheet blank material (shiny sections) on the non-heat treated AISI A2 die sample contact surface after test

3.1.4 Discussion on proof-of-concept tests

Two material pairs with relatively distinct mechanical properties were tested in this study, the results were considerably different. In order to make a reasonable comparison between

these two cases, the specific wear rate (k) was used. For the second case (soft-soft pair), although the total sweeping (contact length) was almost half of that for the first case, severe wear formation including galling was observed, and this was verified through the comparison of specific wear rate values as shown in Table 3.4. The specific wear rate for the second case is almost 100 times greater than that of the first case (hard-hard pair). It is not practical to use such kind of soft die- soft sheet material pair in real stamping operations since in the industrial practice the upper limit of specific wear rate for engineering sliding surfaces is accepted to be around $1x10^{-6}$ $mm^3/N.m$ (5 times less than that of case 2). Nevertheless, it was found that the developed wear test method and device was able to handle both cases with rapidity and with reasonable accuracy.

Table 3.4 Specific wear rates for tested die samples

Die Sample	Specific Wear Rate ($mm^3/N.m$)
Heat Treated D2 (58-60 HRC)	$5.64x10^{-8}$
Non Heat Treated A2 (18 HRC)	$5.11x10^{-6}$

3.1.5 Conclusions on the phase 1 proof-of-concept experiments

The proposed wear testing method was validated based on the 1st generation test device as described in the previous section. It was demonstrated that the test method has the ability to handle extreme contact conditions, which were hard-hard and soft-soft contact pair in this case. For the first case (Case I), a conventional, commonly used die material AISI D2 was tested on advanced high strength steel grades (DP 600, 800 and

1000). Although the load level was not as high as in stamping operations, the wear obtained was in the acceptable limits. In the second case (Case II), relatively softer (non heat treated) die sample AISI A2 was tested on widespread used cold rolled AISI 1008 sheet blanks. The reason to choose this kind of contact pair was to verify the suitability of the proposed test setup for and lower material hardness oriented applications.

In the next phase of this study, we will focus on verifying the wear test method by testing the material pairs under higher contact stress conditions by means of samples with smaller contact areas.

3.2 Testing Alternative Die Materials with 1st Generation Robot-based Die Wear Test Setup[1]

To authenticate the proposed wear test method and device, seven (7) different contact pairs with industrial relevance were tested in this section as tabulated in Table 3.6. For this section, the bullet-type uncoated die samples, given in Figure 3.12, were used. Figure 3.13 shows the actual die sample shape and SEM photo of the tip. During the experiments, a normal load of 220 N (average) was applied, and the corresponding average and maximum contact stresses were calculated to be 1.5 and 2 GPa respectively according to Hertzian contact stress theory. A sample calculation is given in Appendix A. Contact stresses experienced on the die samples were in agreement with the reported values available in

literature [Eriksen, 1997; Pereira et al., 2008; Klocke et al., 2006]. All die specimens were tested along a 2 km track distance to achieve significant amount of wear. Sliding speed was selected as 0.3 m/s based on the industrial practice range and reported values in the literature also [van der Heide et al., 2001, 2006; Klocke et al., 2006]. For replication purposes, first, three Caldie samples were tested. Upon obtaining a good repeatability, single tests were performed for other die material cases die to limitations on sheet blank and die samples. Hot-dip galvaannealed (HDGA) DP 600 grade AHSS sheet blanks were used in all seven test cases. The sheet blank dimensions were 330x330x1 mm. The typical chemical composition of DP 600 is given in Table 3.5. Average hardness value for sheet blanks (DP 600) was measured as 84 HRB (Rockwell Hardness Scale B with 100 kg.f indentation load) and 201 HV_1 (micro Vickers hardness with 1kg load).
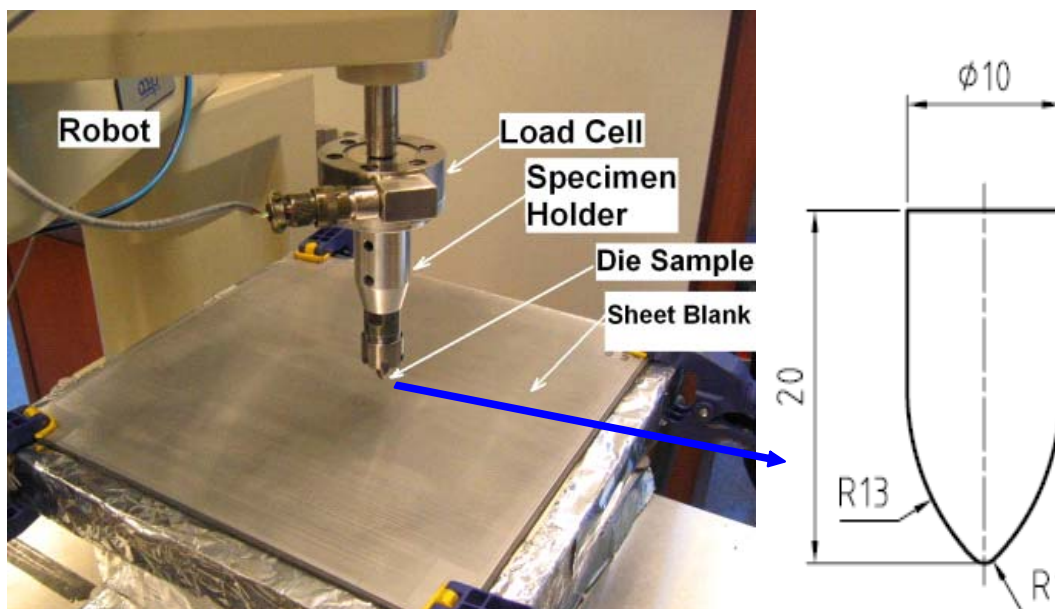
Figure 3.12 Developed robot-based die wear test system, and the bullet-type die sample configuration
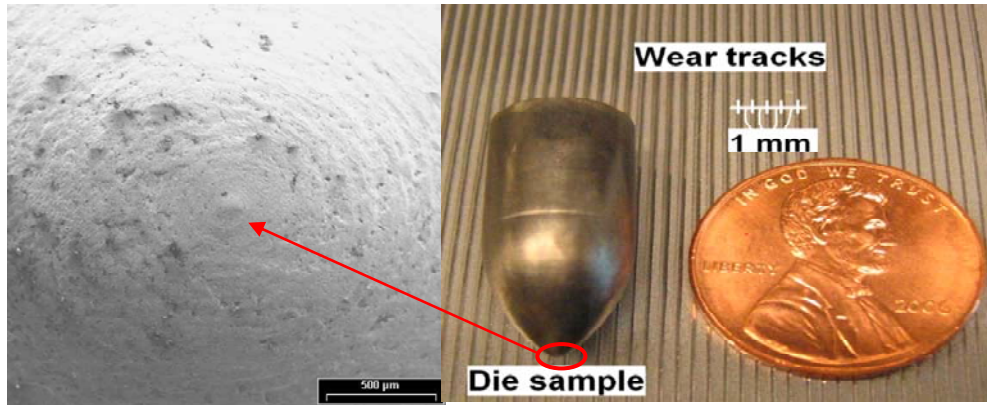
Figure 3.13 Actual die sample view and SEM view of its tip before tests

Table 3.5 Typical chemical composition of DP 600 steel sheet blanks [*Cuddy et al., 2005*]

Material Grade	Chemical Composition					
	C	Mn	Si	Al	S	P
DP 600	0.106	0.800	0.310	0.044	0.005	0.01

3.2.1 Description of seven (7) die materials used in the experiments

Seven (7) different die materials were tested to compare their wear resistance. None of them had coating or any surface conditioning other than the heat treatment as suggested by their respective suppliers as explained later. AISI D2 is a chromium-molybdenum-vanadium alloyed conventional tool steel. Although it has been used in several forming operations for many years, it is considered not to be an appropriate choice for AHSS

stamping since its chipping and cracking performance is insufficient in long-run productions. It was included in this study as a base material for comparison purposes. Vanadis 4 Extra is chromium-molybdenum vanadium alloyed powder metallurgical cold work tool steel characterized by high abrasive-adhesive wear resistance and very good ductility. Vancron 40 is a Cr-Mo-W-V-N alloyed powder metallurgical cold work tool steel that provides an excellent combination of galling resistance and adhesive wear resistance. Caldie is a chromium-molybdenum-vanadium alloyed tool steel, and characterized for its good wear resistance and very good chipping and cracking resistance. It is suitable for short to medium run tooling. Caldie is preferred when surface coating is necessary since it is a very successful substrate steel. K340 Isodur is a cold work tool steel with a uniquely balanced chemical composition for stamping, cutting and forming operations. The high yield strength and excellent toughness characteristics makes this tool steel a good choice for applications where chipping or premature wear is a problem. Carmo is a high-strength, flame-, induction- and through hardening cold work tool steel [Böhler-Uddeholm Product Specification Sheets, 2009]. 0050A (SAE J435) cast steel is one of the alternative and cost-effective die materials being considered in the automotive industry [Steel Casting Handbook, 1999; Automotive Steel Design Manual, 2002; Metals Handbook, 1990]. All the tested materials are used for some selected, trial-purpose cases in the automotive industry. Caldie is used in trim dies, and Carmo in the draw punches for stampings used in the Ford 500 and Freestyle models [Kuvin, 2006]. 0050A cast steel material is used as a body-side die material for the Daimler-Chrysler PT production line

71

[Bay Cast Inc., 2009]. Typical chemical compositions and some mechanical properties of the tested materials are presented in Table 3.6.

Die materials were machined to the dimensions given in Figure 3.12 by means of CNC turning. It was not possible to take surface roughness measurements (with a contact type profilometer) before the tests on samples' tips since the contact surface areas were too small. Measurements on the lateral surfaces of the samples resulted in the average surface roughness value of 0.03 μm or less. All die samples were heat treated according to the suggestions by the suppliers and the resulting hardness values compared with the suggested values in Figure 3.14. Error bars denote the range of suggested hardness values for the materials by their providers. Except Caldie, all the die samples have attained the suggested hardness levels before wear tests. Failing to achieve the suggested hardness value for Caldie resulted in considerable performance loss as it will be discussed in results section.

Table 3.6 Chemical compositions and some mechanical properties of the tested die materials [*Böhler-Uddeholm Product Specification Sheets, 2009; Steel Casting Handbook, 1999; Automotive Steel Design Manual, 2002; Metals Handbook, 1990; Miller; 2009*]

Die Materials	C	Cr	Mo	Mn	V	Si	N	W
D2	1.55	11.8	0.8	0.4	0.8	0.3		
Vanadis 4	1.4	4.7	3.5	0.4	3.7	0.4		
Vancron 40	1.1	4.5	3.2	0.4	8.5	0.5	1.8	3.7
Caldie	0.7	5	2.3	0.5	0.5	0.2		
K340 Isodur	1.1	8.3	2.1	0.4	0.5	0.9		
Carmo	0.6	4.5	0.5	0.8	0.2	0.35		
0050A	0.4			0.5				

Die Materials	Density (kg/m³)	Young's Modulus (GPa)	Yield Strength, R_p, (MPa)	Tensile Strength R_m (MPa)	Compressive Yield Strength $Rc_{0.2}$ (MPa)
D2	7610	210			2200
Vanadis 4	7700	206	2140	2480	2480
Vancron 40	7820	209			2500
Caldie	7700	213			2230
K340 Isodur	7680	210			
Carmo	7700		670	870	
0050A	7800	214-217	310 - 415	586 - 787	
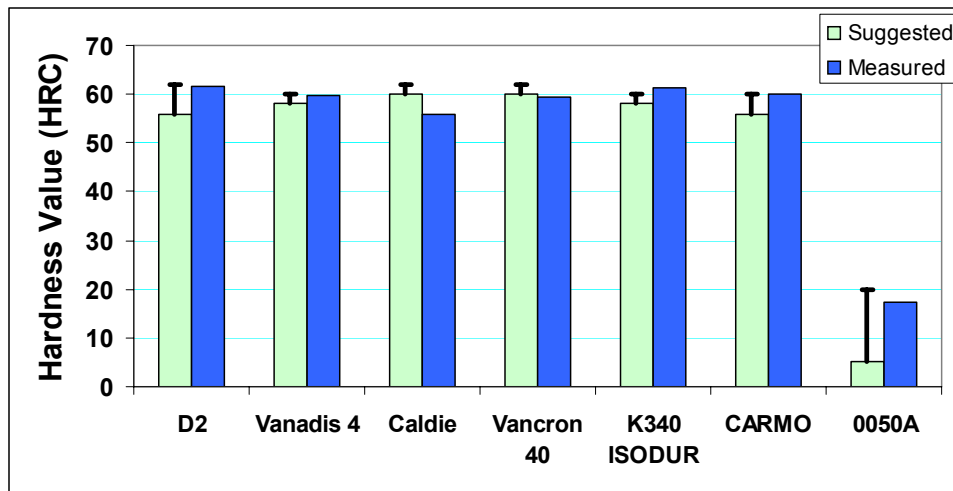
Figure 3.14 Suggested [*Böhler-Uddeholm Product Specification Sheets, 2009; Steel Casting Handbook, 1999; Automotive Steel Design Manual, 2002; Metals Handbook, 1990*] and measured hardness values for tested die materials

3.2.2 Experimental results

3.2.2.1 Micrographs and 3-D Surface Mapping

Microscopic examination procedure applied for every die sample before and after tests. Figures 3.15-3.21 present the after-test die sample microscopic observations, and 3-D surface topography, which were obtained by combining the regularly spaced line surface roughness measurements. In the same figures, directions for sliding and stylus

measurements are shown with dashed red and solid blue arrows, respectively. Due to restrictions in stylus measurements, plotted area is rectangular instead of original circular shape.
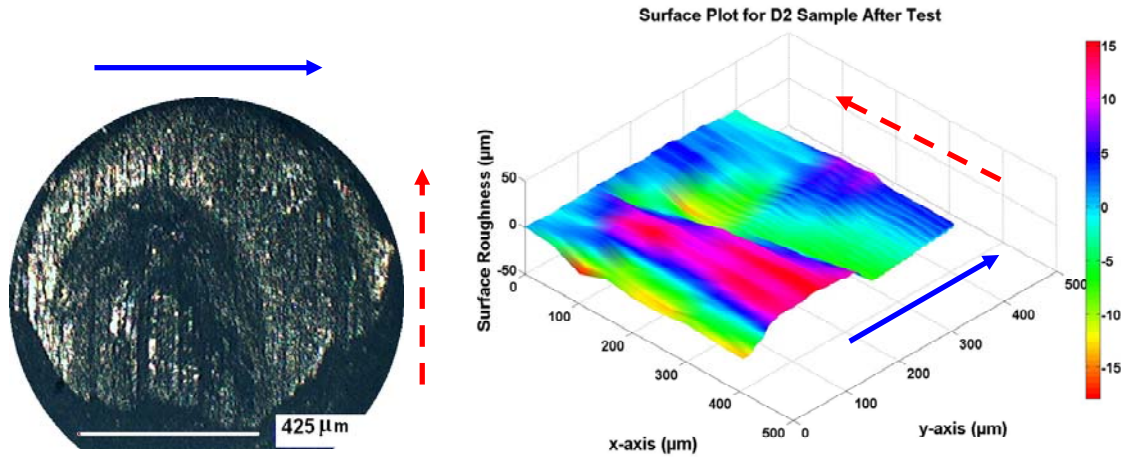
Figure 3.15 Micrograph and surface map for D2 specimen after test
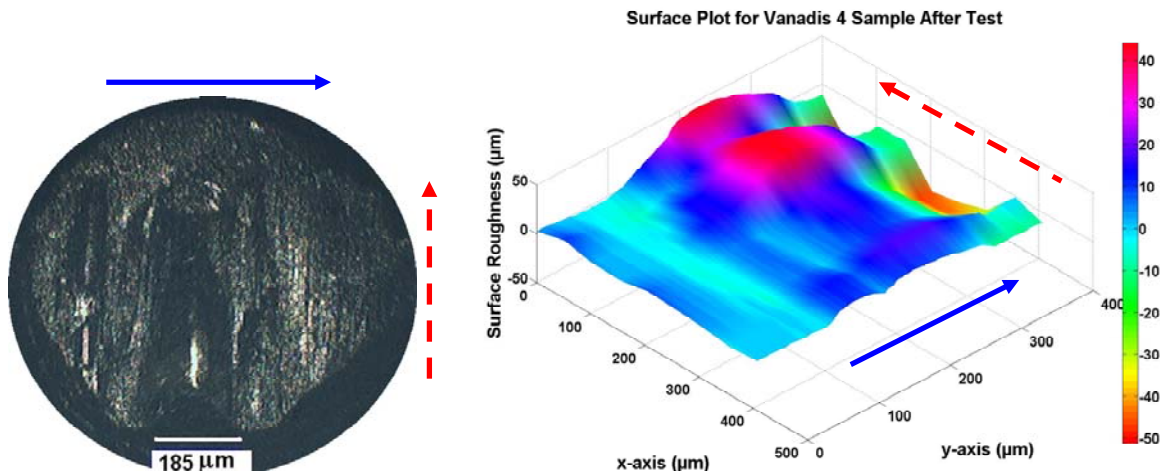
Figure 3.16 Micrograph and surface map for Vanadis 4 Extra after test
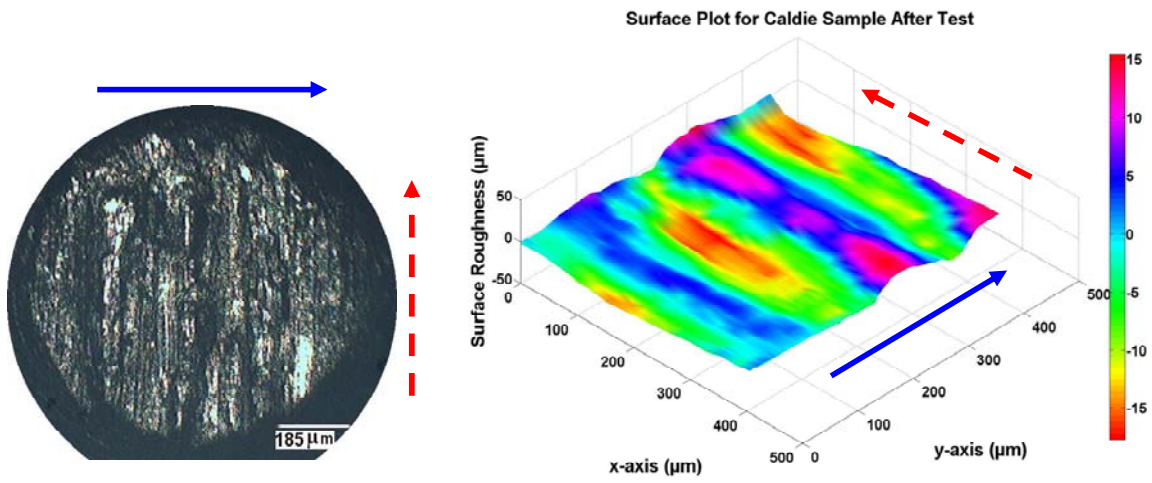
Figure 3.17 Micrograph and surface map for Caldie specimen after test
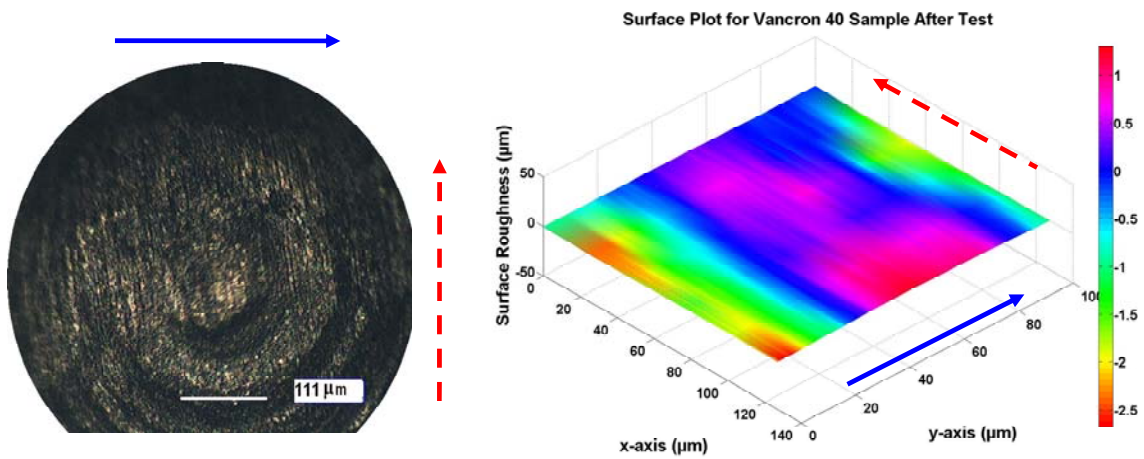
Figure 3.18 Micrograph and surface map for Vancron 40 after test
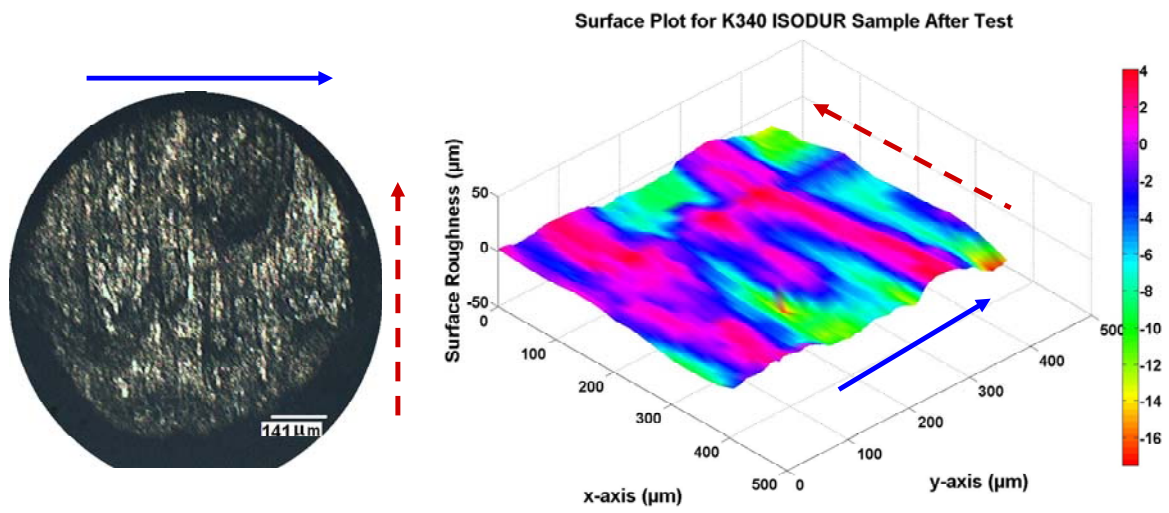
Figure 3.19 Micrograph and surface map for K340 after test
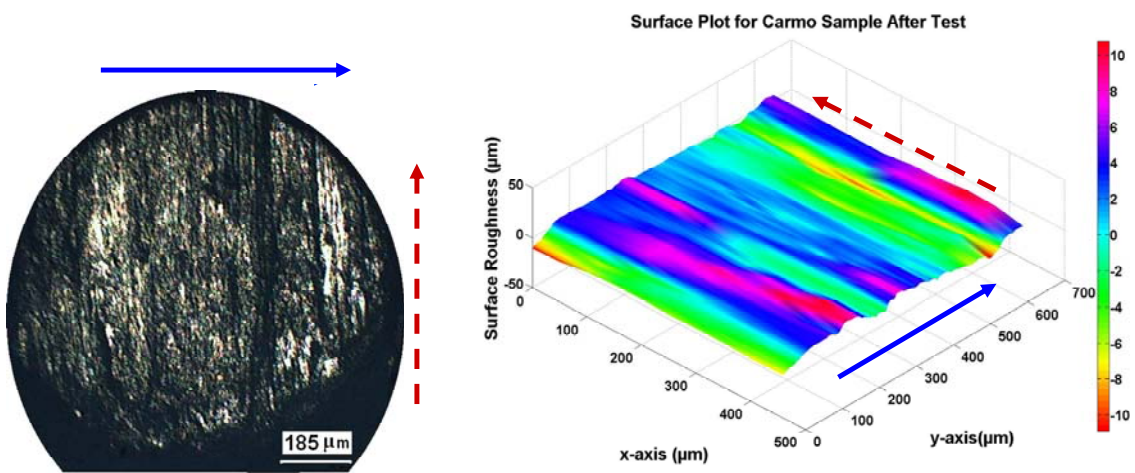
Figure 3.20 Micrograph and surface map for Carmo after test
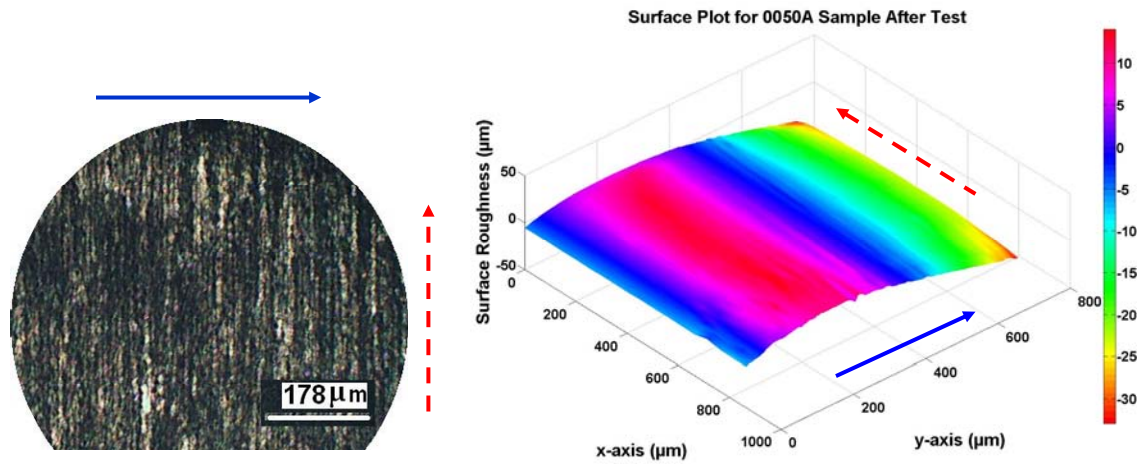
Figure 3.21 Micrograph and surface map for 0050A Cast Steel after test

3.2.3. Surface roughness measurements

3.2.3.1 Stylus Measurements for Average Surface Roughness (R_a)

After each wear test, contact surfaces of all die samples were measured with a contacting stylus type profilometer (Ambios XP-1, high resolution surface profiler). Since the contact surface area was too small (~Ø1 mm), a limited number of measurements could be taken. Measurements were taken along a direction normal to the sliding direction which was followed during the test. Schematic representation of the measurement procedure is presented in Figure 3.22. An average surface roughness value was calculated by averaging the line surface roughness values measured. Average surface roughness values (R_a) for each die sample are plotted in Figure 3.23. Vancron 40 performed the best; its average surface roughness (R_a) is 0.031 μm with a minimum variation, whereas R_a for D2 is 0.292 μm, which is the worst in terms of the R_a comparisons. Interestingly, 0050A (die cast material) has a lower average surface roughness value when compared to D2 and some

77

other specially alloyed and expensive tool materials although it experienced significant mass loss as will be discussed later. Surface roughness differences between Carmo and 0050A samples can easily be distinguished when 3-D optical profilometer pictures given in Figure 3.24 and the values in Figure 3.23 are assessed together.

(a)   (b)
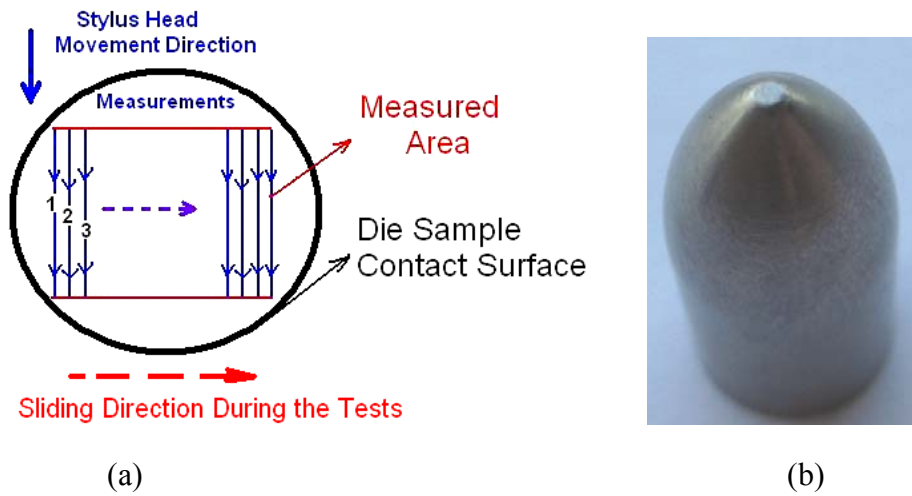
Figure 3.22 (a) Surface roughness measurement procedure with stylus, (b) Typical view of die sample after test (note the flattened/worn tip)
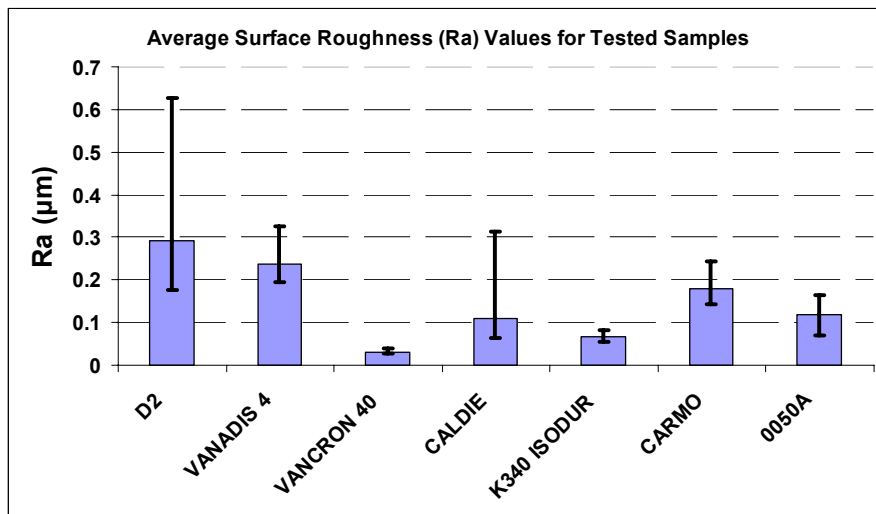
Figure 3.23 Average surface roughness values (Ra) after tests for each tested material

D'Agostino and Pearson omnibus normality test using Prism software v.5 revealed that the surface roughness data obtained for AISI D2 and Caldie, in which big surface roughness variations were seen as given in Figure 3.23, samples were not in Gaussian distribution form. Varying number of contact roughness measurements (6-18 measurements) was taken on the sample surfaces depending on the contact area. The number of data (6 measurements) taken for Vancron 40 was not enough to perform normality test. Average surface roughness data for other samples passed the normality test with not significant P values. The average surface roughness data, then, were subjected to one-way ANOVA analysis assuming non-Gaussian data distribution and using non-parametric Kruskal-Wallis test. The results showed that medians varied significantly (P<0.005).

3.2.3.2 Surface Area Roughness Measurements

Apart from the line average surface roughness (R_a) measurements with contact type of profilometer, some surface area roughness measurements (S_a, S_q, S_{sk}, S_{ku}), which are more informative over the complete 3-D surface texture, were also obtained for some die samples after the tests (Figure 3.24 and Figure 3.25). In these measurements, results were obtained by non-contact, 3-D optical profilometers (Nanovea 3-D Profilometer, MicroPhotonics Inc., CA, USA; and MicroXAM white light interferometer, KLA-Tencor Corp., CA, USA). Average roughness in 3-D (S_a), root-mean-square roughness in 3-D (S_q), skewness (S_{sk}), kurtosis (S_{ku}) are given for some of the tested samples in Table 3.7.

79

<div align="center">a)   b)</div>
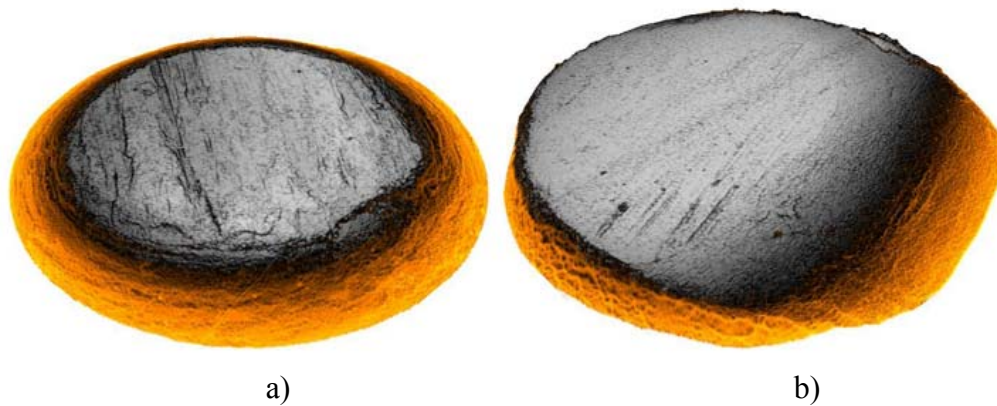
Figure 3.24 3-D optical profilometer pictures of Carmo (on the left) and cast steel 0050A (on the right) samples (with Nanovea 3-D Profilometer, MicroPhotonics Inc., CA, USA)

Table 3.7: 3-D surface roughness parameters for some of the tested samples

Die Sample	S_a (μm)	S_q (μm)	S_{sk}	S_{ku}
D2	5.98	7.47	0.179	2.79
Vancron 40	0.878	1.144	-0.15	3.51
Carmo	3.26	4.11	0.118	3.02
0050A	0.722	1.05	1.58	48.3

Since R_a measurements neither make a distinction between peaks and valleys nor provide information about the surface spatially; S_a and S_q are frequently used to characterize the texture. S_a is preferred for machined surfaces while S_q is used for optical surfaces. When Table 3.7 is examined with Figure 3.23; it is seen that S_a and S_q values for cast steel sample 0050A are lower than the ones for Vancron 40, which was not the case when the R_a values of those samples are compared. S_{sk} is defined as the degree of symmetry of the surface heights about the mean plane and its sign determines the dominance of peaks (i.e. $S_{sk}>0$) or valleys (i.e. $S_{sk} <0$) over the surface. The negative S_{sk} value for Vancron 40

sample indicates the presence of the valleys which can be noticed around the center point of the surface given in Figure 3.25.b. Contrary to Vancron 40, D2 sample has a skewness value with a positive sign designating the peaks which can be visible in Figure 3.25.a. S_{ku} points out the degree of peakedness of a surface height distribution or existence of disorderly high peaks or deep valleys. In case of presence of high peaks and deep valleys, its value is greater than 3, otherwise it is less than 3. S_{ku} value given in Table 3.7 and Figure 3.24.b undoubtedly clarify that the cast steel sample has inordinately high peaks due to excessive shape deformation on the contact surface.

(a)   (b)
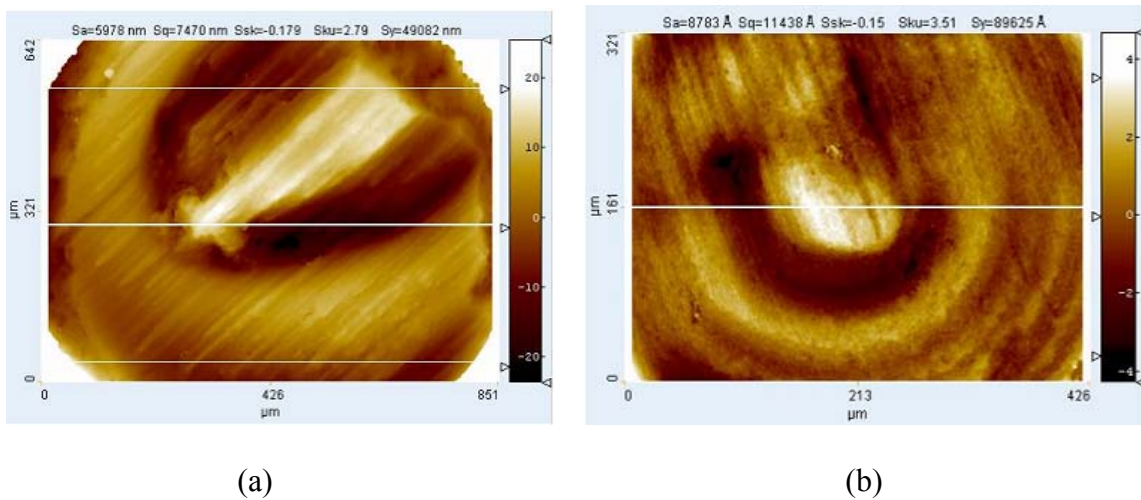
Figure 3.25 White light interferometer photo of (a) D2, and (b) Vancron 40 specimens with MicroXAM (provided by KLA-Tencor Corp., CA, USA)

3.2.4. Specific wear rates

Several parameters were developed to quantify the wear performances of materials [van der Heide et al., 2006; Meng, and Ludema, 1995]. Two of the widely used parameters to compare the wear performance of the materials are wear coefficient and specific wear rate. Coefficient of wear is rather irrelevant in tool wear studies since it includes a variable

workpiece hardness parameter [Holmberg, 2005]. Thus, specific wear rate is more preferred and was given in Eq.1 in Chapter I. The specific wear rates for each tested die sample are tabulated in Table 3.8. Similarly Figure 3.26 illustrates the specific wear rate values for tested die samples, respectively. Since the mass losses are measured after the tests, the wear volumes are obtained by dividing the mass loss value to the density of each material. Smaller values for specific wear rate means higher wear resistance performance. As it can be observed from the Table 3.8, and Figure 3.26 that Vancron 40 specimen has the highest and 0050A has the lowest performance among the tested materials. Industrial upper limit of specific wear rate for engineering sliding surfaces is accepted to be around 1×10^{-6} mm^3/N.m by some researchers [van der Heide et al., 2006]. As can be seen from the Table 3.8, all the tested materials are well below this limit value.

Table 3.8 Specific wear rates for die materials tested

Material	Specific Wear Rate (mm^3/m.N)
D2	19.62×10^{-8}
Vanadis 4	5.993×10^{-8}
Vancron 40	2.625×10^{-8}
K340 Isodur	6.254×10^{-8}
Carmo	8.922×10^{-8}
0050A	24.592×10^{-8}
Caldie	20.705×10^{-8}
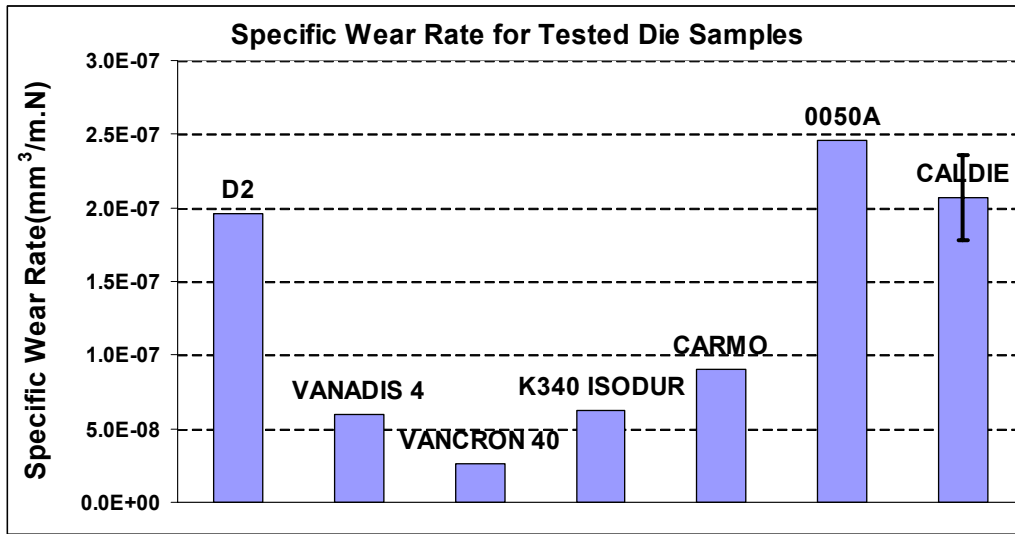
Figure 3.26 Specific wear rates chart for tested materials

3.2.5. Discussion on wear tests of uncoated die samples

This study aimed to investigate the wear performance of seven different die samples under the same contact conditions such as contact stress, sliding speed, and sliding distance. Although the effect of maximum contact pressure and its threshold level for galling [Podgornik et al., 2004; Gåård,et al., 2007, Yan, 2006] were not examined in this study; D2 was the only specimen that galling scars were clearly visible among the tested samples. The highest mass loss was recorded for 0050A cast steel sample, however; no galling effect was observed on its contact surface. Plastic squeezing is thought to be more effective than adhesive wear mechanism for the cast steel sample. In this phenomenon, surface texture change is mainly resulted from the redistribution of material by plastic flow without weight loss [Nilsson et al., 2002]. Relatively higher tip shape deformation occurred on the 0050A tip; consequently the contact surface enlarged and contact stress was lowered. 0050A was the softest material among the tested seven die materials as can

be seen from Figure 3.14. The highest mass loss obtained for 0050A is probably resulted from the relatively close hardness values of die material and sheet blank (87.4 HRB, 203 HV_1 for DP600 sheets, 96 HRB for 0050A cast steel material). This is verified by the average surface roughness value for the 0050A specimen that it was less than that of D2, Vanadis 4 and Caldie samples. The sheet blank surface after 0050A tests was shiny with very shallow scratches. During the tests, wear scars on the sheet surfaces were also observed since those are the reflection of die contact surfaces. For the same force levels, similar wear scars and depths were observed for all tests except for 0050A and K340 Isodur. In some part of the K340 Isodur tests, depth of wear tracks on sheet blank was shallower and the sheet surface was shiny. It is concluded that this material is more prone to material stacking on the surface and coating might be necessary for some cases.

For the Vancron 40 specimen, the wear pattern was almost uniform along the contact surface. Moreover, sliding direction could not be identified due to the lack of direction oriented wear scars (Figure 3.18). Homogeneity in the wear pattern could possibly be resulted from uniform fine particle distribution utilizing powder metallurgy process. Powder type structure contains small particles and has higher degree of regularity in microstructure so that it reduces the risk of galling mechanism which is initiated by micro-welding at the die sample-sheet interface and results in material removal from the die surface. Similar to die wear pattern, chips removed from the sheet surface were in smaller sizes for Vancron 40 with respect to ones in other tests. It is undoubtedly clear that the Vancron 40 die sample, which is a nitrided and wolfram added powder metallurgy tool steel, has the best wear resistance performance among the die samples tested. Similar

84

outstanding performance of Vancron 40 compared to ANSI D2 tool steel has been verified by researchers in academia as well as from industrial experience [Gåård et al, 2007; 2009; Emanuelsson, 2008].

The specific wear rate values for Vanadis 4 extra, K340 Isodur, and Carmo were close to each other (Figure 3.26). Lower performance for Caldie could be due to the fact that the test samples had lower hardness values than the suggested levels by the supplier. Since the hardness is one of the most influencing material related parameters in wear, it can be concluded that the performance of Caldie would have been improved if we had the right samples with the suggested hardness levels; however results are still conformable with the ones available in the literature [Böhler-Uddeholm Product Specification Sheets, 2009; Steel Casting Handbook, 1999; Automotive Steel Design Manual, 2002; Metals Handbook, 1990].

3.3 General Evaluation of 1st Generation Die Wear Test System

The proposed and validated test method can be improved and used in a variety of cases and applications as it has premises of much shorter, rapid and accurate wear characterization. The development and demonstration of this rapid and cost-effective wear test method is expected to offer researchers a variety of opportunities to develop optimized die coating/enhancement methodologies using traditional (such as CVD, PVD, TD, thermo-reactive diffusion-TRD) as well as newer (such as selective laser sintering, laser deposition, laser peening/cladding, burnishing, etc.) techniques for increased tool life and

robust production. Second phase studies also aim to determine the effects of substrate hardness (coated/uncoated), type of coating, and substrate (die) materials.

The distinguished features of the proposed test can be summarized as follows;

1) Tested die specimen is continuously in contact with fresh (virgin) sheet blank surface,

2) It is a very compact apparatus that requires relatively small space and no auxiliary equipment in comparison to other test methods such as strip pulling, draw bead and u-bending tests,

3) Both sides of sheet blanks can be used and this saves test material,

4) It has flexibility to choose die sample configurations such as disks; cylindrical, square specimens can be tested.

5) Regular sheet metal blanks just coming out of steel mills, coated/uncoated sheets and/or die samples can be used; and experiments with different lubricants can be performed,

6) Friction and wear tests at elevated temperatures are possible with the installation of heaters on the periphery of die specimen.

The only drawback for this current test setup is the limitation of the load that can be applied by robot. With the current test system of the 1st generation design and the specified die specimen dimensions as above, low contact stress levels up to 50 MPa can be achieved.

CHAPTER 4

2nd Generation Die Wear Test System and Wear Tests

After successful implementation of the robot-based die wear test system, it was planned to advance the test setup and perform additional tests to investigate the effect of various parameters on wear resistance of die materials. Therefore a CNC (computer numeric control)-based test system was built to offer robustness and higher contact load capability. This chapter covers description of new system and wear test results of numerous coated samples.

4.1 Description of 2nd Generation Die Wear Test System (CNC-based Wear Test System)

The CNC-based die wear test system is based on the use of precise and controlled motion of a vertical machining center (HAAS VF-3 CNC)'s x-, y- and z-axes and spindle (no rotation). A load sensor was mounted on the spindle through a holder which also houses the die sample of interest. AHSS sheet blanks are laid on the x-y table with clamps at four corners as can be seen in Figure 4.1. The CNC machine was programmed for the precise pressing of die sample and one-way scratching/sweeping on the AHSS sheet blank. Bullet-form die samples with dimensions shown in Figure 3.12 and 3.13 were used in wear

tests. Normal and shear forces occurring at the die and blank interface were measured during the tests by means of SlimLine sensors model # 9134B21 and 9144B21 from KISTLER (Kistler Instrument Corp., Amherst, NY, USA). Signals obtained by sensors are amplified by an industrial charge amplifier and transmitted to data acquisition card DAQCard-6024E through CB-68LP connector block (both are products of National Instruments Corp., Austin, TX, USA). Sampling rate during the data acquisition was selected as 10 Hz, and data is stored in a PC installed next to the test setup using Labview v.7.0 software (National Instruments Corp., Austin, TX, USA). The Labview code flow-chart used to store load sensor data is given in Appendix B.
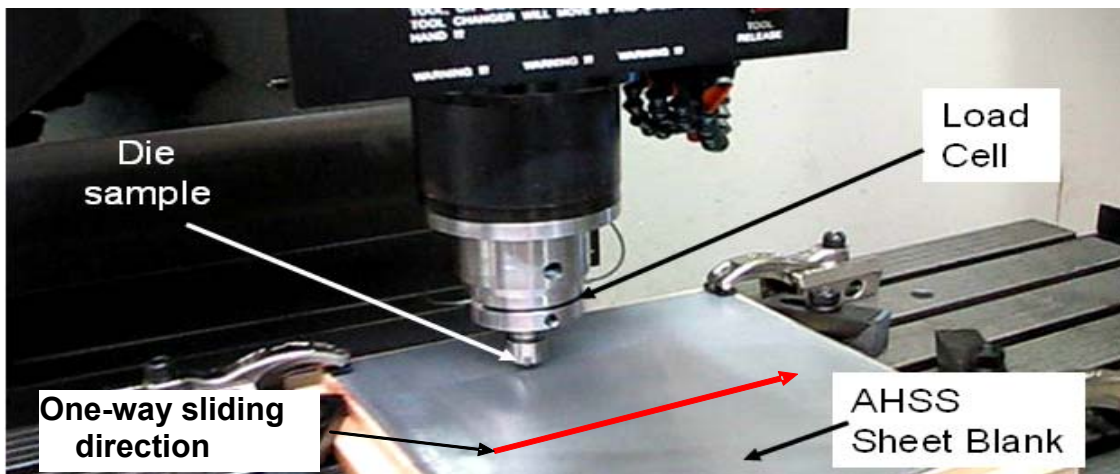
Figure 4.1 2nd generation die wear test system

4.2 Die Wear Experiments and Experimental Conditions with the CNC-based Wear Test System

In order to investigate the effect of different parameters on die wear, an experimentation plan is prepared in collaboration with project partner companies including Daido Steel Co., (Japan) , International Mold Steel Inc. (Kentucky, USA), and General Motors as tabulated in Table 4.1. Different substrate materials with specific hardness values, different coating types were tested according the test plan. The main parameters investigated were effect of substrate hardness without coating (samples 1-3), effect of substrate hardness for coated specimens (samples 4-6), effect of coating type (samples 5-9), and effect of substrate material for coated samples (samples 10-12). Each test condition is further described in Table 4.1, and was intended to be repeated three (3) times. However; since the test matrix was relatively large and required a large amount of sheet blanks and since we were limited in terms of the materials provided, some die samples were not tested on the same type of sheet blank. Hence, the entire experiment matrix was divided into several small groups that the same type of sheet blank provided by the same supplier was used in each of those small group tests. Nevertheless, testing of the entire matrix took more than one year, and each group of tests were conducted in very close proximity of time reducing the effect of environmental variables such as seasonal temperature changes, machine settings, etc. Therefore, analyses of small group of tests will be reviewed separately and similar ones will be compared at the end of these analyses under the general discussion part.

Table 4.1 Experimental Plan with 2nd Generation Die Wear Test System

No.	Grade	Hardness (HRC)	Coating	Remarks
1		58-60		
2		60-62	Non-coated	Prepared by IMS
3		62-64		
4		58-60		
5	DC53	60-62	TD coating	
6		62-64		
7		60-62	Radical nitriding +TiCN (PVD)	
8		60-62	TiCN (PVD)	Prepared by Daido
9		60-62	TiC (CVD)	
10	SKD11	58-60	TD	
11	DRM3	64-66	TD	
12	DRM51	62-64	TD	

4.3 Description of Tested Coating Types

As can be seen from the Table 4.1, the test plan includes different coatings including Thermal Diffusion (TD), Chemical Vapor Deposition (CVD), Physical Vapor Deposition (PVD), and radical nitriding + physical vapor deposition. Coatings are used to reduce the friction between contacting parts, increase the chemical and impact resistance and thus lower the shear forces that leads to wear. They are applied onto the substrate which is to be protected in micron level thicknesses. Coating process can either be performed in high temperature as in TD and CVD or low temperature as in PVD coating applications. All the material preparation and coating applications were performed by Daido Steel Co., Japan. The following section provides brief information on the coating types tested in this study.

4.3.1 Chemical vapor deposition (CVD)

Chemical vapor deposition is described as the deposition of a solid on a heated surface by means of a chemical reaction from the vapor or gas phase [ASM Metals Handbook, 1996]. It is preferred when a very uniform coating is necessary and it provides hardness, wear and corrosion resistance. It is appropriate kind of coating for inner side of very deep holes.

Application of CVD coating require high temperatures (800-1100 ºC) to initiate the chemical reaction which limits the choices for substrate material. Since the application temperature is high, hardening and tempering should be performed to restore the desired mechanical properties. Multiple layers and different compounds such as chromium carbide (CrC), silicon carbide (SiC), titanium diboride (TiB_2), alumina (Al_2O_3), diamond-like carbon (DLC) as well as Titanium carbide (TiC), titanium nitride (TiN), and titanium carbonitride (TiCN) can be deposited onto metal surface via CVD technique.

4.3.2 Thermal diffusion (TD)

Thermal diffusion is another type of high temperature coating that metal carbides (mostly vanadium carbide) are produced on the surface of carbon containing substrate materials via diffusion mechanism in a furnace containing a molten salt. It is also known as thermo-reactive diffusion or Toyota diffusion, and consists of several stages such as pre-heating, coating, ultrasonic cleaning, heat treating and post-coating polishing. Vanadium carbide coating offers higher hardness compared to PVD and CVD coatings.

Figure 4.2 symbolizes the carbide layer formation in TD coating process. Atoms or ions of carbon constituents dispersed in the salt bath combine with the carbon atoms available in the substrate material, and then form the carbide layer on the substrate surface. Afterward, the carbide layer is expanded by reaction between the carbon atoms and the carbide constituents on the formed layer by continuous supply of carbon atoms from the substrate [Teikuro TRD, 2009].
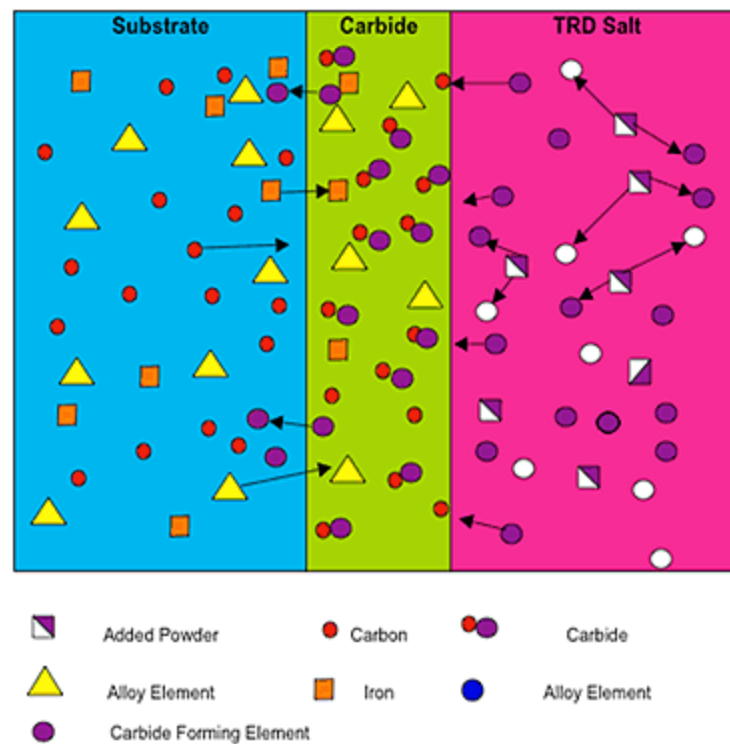
Figure 4.2 Carbide layer formation on a carbon containing substrate in TD coating process [*Teikuro TRD, 2009*]

4.3.3 Physical vapor deposition (PVD)

In this process, various metal ions are positively charged and exposed to reaction with gas ions that are introduced into a vacuum chamber in order to create various coating compositions. The parts to be coated are negatively charged to attract the positively charged ions. Unlike the CVD process, physical vapor deposition takes place at relatively lower temperatures (200-550°C) under vacuum conditions. As a rule of thumb, the annealing temperature of the steel material to be coated must be higher than the coating temperature. TiN is the most deposited type of PVD in industrial applications.

4.3.4 Mechanical and physical properties of coatings

Metal forming processes need wear resistant tool coatings with special qualities such as sufficient hardness, ductility, high compressive strength, and coating thickness,. Although these properties vary depending on the coating process applied, chemical compositions used, typical properties for the coatings type used in this study are summarized in Table 4.2. Hardness values are given in micro-Vickers scale using 50 gf of loading. Corresponding hardness values for these hard type of coatings are in 20-30 GPa levels [Holmberg et. al, 2009].

Table 4.2 Typical physical and mechanical properties for coatings [*After Holleck, 1986; Janoss, 2008, Teikuro TRD, 2009*]

Coating	Density (g/cm^3)	Elastic Modulus (GPa)	Hardness (HV)	Typical Thickness (μm)
TiC (CVD)	4.93	450-470	2800-3300	6-10
TiN (PVD)	5.4	250-590	2100-2900	3-5
VC (TD)	5.41	430	2900-3500	3-10

Coating prices are determined by several factors such as number and/or weight of parts to be coated, pre and post treatments (coating removal, surface finishing, heat treatment). It was reported that CVD coating is approximately 50 percent more expensive than PVD. The high temperatures involved imply pre- and post-hardening and continuous checking of tolerances, which increases substantially the global cost (up to 3-4 times that of PVD) [Lebau, 2003].

4.4. Test Group I: Effect of Substrate Hardness on Wear Performance

In this test group, die samples numbered with 4, 5, and 6 were tested to understand the effect of substrate hardness on the wear characteristics and their comparisons to commonly used AISI D2 and newly developed, high-end die material of Vancron 40 samples. Two (2) samples were tested for both D2 and Vancron 40 die materials. Samples 4-6 were DC-53 die materials with different substrate hardness values ranging from 58 to 64, and all were TD coated, while AISI D2 and Vancron 40 samples were uncoated. Table 4.3 shows the information for the tested die samples. Chemical composition of DC 53 is given in Table 4.4 whereas the same for AISI D2 and Vancron 40 was given in Table 3.6.

Hot-dip galvaanealed DP 600 sheet blanks with 1.4 mm nominal thickness provided by US Steel were used in this Group I tests. Surface roughness (R_a) value for the sheet blanks was measured as 0.25 without any significant variations for both directions in parallel and normal to the rolling direction.

Table 4.3 Substrate hardness and coating specifications for Group I Tests

Sample List #	Substrate Material + Coating Type	Substrate Hardness (HRC)
4-1	DC 53 Sample + TD Coating	58-60
5-1	DC 53 Sample + TD Coating	60-62
6-1	DC 53 Sample + TD Coating	62-64
	AISI D2 #1 AISI D2 #2	62 61
	VANCRON 40 #1 VANCRON 40 #2	60 59

Table 4.4 Chemical composition of DC 53

Substrate	C	Si	Mn	Cr	Mo	V
DC 53	0.96	0.91	0.37	8.1	2	0.26

A total of seven (7) samples were tested, each, along a length of 2km under 200N average contact normal load and with a sliding speed of 0.33m/s. For 2km of wear testing, approximately 2.29 m^2 (~24.6 ft^2) of sheet blank area was needed. Similar surface cleaning procedures were applied before and/or after the tests as explained in Chapter 3.

The calculated specific wear rates are shown in Figure 4.3 for all Group I test cases. Average values and variations for AISI D2 and Vancron 40 samples are also shown in this figure. As expected, coated samples showed higher wear resistance compared to uncoated samples of AISI D2 and Vancron 40. Different from the previous set of tests performed with 1[st]st generation test system, the performances of AISI D2 and Vancron 40 were not distinct from each other. Performances for the coated samples were in close proximity; DC53 sample with 60-62 (Sample # 5-1) substrate hardness was ahead by a neck compared to other two samples' performances, though. Since the coatings were not failed from the substrates entirely, as in scratch tests, it is difficult to evaluate the effect of substrate hardness on anti-wear performance.
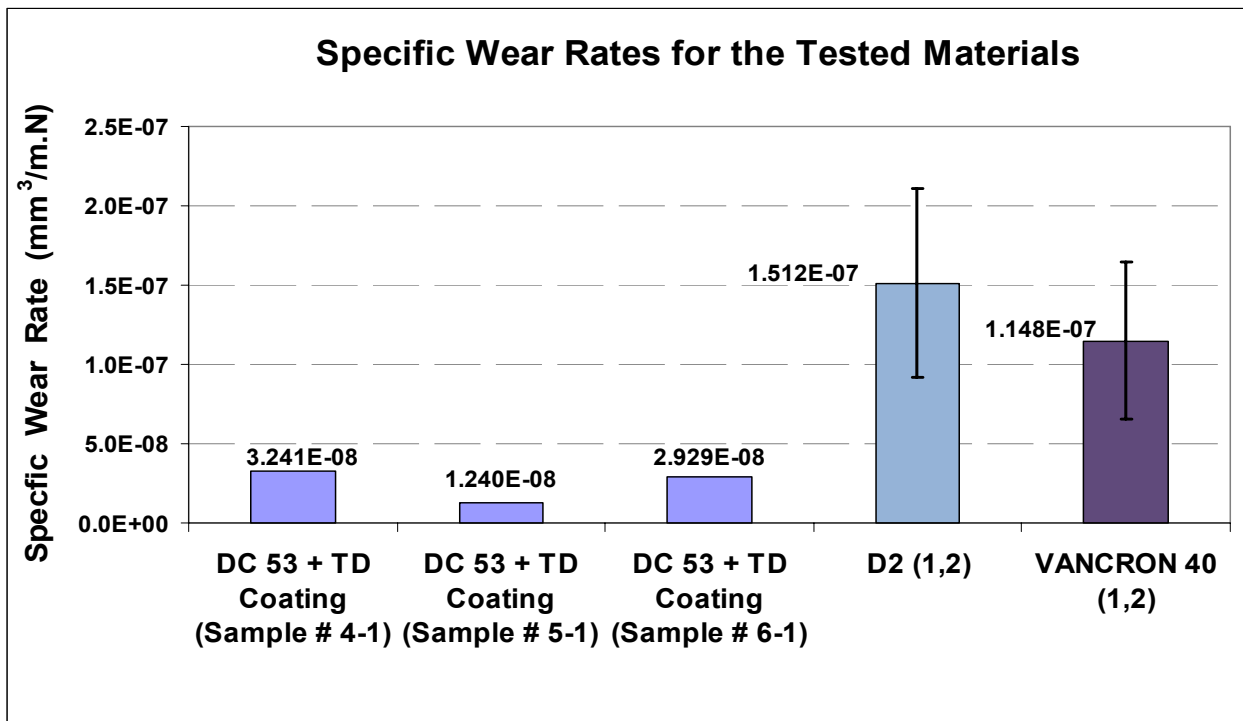
Figure 4.3 Specific wear rates for the tested die samples in Test Group I

Tested samples were examined under confocal microscope (μsurf explorer, Nanofocus-US, Glen Allen, VA), and analyses were performed to obtain 3-D surface roughness parameters. The main distinguished feature of confocal microscopes is that the ability to take several in-focus pictures in z-direction and combines them in one unique three-dimensional image file thus eliminating out-of-focus light problems for the specimens that are thicker than focal plane. Moreover, automated stage use provides stitching multiple set of in-focus pictures in lateral direction which is extending the measurement field. Figure 4.4 demonstrates confocal microscope images obtained by μsurf explorer and its software μsoft analysis v.5 (NanoFocus AG, Germany). Olympus brand lenses with 20X magnification and numerical aperture of 0.6 were used for all measurements. The field of view (measuring field) for the lens type used is 800μm x 800μm. One of the main advantages of confocal microscope use is that the peak and valley regions can easily be differentiated from each other looking at 3D picture of the surface, which is not possible with regular microscopes. SEM observations for coated die samples given in Figure 4.5 – 4.7 demonstrated insignificant coating damages and small particles stuck to die sample surface from sheet blank.
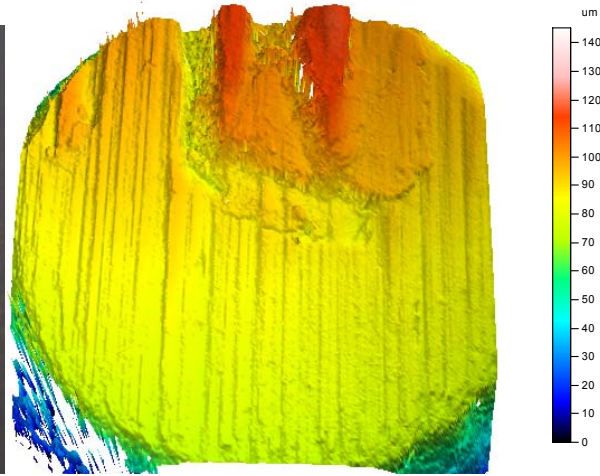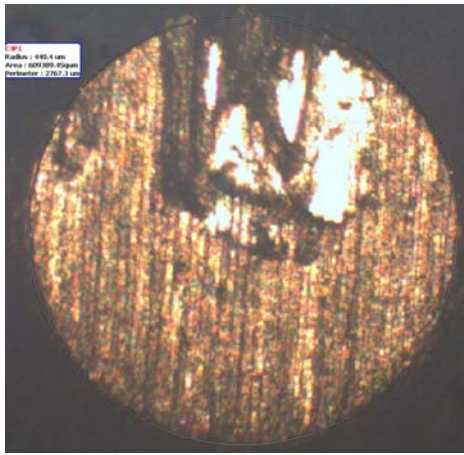
a) Uncoated AISI D2 #1
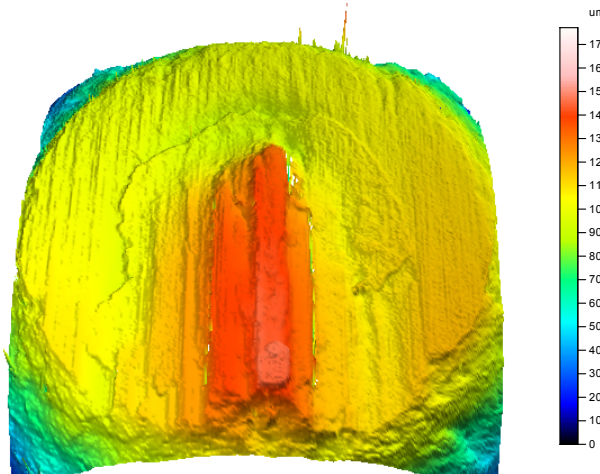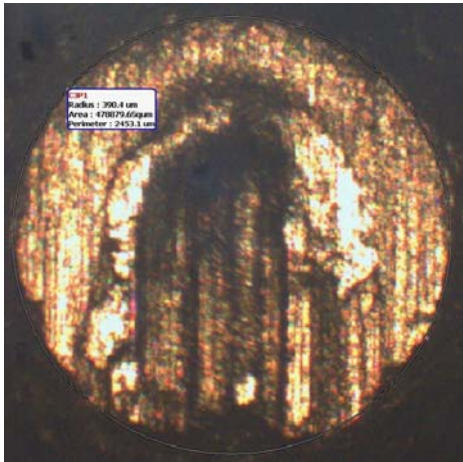
b) Uncoated AISI D2 #2
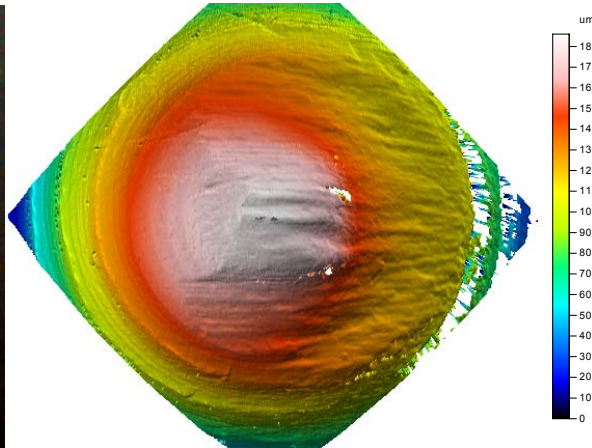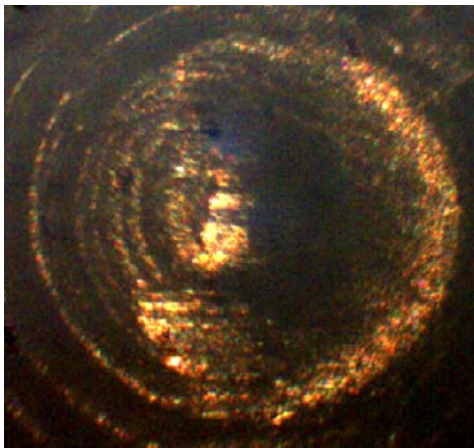
c) Uncoated Vancron 40 #1
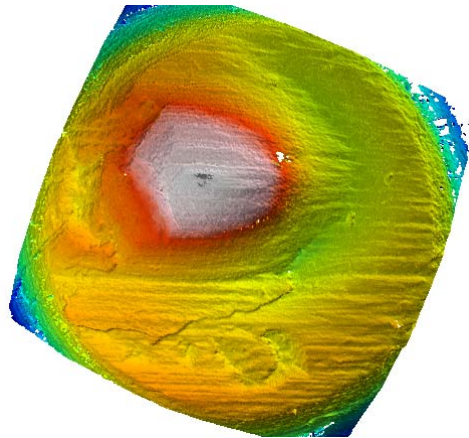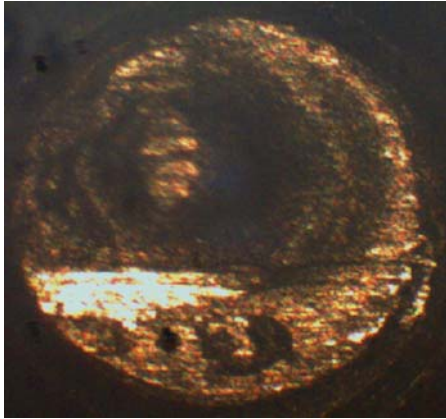
d) Uncoated Vancron 40 #2
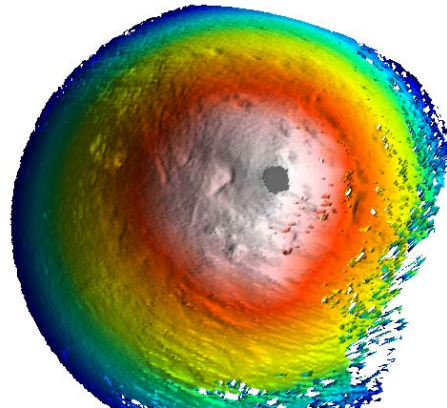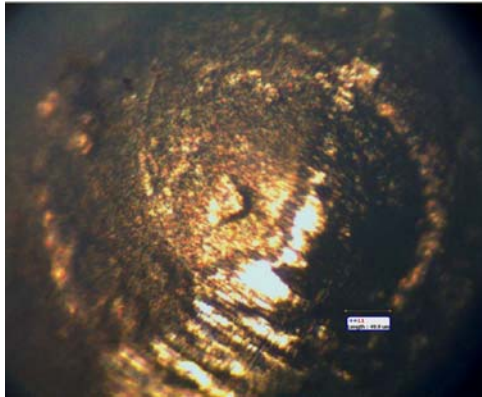
e) TD coated DC 53 die sample (Sample # 4-1)
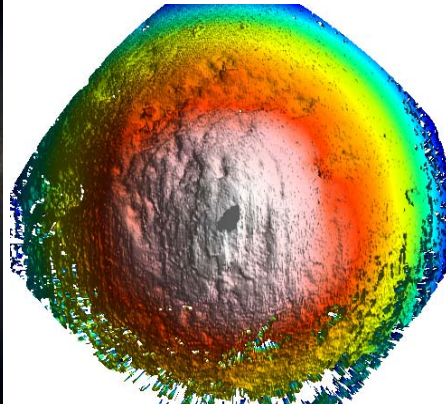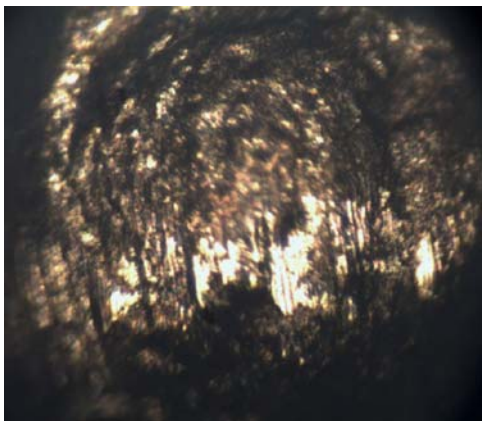
f) TD coated DC 53 die sample (Sample # 5-1)
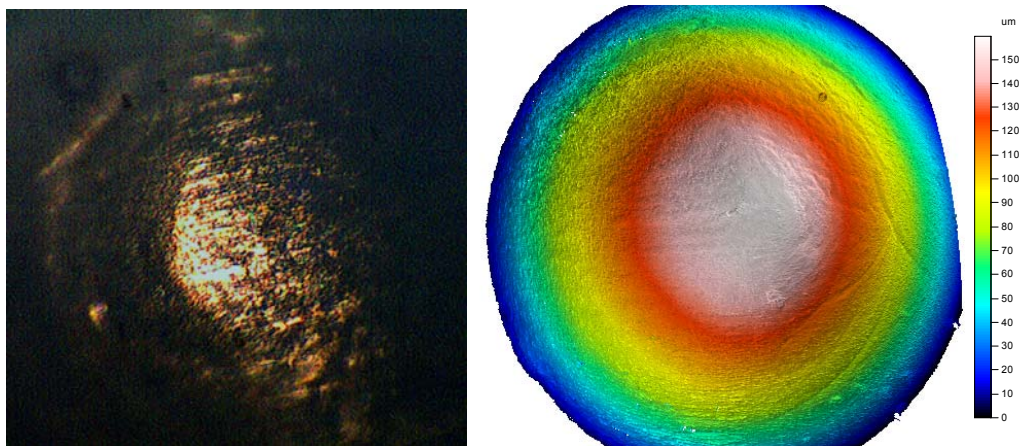
g) TD coated DC 53 die sample (Sample # 6-1)

Figure 4.4 Optical microscope (on the left) and 3-D confocal microscope pictures (on the right) of the tested die samples
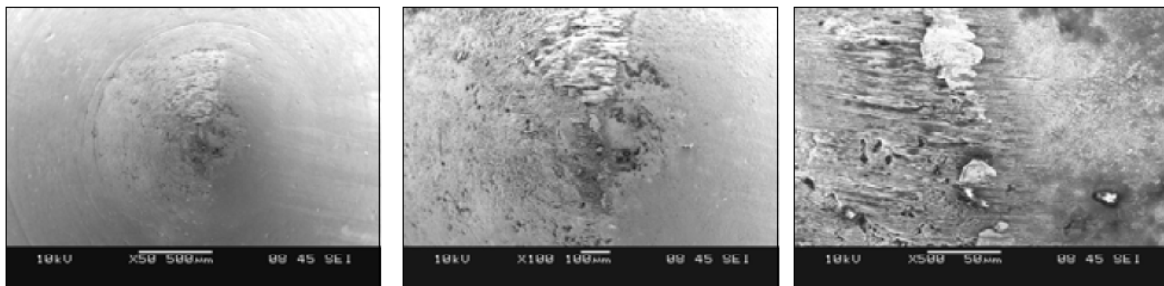
(a)   (b)   (c)

Figure 4.5 SEM picture of TD coated DC 53 (59.3 HRC) die sample (Sample # 4-1) at the tip (magnifications: a) 50X b) 100X c) 500X)
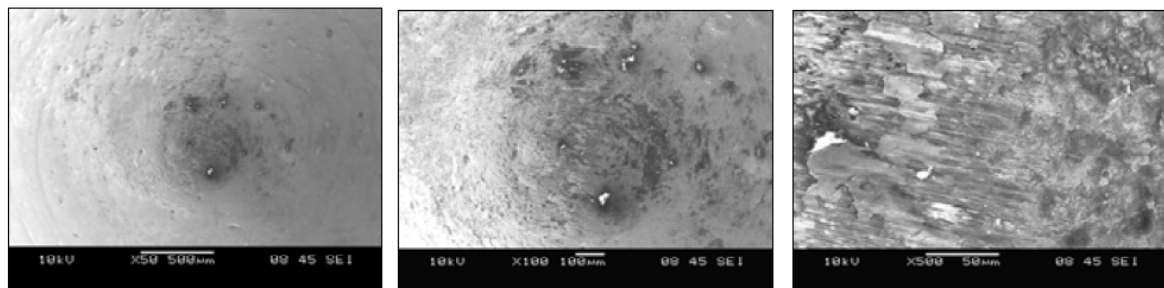
(a)   (b)   (c)

Figure 4.6 SEM picture of TD coated DC 53 (63.1 HRC) die sample (Sample # 5-2) at the tip (magnifications: a) 50X b) 100X c) 500X)

100

(a)	*(b)*	*(c)*
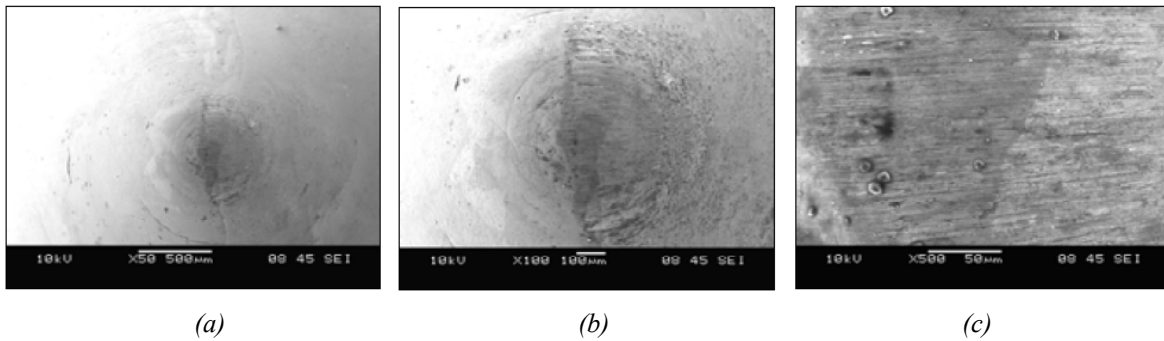
Figure 4.7 SEM picture of TD coated DC 53 (61.9 HRC) die sample (Sample # 6-1) at the tip (magnifications: a) 50X b) 100X c) 500X)

4.4.1 3-D Surface roughness analyses for Test Group I

3D surface roughness analyses, to characterize contact surface after the tests, were also performed based on confocal microscope measurements. Although the die sample contact surfaces do not have uniform wear patterns; and different from machined or optical surfaces that have certain imposed textures, 3D surface finish analysis gives valuable information about the wear characteristics (galling effect, material pile-up or removals etc.) of the tested material. Analyzing the surface in 3D give more accurate information compared to 2D analysis which is usually obtained by contact type profilometers with line measurements. 2D analyses are direction oriented and insensitive to directional texture differences; and require multiple measurements to cover the area of interest. Conversely, 3D analysis provides surface texture information for the same particular area eliminating the directionality problem.

The surface texture consisted of four components; form, waviness, roughness, and micro-roughness as can be seen in Figure 4.8. Form is a component of surface finish with a long wavelength similar to the wavelength of the object measured. Form needs to be

101

removed in order to analyze surface texture (i.e. waviness and roughness). Waviness is the surface texture component that varies slowly depending on the horizontal position. Waviness, for example, may result from low frequency vibrations between the workpiece and the machining tool and stringently affects the mechanical contact (machining faults, gaskets, bearings). Wavelength range for waviness is defined in the range of 0.5-2.5mm. Roughness, in contrast to waviness, is regarded as surface texture component that varying rapidly depending on the horizontal position and gives indication on the nature of the material and the machining type used. It is accepted to be represented by wavelengths ranging from 20 - 500μm. Micro-roughness is regarded as the finest component of surface texture. It is defined as the set of high frequencies (the smallest wavelengths) in a measurement, and can be caused by sampling noise or from the microscopic relief and the structure of material. Microroughness must be filtered before calculating the roughness parameters and usually discarded by band-pass filtering using microroughness cut-off filters ranging 2.5 to 25μm. Filtering microroughness is often omitted on surfaces because of the relatively low resolution in points per profile. [Nanafocus μsoft user's guide, 2009].
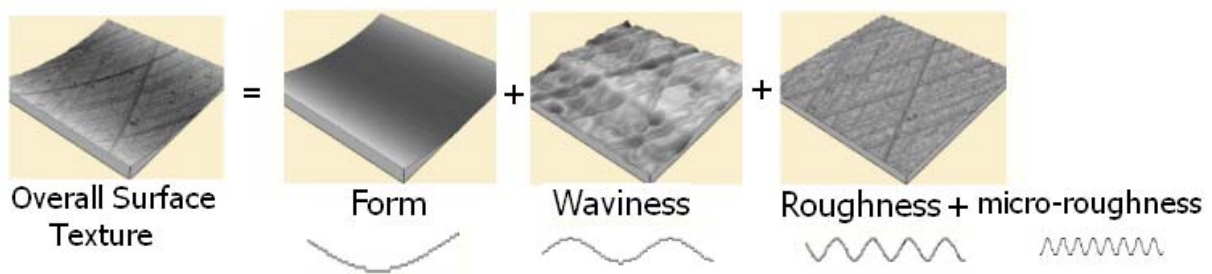
Figure 4.8 Components of surface texture [*After Nanafocus μsoft user's guide, 2009*]

In order to obtain roughness profile itself, waviness and form components should be subtracted from the overall surface profile using suitable filter sizes. Following procedure given in Figure 4.9 were applied to obtain the roughness and waviness profiles in μsoft analysis software:

a) Boundary of measurement interest selection was made on the source surface obtained by confocal microscopy

b) Form removing were performed by choosing numerical preferences (polynomial order of 2)

c) Filter type (Gaussian), and cut-off wavelength filter size to separate the waviness and roughness were selected as 0.25 mm.

a)   *b)*

c)

d)   *e)*
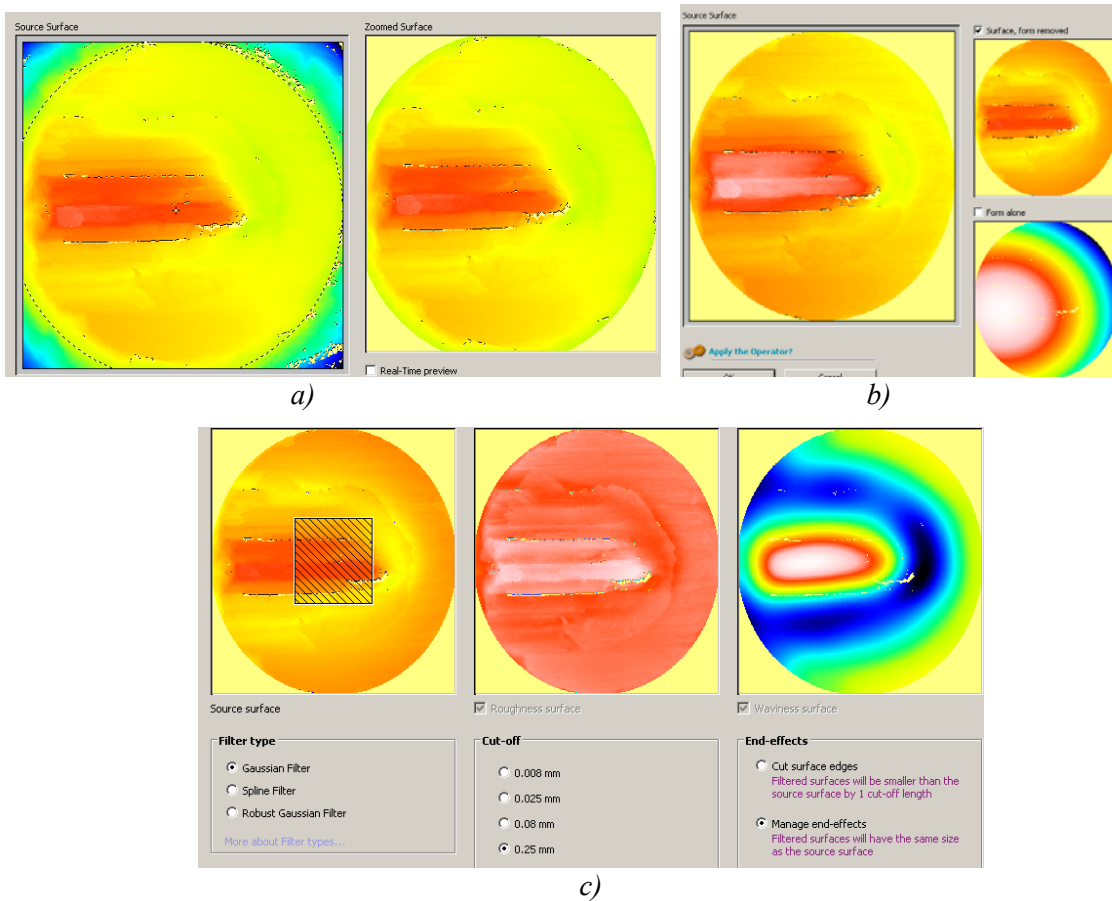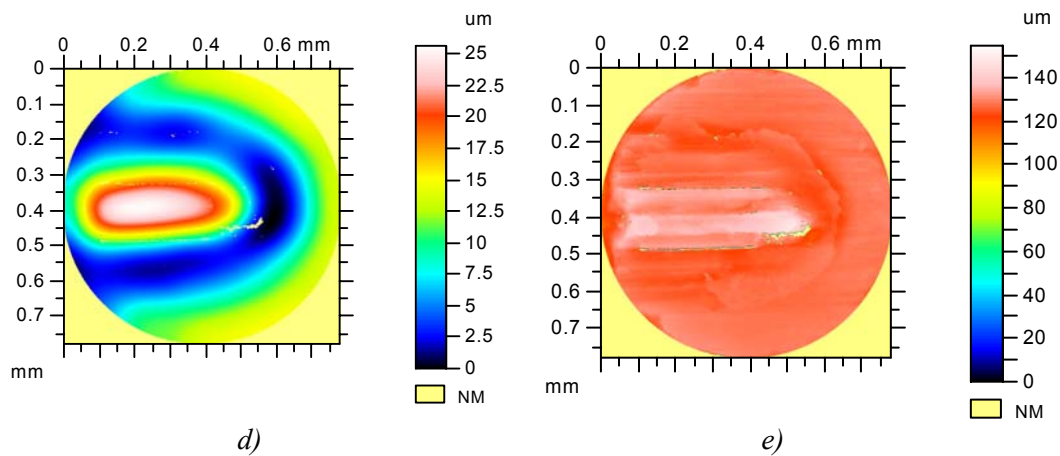
Figure 4.9 Procedure applied to obtain the waviness and roughness in μsoft analysis software. a) Reference measurement area selection on source surface, b) form removal using numerical preferences, c) filter type and cut-off filter size selection d) obtained waviness profile, e) obtained roughness profile

The 3D surface texture measurements obtained for Test Group 1 are tabulated in Table 4.5. Average (S_a), root-mean square roughness in 3D, (S_q), and ten point heights (S_z) were obtained as the lowest for the DC 53 # 6-1 TD coated sample. Negative value of skewness (S_{sk}) signifies the presence of valleys for all tested samples. Kurtosis (S_{ku}) values were obtained as higher than zero that stand for high peak and valleys on the measurement area. Maximum peak heights (S_p) were higher for D2 samples than other tested samples as can also be seen from Figure 4.5.

Table 4.5 3D surface roughness parameters for the Test Group 1 samples after the wear tests

Roughness Parameter	D2 #1	D2 #2	Vancron40 #1	Vancron40 #2	DC 53 #4_1 (TD Coated)	DC 53 # 5_1 (TD Coated)	DC 53 # 6_1 (TD Coated)
$S_{q\ (\mu m)}$	4.92	6.13	3.5	4.13	5.52	7.04	1.63
S_{sk}	-9.03	-9.21	-8.28	-3.68	-4.09	-7.91	-7.37
S_{ku}	149	146	216	86.1	60.9	98.3	211
$S_{p\ (\mu m)}$	27.3	34.6	12	12.5	23	22	14.1
$S_{v\ (\mu m)}$	98.2	118	141	113	119	122	62.7
$S_{z\ (\mu m)}$	125	153	153	126	142	144	76.8
$S_{a\ (\mu m)}$	1.91	2.98	2.29	2.98	2.77	3.08	1

4.5 Test Group II: Effect of Coating Type on Wear Performance [2]

Group II tests were aimed to investigate the effect of coating type on wear resistance. Four (4) different coatings, namely TD, PVD, radical nitriding + PVD, and CVD, were tested on the same substrate material of DC 53 and against the hot-dip galvaannealed DP 600 sheet blanks (provided by US Steel) for 2km under 200N average contact normal load.

Table 4.6 and Table 4.7 show hardness and average surface roughness values before tests for sheet blank and die samples, respectively. Hardness measurement for sheet blank performed with micro-Vickers hardness tester applying 1kg.f, while hardness values for substrate materials of die samples were measured using conical type indenter and 150kg.f load.

Coated die samples were provided by Daido Steel Co. Ltd (Japan) and were prepared according to the following procedure: Firstly, all the samples are roughly machined before pre-heat treatment. In the heat treatment die samples were exposed to gas quenching at 1030° C, then tempered for 1 hour at 550° C. After the heat treatment applied; the die samples are machined to final dimensions and polished prior to coating process (Thermal Diffusion: TD, Physical Vapour Deposition: PVD, and Chemical Vapour Deposition: CVD). In particular, the second sample is radically nitrided before its PVD coating. In radical nitriding process, different from conventional nitriding, the coating process is done under NH_3 and H_2 environment and it eliminates the formation of "white layer" which is brittle and needs to be cleaned prior to PVD coating process. The combination of radical nitriding and PVD coating provides increased hardness and peel off resistance for coatings. TD and CVD coated samples are heat treated after coating process once again. The final procedure for the sample preparation is polishing of coated samples. Typical coating thicknesses for all the samples tested were estimated by provider in the 5-10 μm range. The measurements and microscope analyses mentioned in previous sections were performed for this group of samples, too.

Table 4.6 Hardness and average surface roughness (Ra) values for DP 600 sheet blank

Hardness Measured (HV$_1$)	Average Surface Roughness Ra (μm)
203	0.24

Table 4.7 Die samples tested, hardness values and average surface roughness values (Ra)

Sample #	Substrate (die sample) + coating configuration	Substrate Hardness Measured (HRC)	Average Surface Roughness, Ra, Before Test (µm)
5-2	DC 53 + TD Coating	61.4	0.025
7-1	DC 53 + Radical nitriding TiCN (PVD)	61.9	0.063
8-1	DC 53 + TiCN (PVD)	61.1	0.051
9-1	DC 53 + Multi-layered CVD (TiC + TiCN + TiN)	62.9	0.079

4.5.1   Experimental results and discussion for Test Group II

Performance evaluation of die samples was based on the following measurements (1) mass loss, (2) surface profile (roughness) and (3) microscopic evaluations. In order to measure the surface roughness, contact surface of die samples are measured with a stylus (AMBIOS XP-1, Ambios Tech., CA, USA) which is a contact-type of device. All measurements were taken normal to the sliding direction which was followed during the test. 2-D surface roughness measurements are given in Table 4.8. It can be observed that there is no significant difference between initial and resultant surface roughness values for the die sample contact surfaces when Table 4.7 and Table 4.8 are compared. Even, the surface roughness is improved for all the die samples except PVD coated sample. Surface roughness data obtained after tests for all samples passed the normality tests and significantly different means and variances ($P<0.005$) were obtained applying one-way ANOVA method. Figures 4.10 – 4.13 depict the micrographs for the resultant contact surfaces and their 3D topographies obtained by using a HIROX digital microscope KH-

7700 (Hirox-USA Inc., NJ, USA). Some additional analyses on the samples were performed by Dr. Kunio Namiki of Daido Steel Co., Ltd (Japan) upon the sample preparation depicted in Figure 4.14. SEM observations of the tested samples at their tips with different magnification levels are given in Figure 4.15 – Figure 4.18. From optical microscope and SEM images, it is indisputably obvious that the contact surfaces of the PVD coated (sample # 7-1, 8-1) samples underwent considerable changes compared to TD and CVD coated samples. Sliding directions are clearly visible for those samples and adhesion type of wear observed on contact surfaces.

Table 4.8 Measured surface roughness values for tested samples

Sample #	Test Material + Coating	R_a(µm)	R_{ku}(µm)	R_q(µm)
5-2	I) DC 53 + TD Coating	0.018	9.057	0.025
7-1	II) DC 53 + Radical nitriding TiCN (PVD)	0.059	6.218	0.080
8-1	III) DC 53 + TiCN (PVD)	0.068	5.393	0.092
9-1	IV) DC 53 + multi-layered CVD (TiC, TiCN, TiN)	0.053	4.88	0.071

(a)

(b)
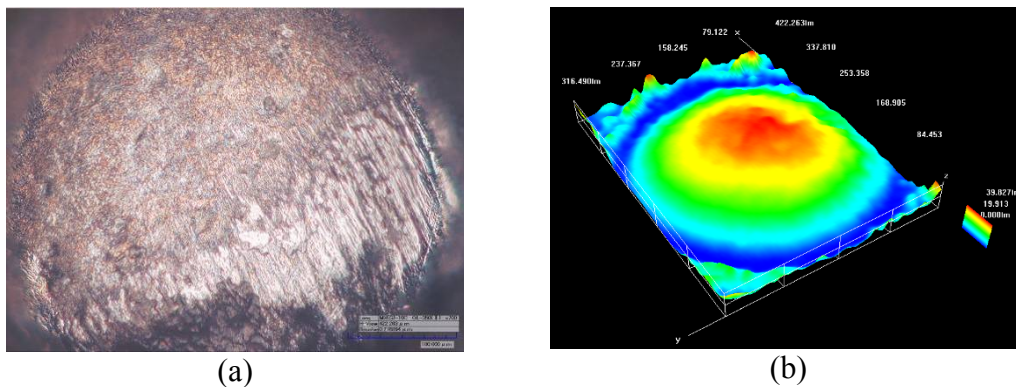
Figure 4.10 (a) Micrograph of DC 53 die sample with TD coating (700X); (b) 3-D topography of the worn surface

(a)   (b)
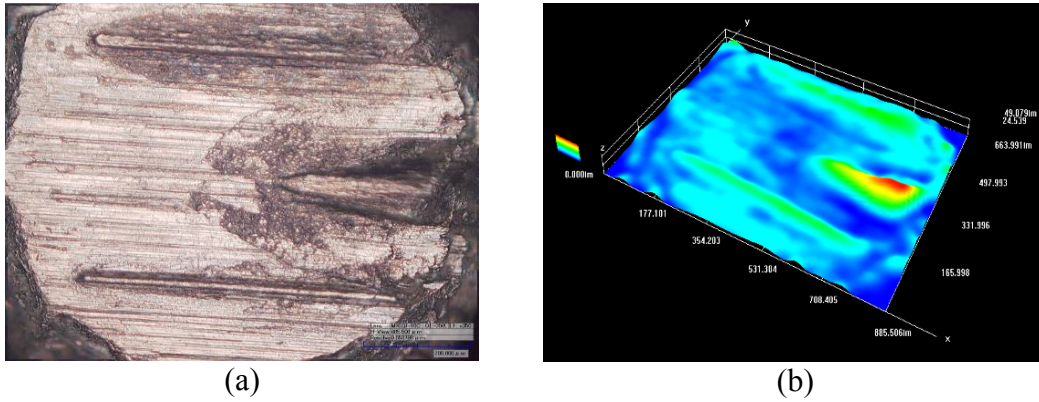
Figure 4.11 (a) Micrograph of DC 53 die sample with radical nitriding + TiCN (PVD) coating (350X)); (b) 3-D topography of the worn surface

(a)   (b)
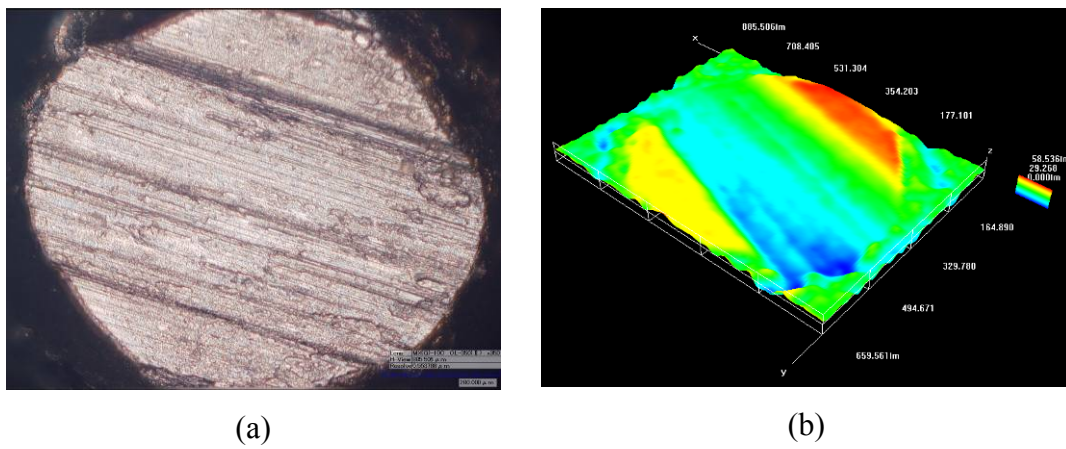
Figure 4.12 (a) Micrograph of DC 53 die sample with TiCN (PVD) coating (350X); (b) 3-D topography of the worn surface

(a)   (b)
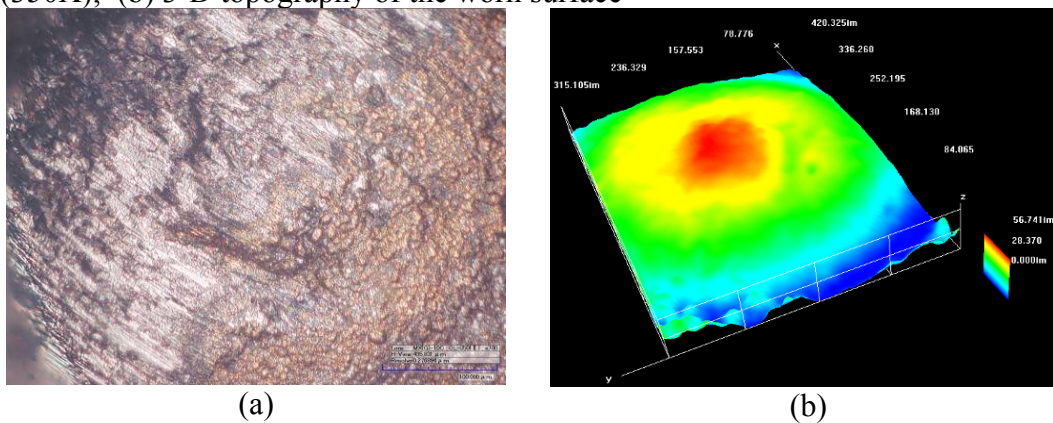
Figure 4.13 (a) Micrograph of DC 53 die sample with multi-layered CVD (TiC, TiCN, TiN) coating (700X) ; (b) 3-D topography of the worn surface

109
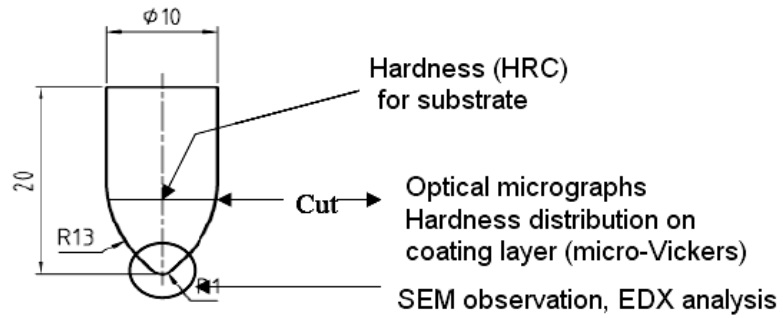
Figure 4.14 Sample preparation and list of analyses (by Daido Steel Co., Ltd, Japan)

(a)	(b)	(c)
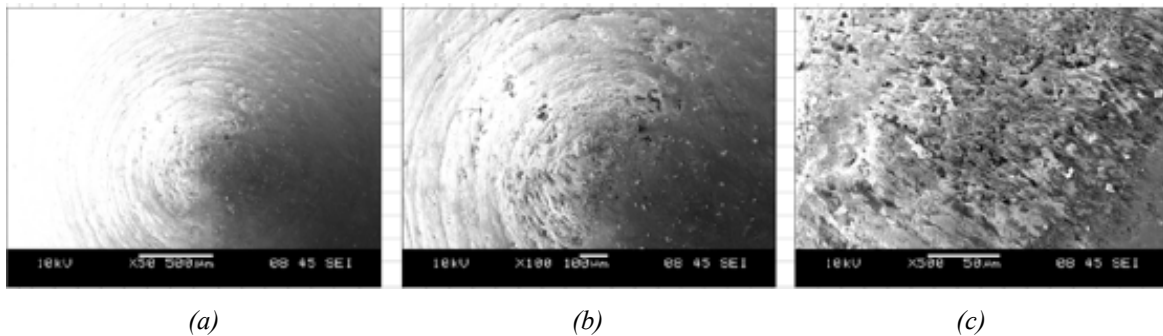
Figure 4.15 SEM picture of DC 53 die sample with TD coating at the tip (magnifications: a) 50X b) 100X c) 500X)

(a)	(b)	(c)
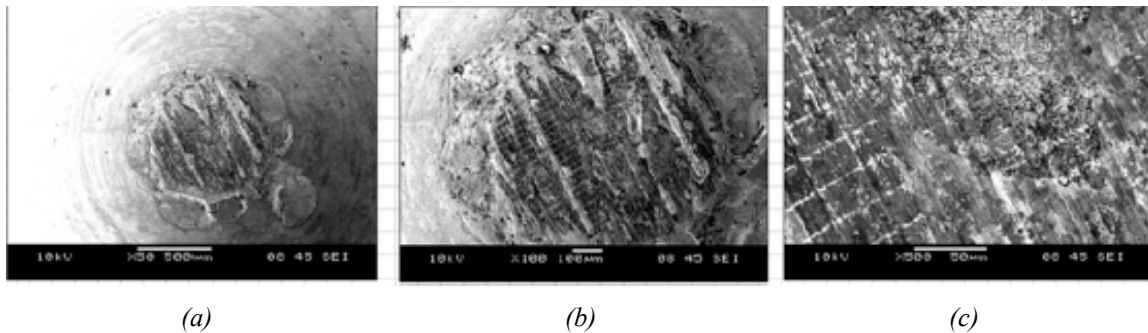
Figure 4.16 SEM picture at the tip of DC 53 die sample with radical nitriding + TiCN (PVD) coating (magnifications: a) 50X b) 100X c) 500X)

(a)   *(b)*   *(c)*
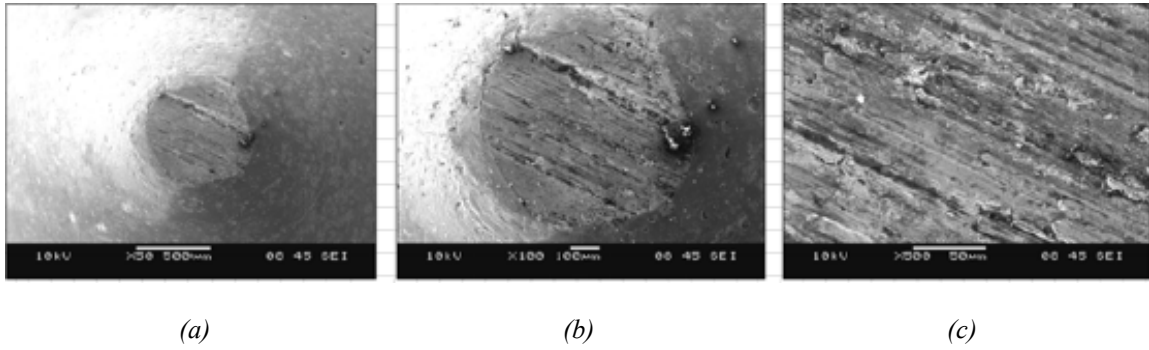
Figure 4.17 SEM picture at the tip of DC 53 die sample (III) with TiCN (PVD) coating (magnifications: a) 50X b) 100X c) 500X)

(a)   *(b)*   *(c)*
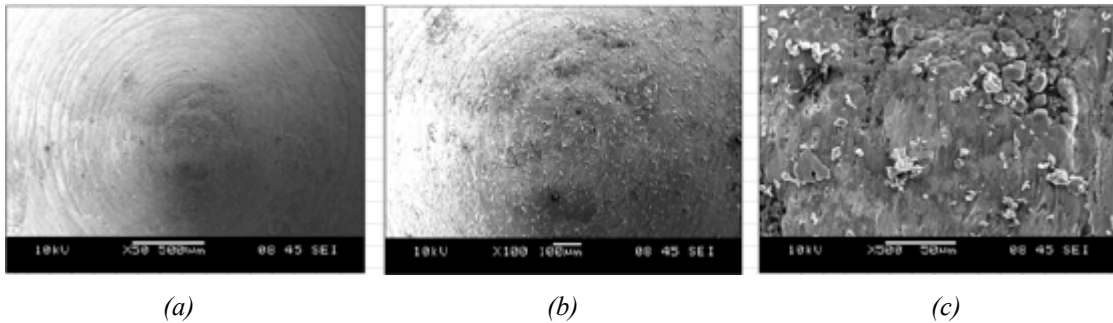
Figure 4.18 SEM picture at the tip of DC 53 die sample (IV) with multi-layered CVD (TiC, TiCN, TiN) coating (magnifications: a) 50X b) 100X c) 500X)

Energy dispersive x-ray (EDX) analyses, shown in Figures 4.19 – 4.22, were also performed for tested samples on coating layers. In addition to carbon content, vanadium, which is main ingredient in TD coating, was detected on the coating layer of Sample I while; titanium (Ti) was detected on coating layers of other three samples as expected. Specifically, for the multi-layered CVD coated sample (Sample IV), a TiC layer just above the substrate, and TiN on the top of coating layers and, a TiCN layer in between those were detected as can be seen in Figure 4.22.
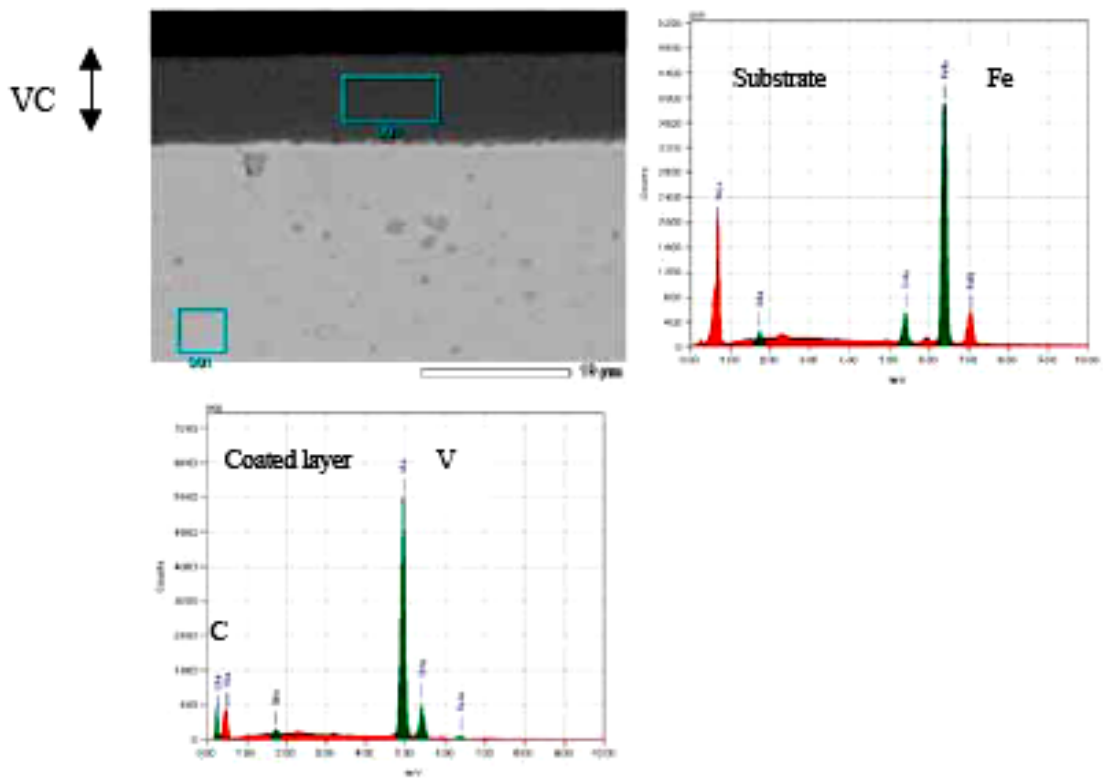
Figure 4.19 SEM-EDX analyses for TD coated sample
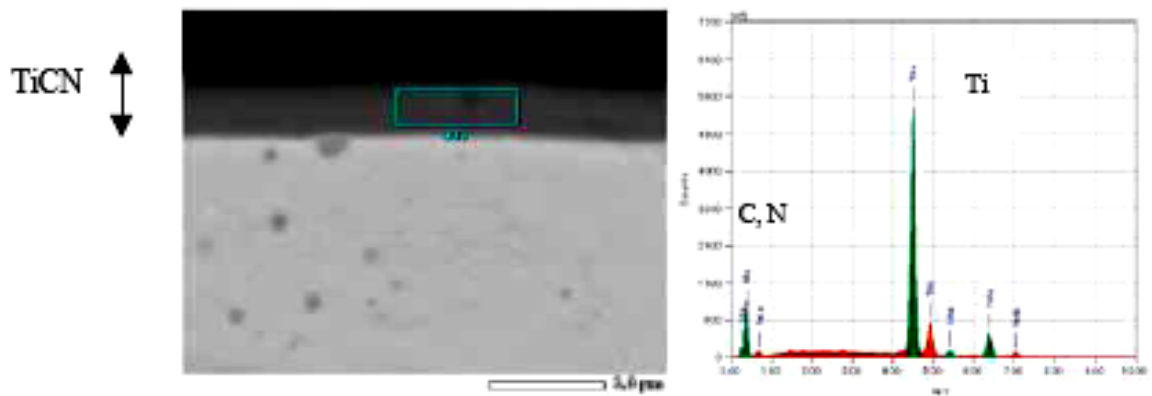
Figure 4.20 SEM-EDX analyses for radical nitriding + PVD (TiCN) coated sample

112
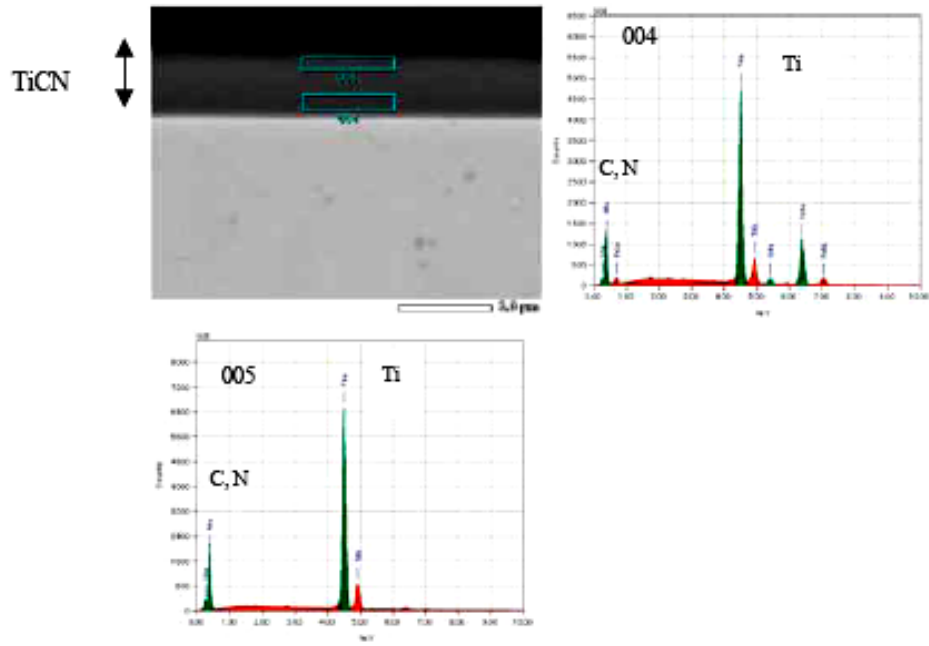
Figure 4.21 SEM-EDX analyses for PVD (TiCN) coated sample
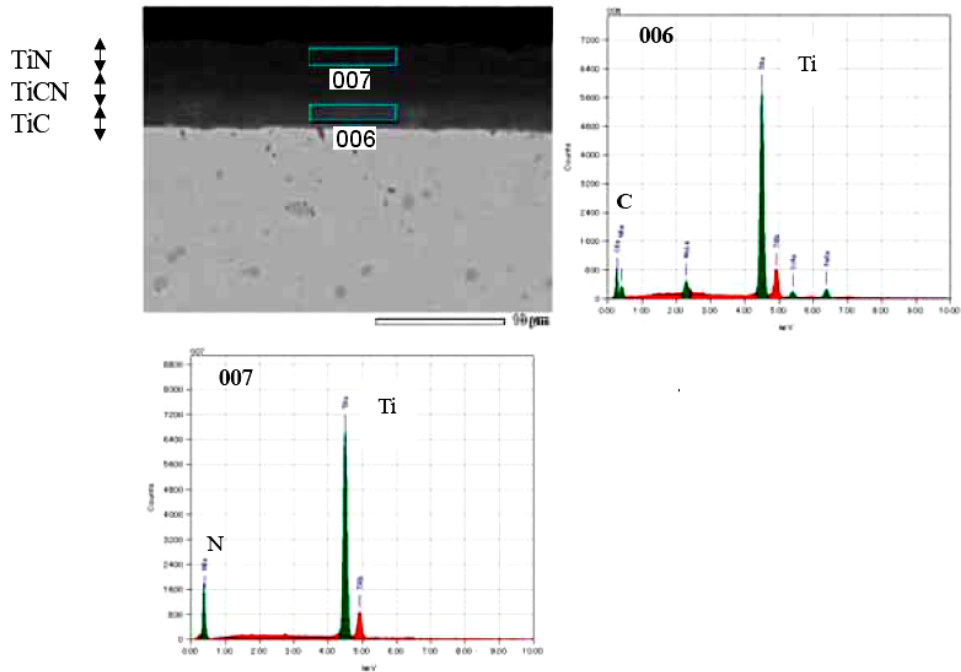
Figure 4.22 SEM-EDX analyses for CVD (TiN+TiCN+TiC) coated sample

From Figures 4.10 and 4.13, it can be observed that the coating is not completely removed from the specimens' contact surface. Specifically, amount of wear debris for the test of TD coated sample was higher than any other sample; although the mass loss of that sample was the least among the test samples. It is concluded that the durable and tough TD coating produced more wear debris on the sheet blank compared to the other samples coated with different coatings. These facts have been verified with the specific wear rate measurements. Wear volume measurement is based on the values of measured mass loss and density of the substrate and coating material. For the die samples coated with TD and CVD coatings, in which the wear is only on the coating, the coating densities were included in calculations. For the other die samples coated with PVD and radical nitriding + PVD coatings specimens (sample # 7-1 and 8-1), both coating and substrate material densities were taken into account in calculating specific wear rate values. Density of the substrate material was reported as 7870 kg/m^3 by sample provider. Other coating density values (4930, 5400, 5410, 5250 kg/m3 for TiC, TiN, VC, TiCN respectively) are obtained from the literature. [Holleck, 1986; Russias et. al, 2007]. Sliding distance is 2 km and average normal load is 200 N as mentioned above. Tabulated results and bar chart form for specific wear rates of the test samples are given in Table 4.9 and Figure 4.23 respectively. The smaller value stands for higher wear resistance. Figure 4.24 shows micro-Vickers hardness measurements on the cut samples from coating surface to substrate. It is noted that the hardness values obtained on DC53 substrate (starting from approximately 0.10 mm in horizontal axis) were in good agreement for all samples. For the coated portions, radical

114

nitriding+PVD coating had relatively higher hardness value due to its characteristic feature.

Table 4.9: Calculated specific wear rate values for tested samples

Sample #	Die Material + Coating	Specific wear rate (mm^3/m.N)
5-2	DC 53 + TD Coating	4.223×10^{-8}
7-1	DC 53 + Radical nitriding +TiCN (PVD)	1.844×10^{-7}
8-1	DC 53 + TiCN (PVD)	1.099×10^{-7}
9-1	DC 53 + multi-layered CVD (TiC, TiCN, TiN)	4.353×10^{-8}
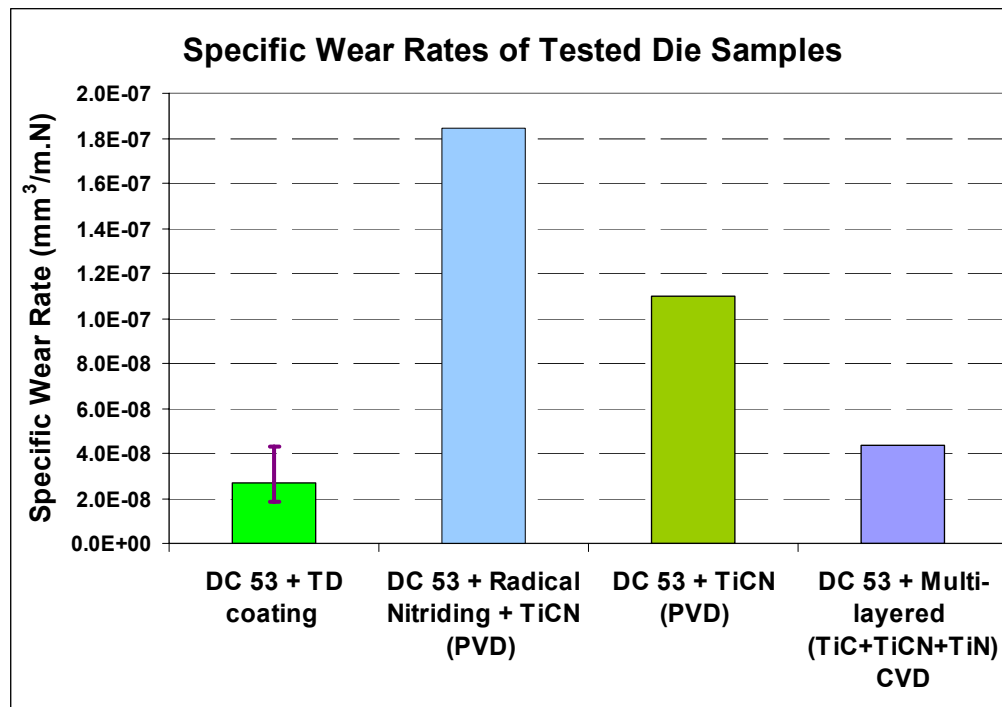
Figure 4.23 Specific wear rates for tested samples in Test Group II
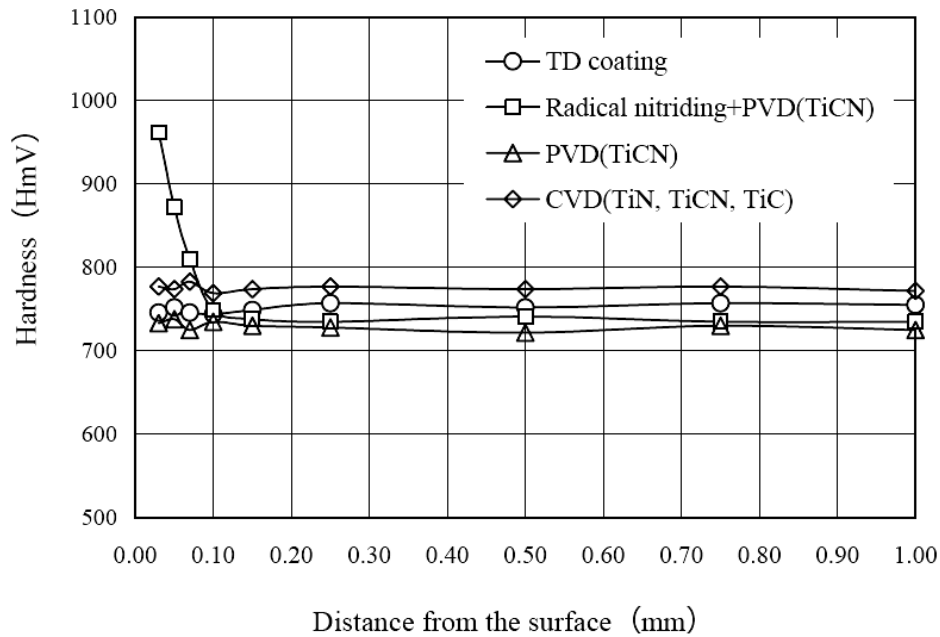
Figure 4.24 Vickers micro-hardness values for the tested samples from coating surface to inner substrate

As reported from the previous studies [Sakamotoa et. al, 2001; Lee and Park, 2007] and experienced in this study, combination of radical nitriding and PVD coating process resulted in higher coating hardness value when the Sample #7-1 and 8-1 are examined. Contrary to expectations, sample # 7-1, with the highest coating hardness, did not perform the best. Die sample # 7-1, coated with radical nitriding and PVD and with a hardness of 61.0 (HRC) on the substrate and 980 (HV) on the coating, performed relatively low compared to other tested samples.

Optical microscope pictures given in Figure 4.25 revealed that the coating differences were different for tested samples. The die samples showing higher wear resistance, namely TD and CVD coated ones, had 6-8 μm coating thickness while PVD, and radical nitriding+ PVD coated samples had the coating thicknesses in the 2-3 μm range.

116

It is clearly seen that the performance of the TD and CVD coated samples are very close to each other, and far better than PVD coated samples. As discussed above, these samples were the ones in which coating was not removed from the contact surface completely. The main factor that led to wear resistance performance differences for tested samples is believed to be coating thickness differences.

The disadvantage for the TD and CVD coating technologies is the limitation of the coating replacement. Typical CVD and TD coatings are applied at temperatures greater than 980°C (~1800°F) to increase molecular activity within the substrate. During these high temperature coating processes, atomic diffusion occurs from substrate to surface and forms a third compound combining with the coating material as described in Figure 4.2. This can produce a hard coating, but the diffusion towards surface is limited. Thus, as tools and coatings wear, the second application of these coatings usually lasts about 70 percent as long as the first application; a third application generally has a life only 30 percent that of the original tool. When the diffusion is not feasible anymore, the process ceases to provide any benefits [Metalforming, 2008].
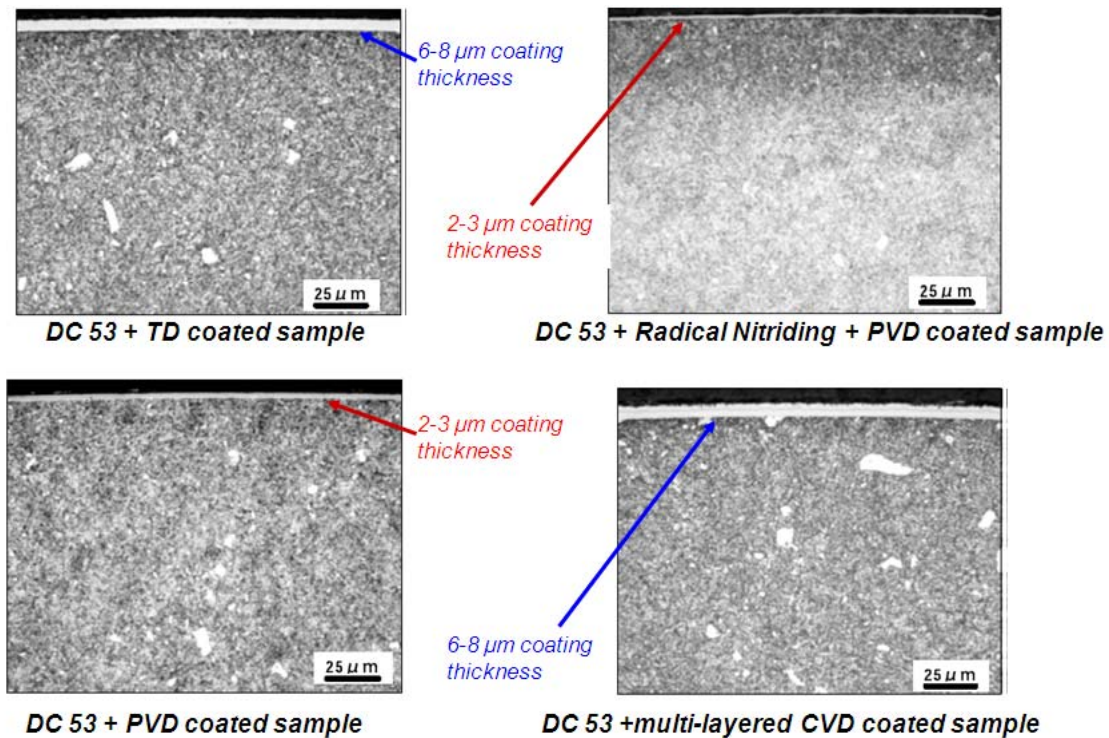
Figure 4.25 Optical microscope images for the coated die samples showing coating thicknesses at their substrate-coating interface

For repetition purposes, three (3) replications were performed with the TD coated case (one of the samples were tested as part of Test Group I, and the other sample was tested as part of Test Group III). Based on good results obtained from replications as depicted in Figure 4.23, as well as limited availability of die samples provided, repetitions for other cases were not performed. The coating was not removed from the substrate completely in any repetition test, which strengthened the consistency of test results. Although there is no agreed upper limit for specific wear rate to assess the performance of materials, all of the specific wear rate values for the tested materials are well below

compared to 1×10^{-6} mm^3/m.N which is regarded as limit value by some researchers [van der Heide et., al, 2006].

As reported in the literature, several researchers investigated the effect of coating applications on wear. In their work, Weist et. al. studied the effect of various coatings including nitrided layers, hard chromium plating as well as PVD, CVD or ion implantation on tool wear. They noted that the best results were obtained for PVD and TD coated punches in a quest for reduction of wear in bulk metal forming processes [Weist et. al, 1986]. In another study by Dubar et. al., the performance of cold forging tool coated with PVD and CVD coatings was examined and the findings showed that the better friction and lifetime results were obtained by CVD coated tools [Dubar et. al, 2005]. As can be understood from these studies and several others, there is no best coating technique that can handle all conditions. The best choice requires finding the optimum combination of substrate and coating material which vary with operation variables. The compatibility of the substrate material and the coating applied is crucial for anti-wear properties as well as the formation of strong bond between substrate and coating material. Higher coating hardness values may contribute less peel-off resistance due to brittleness effect. The uncontrollable coating thickness differences may also contribute to the performance of the tested samples as experienced in this study.

4.6 Test Group III: Effect of Substrate Material

As aforementioned in Section 4.2, one of the parameters to be investigated in the test plan was determined as "effect of substrate material". Samples numbered with 5, and

10-12 given in Table 4.1 were employed in this study. Different from the previous group test materials, SKD 11 (equivalent of AISI D2, and DIN 1.2379 in Japanese standards), DRM 3 (Matrix type high speed steel used in cold forging dies, developed by Daido Steel) and DRM 51 (Another matrix type high speed steel by Daido Steel). DRM series matrix type tool steels are characterized by their superior balance of toughness and hardness that find wide range of applications from hot to cold forging dies. They are regarded as economic alternative to powder metallurgical tool steels. Alloy designing to optimize the carbide type and the amount of carbides and refinement of primary carbides to control carbide solution are the fundamental concepts in their development [Nakahama et. al, 2005]. All the substrate materials were coated with TD coating and tested along 2.2 km track distance under an average normal load of 220N with a sliding speed of 0.33 m/s utilizing the above mentioned system. HDGA DP 600 (US Steel) sheet blanks of 330x330x1mm were used in tests. Chemical compositions for the substrate of die samples, tested material-coating combination, and hardness values for the die samples are tabulated in Table 4.10 and Table 4.11.

Table 4.10 Chemical compositions of the tested die samples

Material	C	Cr	Mo	W	V
DC 53	0.95	8	2	-	0.3
SKD 11	1.50	12	1	-	0.3
DRM 3	0.60	4	2Mo+W		1.0
DRM 51	Patent pending by Daido Steel Co.				

Table 4.11 Tested die sample configuration, substrate hardness, and density values

Sample#	Substrate material + Coating configuration	Substrate Hardness Measured (HRC)	Substrate Density (kg/m^3)
5-3	DC 53 + TD Coating	62.9	7870
10-1	SKD 11+TD Coating	58.2	7730
11-1	DRM 3 +TD Coating	64.3	7920
12-1	DRM 51+TD Coating	63.8	7970

4.6.1 Experimental results and discussion for Test Group III

Performance evaluation of die samples was based on the same criteria as given before; (1) mass loss, and specific wear rate calculation, (2) surface profile (roughness) measurements and (3) microscopic evaluations. In order to have information about surface roughness, contact surface of die samples are measured with a stylus (AMBIOS XP-1, Ambios Tech., CA, USA) which is a contact-type of profilometer. All the measurements are taken normal to the sliding direction which was followed during the test. Table 4.12 and Table 4.13 show the average (R_a) and root-mean-square (R_q) surface roughness values before and after experiments. As can be noticed from these tables, surface roughness values were improved during the tests. Microscopic examinations obtained before and after tests, and given in Figure 4.26 through Figure 4.29 showed that the coatings were not peeled-off from the substrate surfaces at all; sliding tracks were not identifiable except

some minor polishing marks for DRM 3 sample. This is confirmed with SEM micrographs given in Figure 4.30 – 4.33.

Table 4.12 Average surface roughness values (R_a) prior to and after tests

Sample #	Substrate + coating	R_a Before Test (μm)	R_a After Test (μm)
5-3	DC 53 + TD Coating	0.035	0.033
10-1	SKD 11 + TD Coating	0.032	0.018
11-1	DRM 3 + TD Coating	0.020	0.014
12-1	DRM 51 + TD Coating	0.030	0.029

Table 4.13 Root-mean square roughness values (R_q) before and after tests

Die Sample	R_q Before Test (μm)	R_q After Test (μm)
DC 53 + TD Coating	0.050	0.043
SKD 11 + TD Coating	0.048	0.023
DRM 3 + TD Coating	0.028	0.019
DRM 51 + TD Coating	0.047	0.041

(a) *(b)* *(c)*
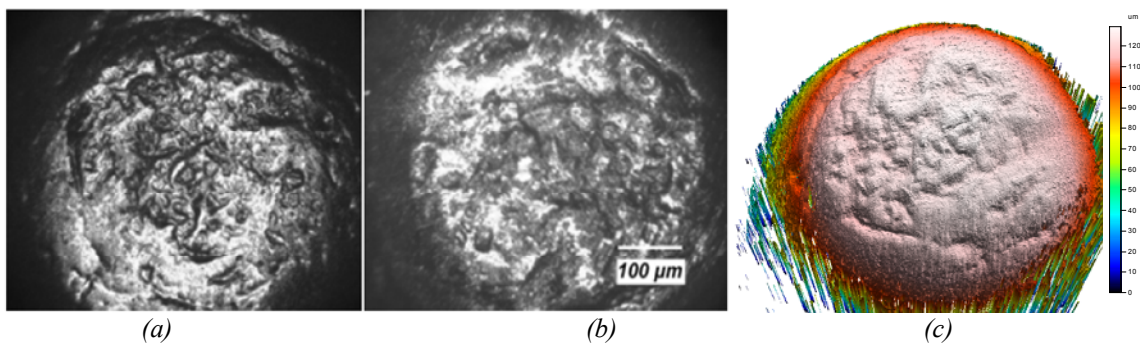
Figure 4.26 Micrographs for TD coated DC 53 die sample (Sample # 5-3) contact surface (a) before test, (b) after test, (c) 3-d view of contact surface after the test using confocal microscopy

(a)   (b)   (c)
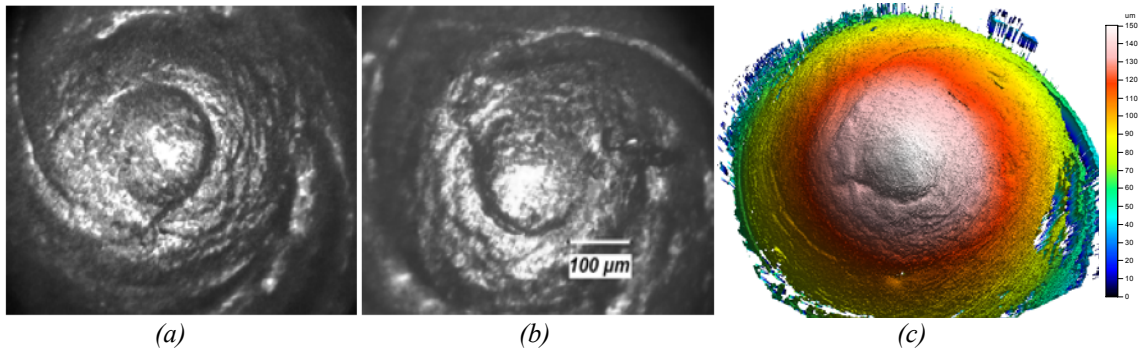
Figure 4.27 Micrographs for TD coated SKD 11 die sample (Sample # 10-1) contact surface (a) before test, (b) after test, (c) 3-d view of contact surface after the test using confocal microscopy

(a)   (b)   (c)
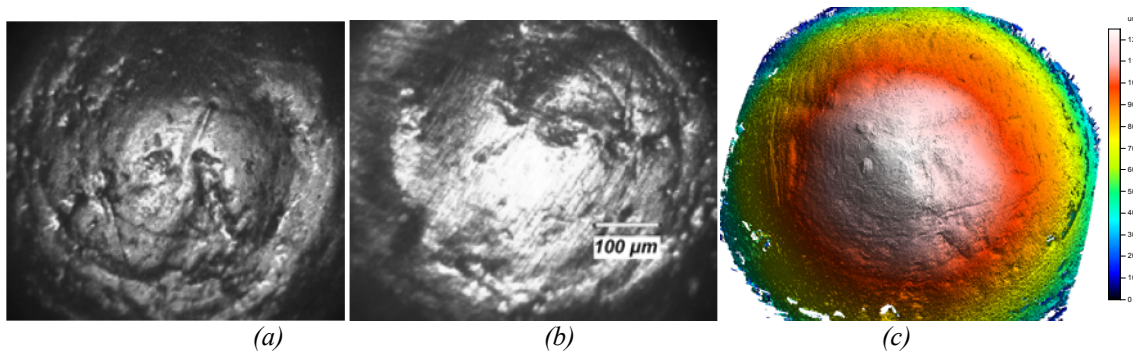
Figure 4.28 Micrographs for TD coated DRM 3 die sample (Sample # 11-1) contact surface (a) before test, (b) after test, (c) 3-d view of contact surface after the test using confocal microscopy

(a)   (b)   (c)
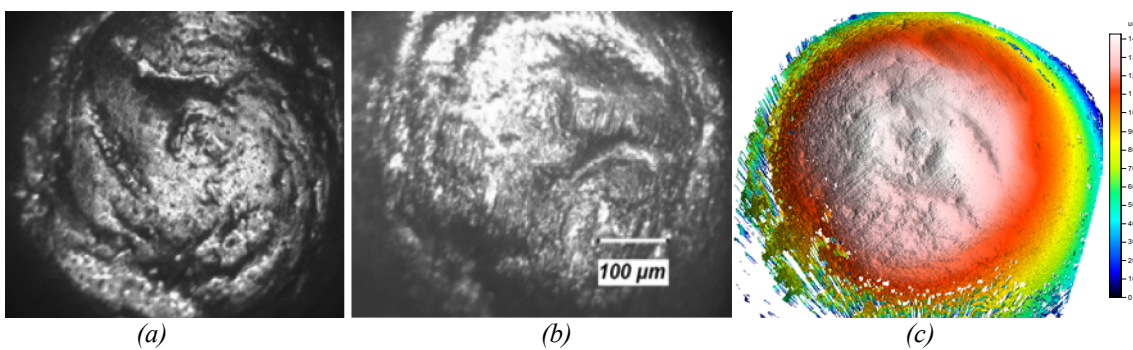
Figure 4.29 Micrographs for TD coated DRM 51 die sample (Sample # 12-1)contact surface (a) before test, (b) after test, (c) 3-d view of contact surface after the test using confocal microscopy

123

3D surface roughness analyses, as tabulated in Table 4.14, were also performed using μsurf explorer confocal microscope. Average (S_a), root-mean-square roughness (S_q), maximum peak heights (S_p), maximum valley depths (S_v), ten points heights (S_z) values were lower for the DRM 3 and SKD 11 samples. On the other hand, relatively higher kurtosis (S_{ku}) values were obtained for those samples. Negative values for skewness (S_{sk}) measurements were experienced for all tested samples, denoting the dominance of valleys on the measured surface. High values for kurtosis were the sign of presence of high peaks and deep valleys for all measured contact surfaces.

SEM pictures given in Figure 4.30 through Figure 4.33 demonstrated that there was not significant coating failure as experienced among Test Group II samples, except minor polishing and sliding tracks in some cases.

Table 4.14: 3-d surface roughness parameters for tested die samples

3-D Surface Roughness Parameter	Tested Die Samples			
	DC 53 + TD Coating	SKD 11 + TD Coating	DRM 3 + TD Coating	DRM 51 + TD Coating
Sq (μm)	6.02	3.55	2.59	6.11
Ssk	-6.96	-6.91	-9.18	-5.33
Sku	86.9	125	192	65.1
Sp (μm)	20.7	15.6	12.3	22.9
Sv (μm)	101	97.7	85.1	107
Sz (μm)	121	113	97.4	130
Sa (μm)	2.94	1.56	1.3	3.12

(a)   *(b)*   *(c)*
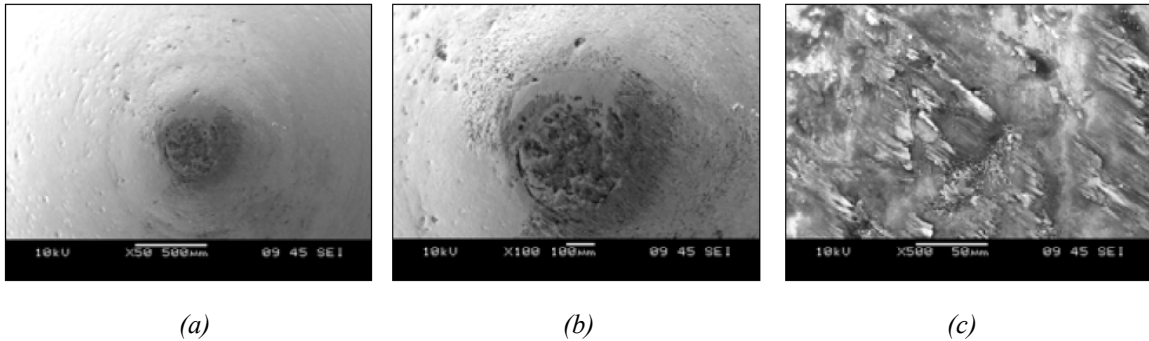
Figure 4.30 SEM picture at the tip of die sample DC 53 with TD coating (Sample # 5-3) with magnifications of a) 50X b) 100X c) 500X

(a)   *(b)*   *(c)*
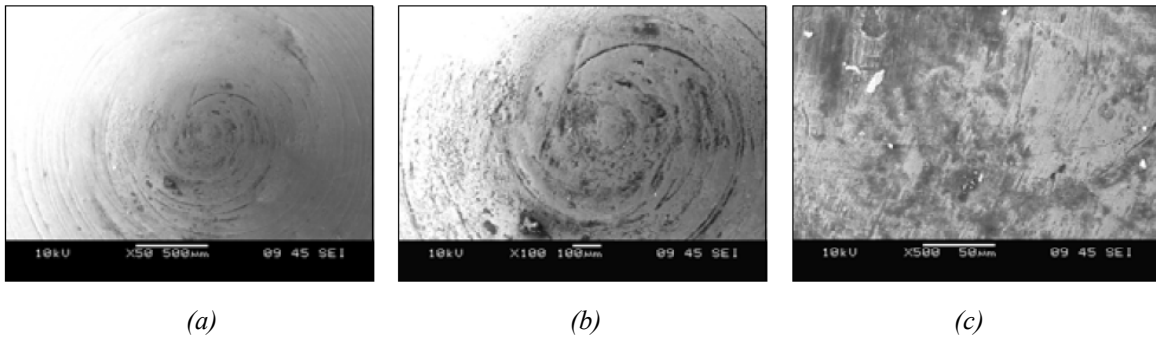
Figure 4.31 SEM picture at the tip of die sample SKD11 with TD coating (Sample # 10-1) with magnifications of a) 50X b) 100X c) 500X

(a)   *(b)*   *(c)*
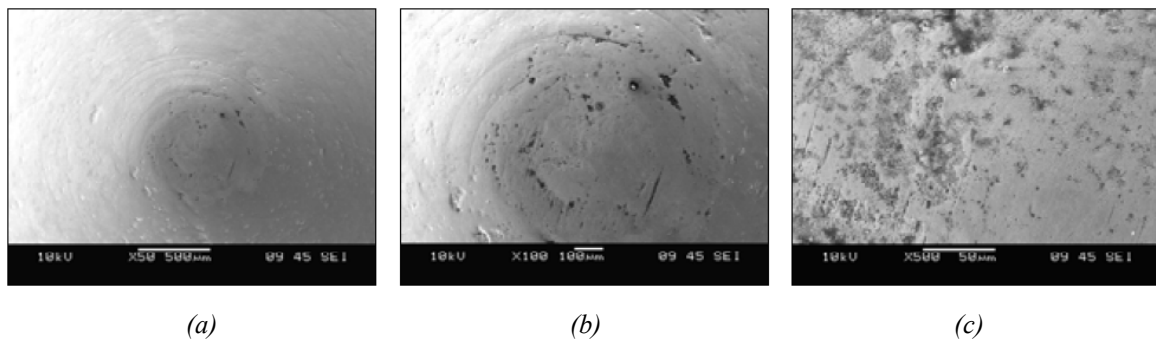
Figure 4.32 SEM picture at the tip of die sample DRM 3 with TD coating (Sample # 11-1) with magnifications of a) 50X b) 100X c) 500X
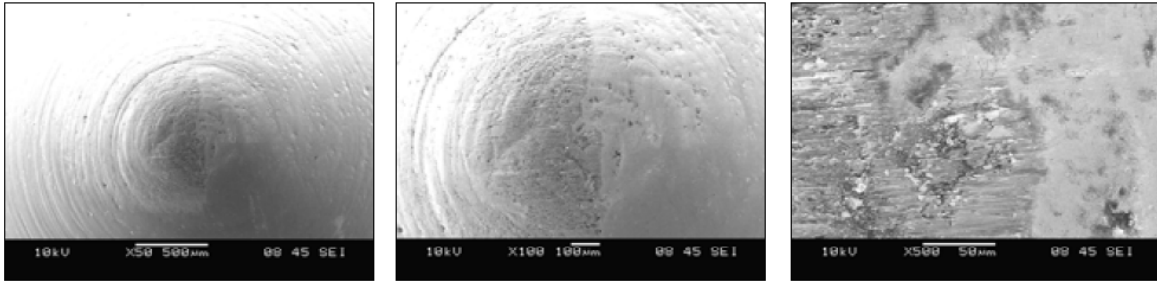
Figure 4.33 SEM picture at the tip of die sample DRM 51 with TD coating (Sample # 12-1) with magnifications of a) 50X b) 100X c) 500X

Specific wear rate calculations based on mass loss measurements were carried out to evaluate the performances of the tested samples, and are given in Figure 4.34. It should be noted that since there was not significant damage on the coating layer and mass losses were insignificant, the specific wear rate calculations did not expose significant differences between tested die samples.

Test results showed that the combination of substrate material and coating technique applied can significantly change the wear resistance compared to performance of the bare/uncoated material. The optimum hardness value for the substrate material and the coating technique applied are the other important factors for improved performance. As can be seen from Table 4.11 that the substrate hardness values for the tested materials varied from 58 to 64 HRC, however, the superiority of the one tested die sample to another is undistinguishable. It is believed that TD coating contributed to improved performance of the tested materials as experienced in previous test stages. In application of TD coating, two separate heat treatments are applied before and after coating process. It is reported by the sample provider that the secondary heat treatment provides higher performance.

Improved surface roughness is verified when the evolution of coefficient of friction during the tests is examined. In particular, friction coefficient for SKD 11 die sample was measured as 0.06 (mean value). It is noticed that the friction coefficient decreases with the increasing load. The stability of coefficient of friction can be explained by the lack of coating removal from the substrate and insignificant topography change on the contact surface.
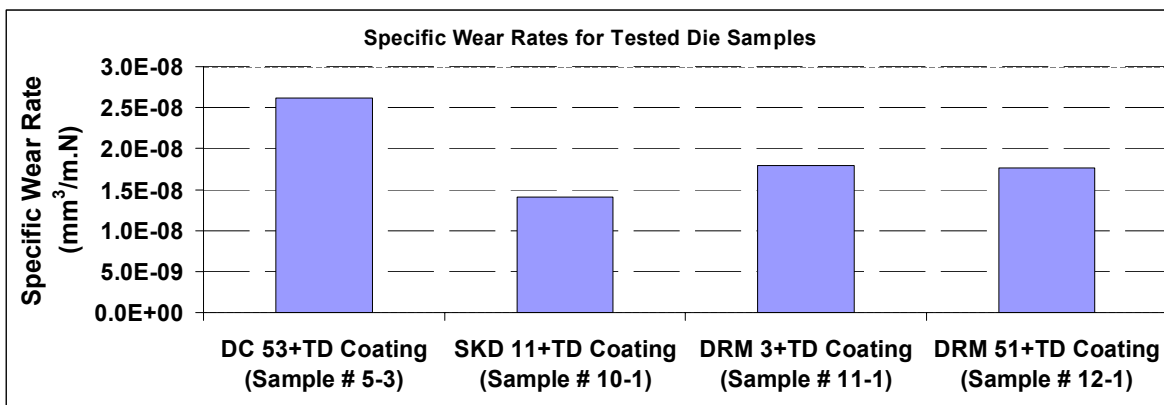
Figure 4.34 Specific wear rates for the tested die samples in Test Group III

4.6.2   Statistical analyses for surface roughness measurements

Similar statistical analyses discussed before were performed on average surface roughness measurements obtained using profilometer. Figure 4.35 demonstrates the average surface roughness variations before and after tests for all tested die samples. In addition to this, normality tests and one-way ANOVA (Analyses of Variables) were performed to evaluate the reliability of surface roughness measurements. It was demonstrated that average surface roughness data for all die samples passed the normality

test. One-way ANOVA statistics resulted in significantly different means and insignificant variance differences (P>0.05) for the used average surface roughness data.
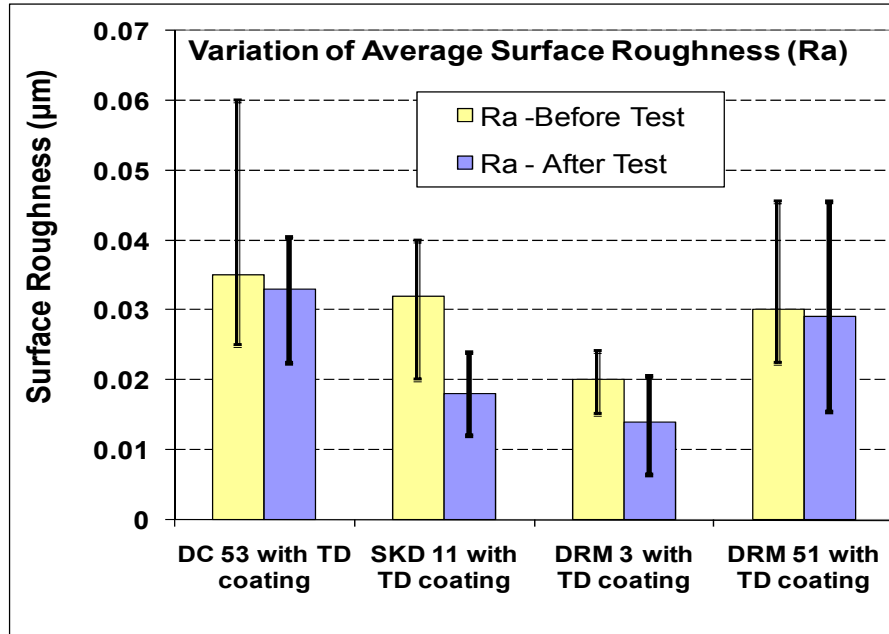
Figure 4.35 Variation of average surface roughness value for the tested die samples

4.7 Test Group IV: Effect of Substrate Hardness, Uncoated DC53 against HDGA DP600

In addition to coated die samples, the test specs given in Table 4.1 include some uncoated die samples, too. Three (3) uncoated DC53 die samples with different substrate hardness values were tested against HDGA DP 600 (US Steel) sheet blanks for 1.6km long test distance. Test length, as can be noticed, was less compared to previous test groups since uncoated surfaces were more prone to wear. When the quantifiable amount of wear experienced in the test of first sample in the list, the duration (or the test length completed

till that time) was set as test length for other samples. Two samples with same substrate hardness value for three different cases, in total six die samples, were used for repetition purposes as can be seen in Table 4.15.

Table 4.15 Test Group IV die sample properties

Sample #	Grade	Hardness (HRC)	Coating
1-1		59.5	
1-2			
2-1	DC 53	60.8	Uncoated
2-2			
3-1		63	
3-2			

4.7.1 Experimental results and discussion for Test Group IV

As expected and observed in testing of uncoated die materials with 1st generation test set-up discussed in Chapter III, the uncoated die samples showed lower wear resistance, resulting in severe form of wear such as galling and scoring. It is also noted that the worn surface area was larger for uncoated samples compared to coated samples that previously tested. Figure 4.36 through Figure 4.41 shows both optical and confocal microscope images of the tested die samples. 3-d confocal microscope images were quite useful in identifying the peak/valley spots which illuminates whether material pile-up from sheet surface or removal from die sample surface occurred. A slight increasing trend in surface texture irregularity was observed with the increasing hardness value of tested material.

129
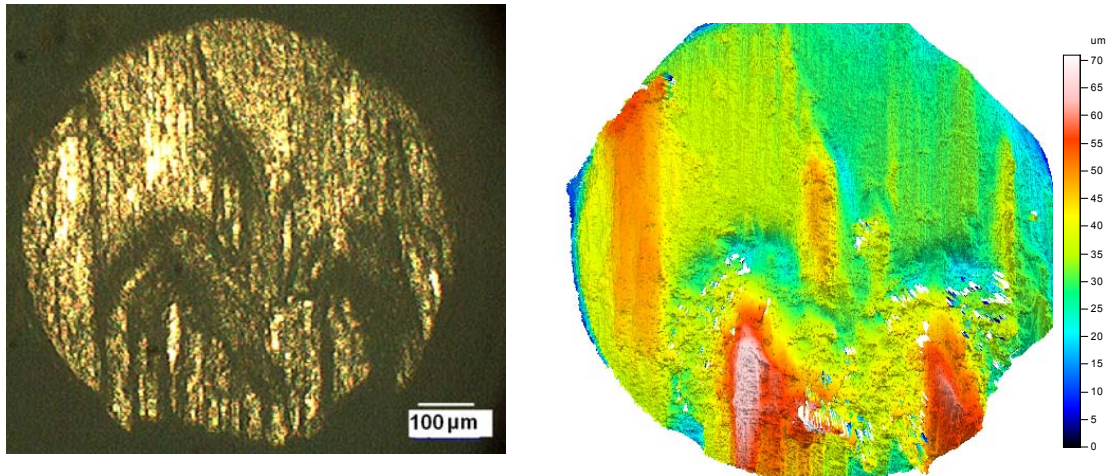
Figure 4.36 Optical (on the left) and confocal (on the right) microscope images of the uncoated DC 53 sample (Sample # 1-1) surface after the test
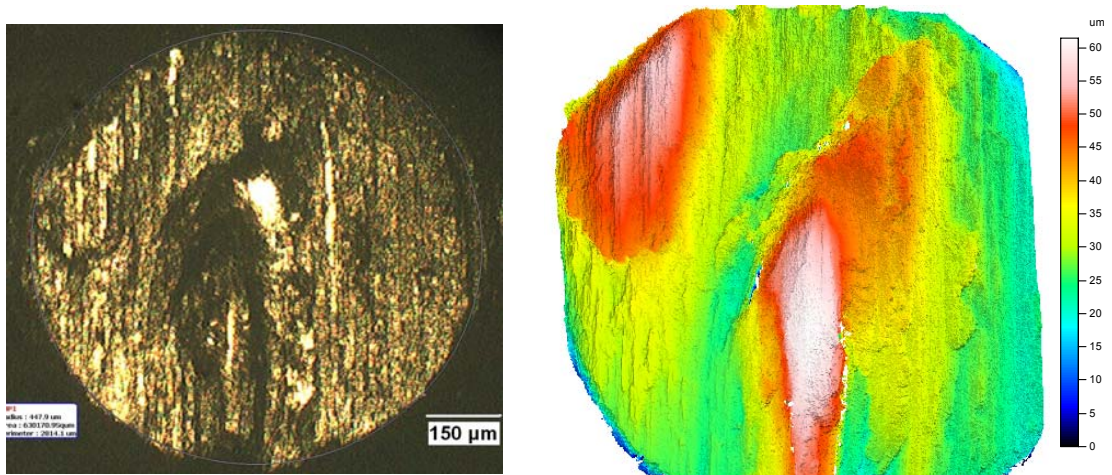
Figure 4.37 Optical (on the left) and confocal (on the right) microscope images of the uncoated DC 53 sample (Sample # 1-2) surface after the test
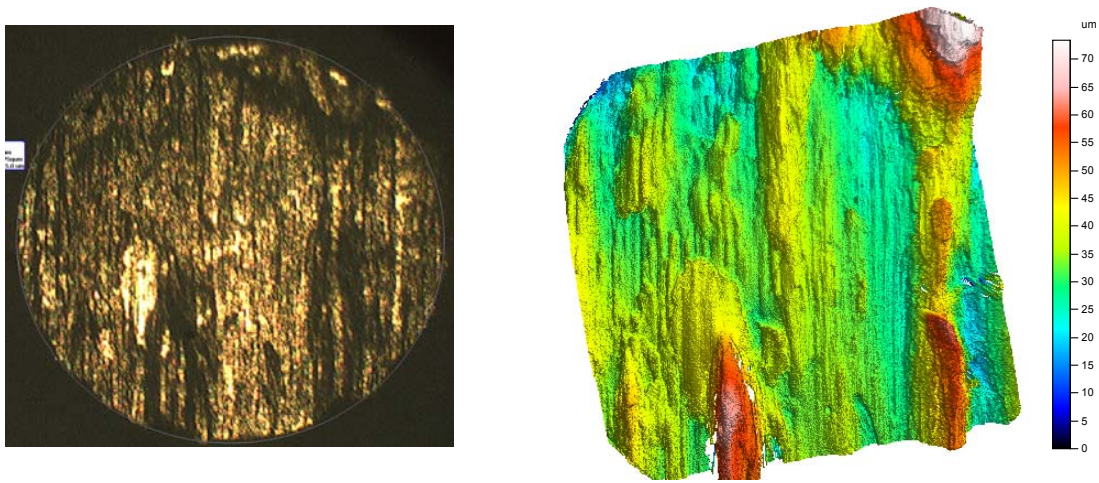
Figure 4.38 Optical (on the left) and confocal (on the right) microscope images of the uncoated DC 53 sample (Sample # 2-1) surface after the test
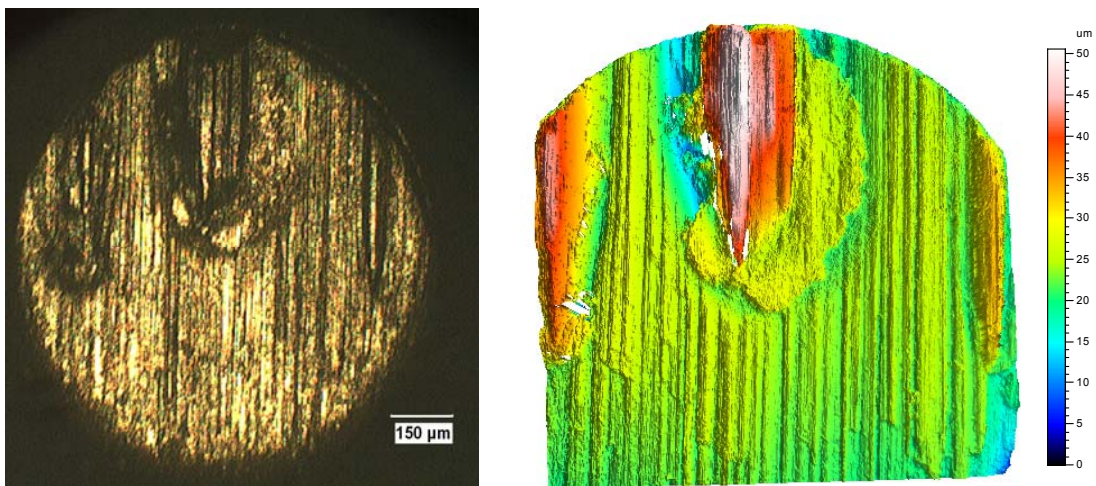
Figure 4.39 Optical (on the left) and confocal (on the right) microscope images of the uncoated DC 53 sample (Sample # 2-2) surface after the test
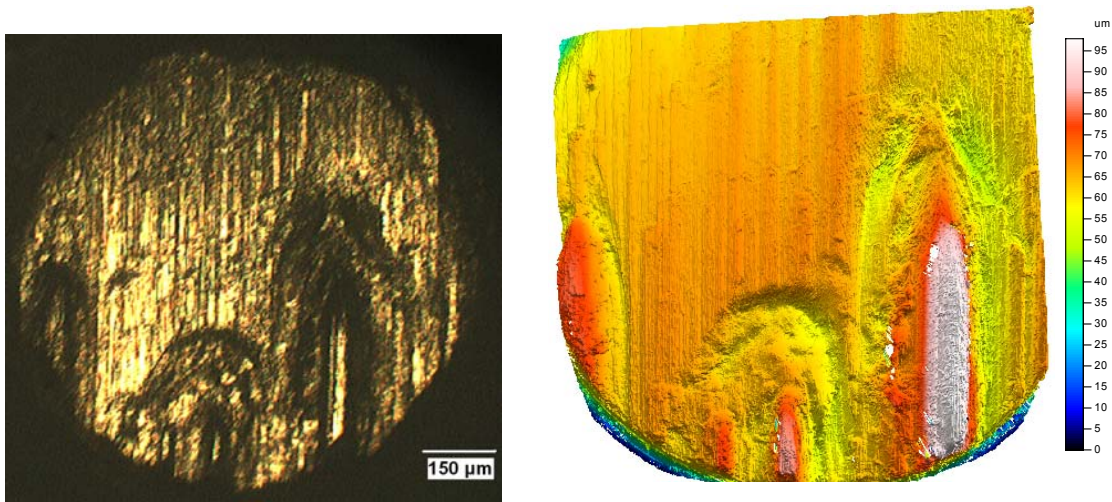
Figure 4.40 Optical (on the left) and confocal (on the right) microscope images of the uncoated DC 53 sample (Sample # 3-1) surface after the test
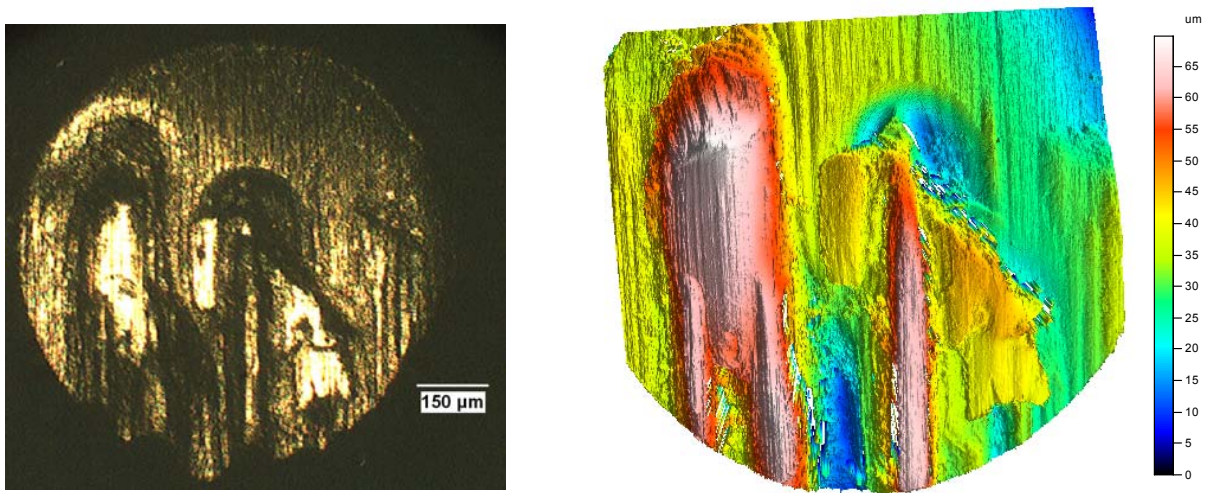
Figure 4.41 Optical (on the left) and confocal (on the right) microscope images of the uncoated DC 53 sample (Sample # 3-2) surface after the test

Specific wear rate calculations given in Figure 4.42 verified the microscopically observed increased wear behavior with increasing substrate hardness value. 3-d surface roughness measurements were also in agreement that the surface roughness values for the

die sample with higher hardness were vaguely higher than the ones for other tested samples. For example, average area, root-mean-square roughnesses, and ten-point-heights, maximum valley depth values were higher for third group of sample as shown in Table 4.16. Skewness values experienced were in narrow range close to zero implying relatively flat and more uniformly worn surfaces compare to previously tested samples.
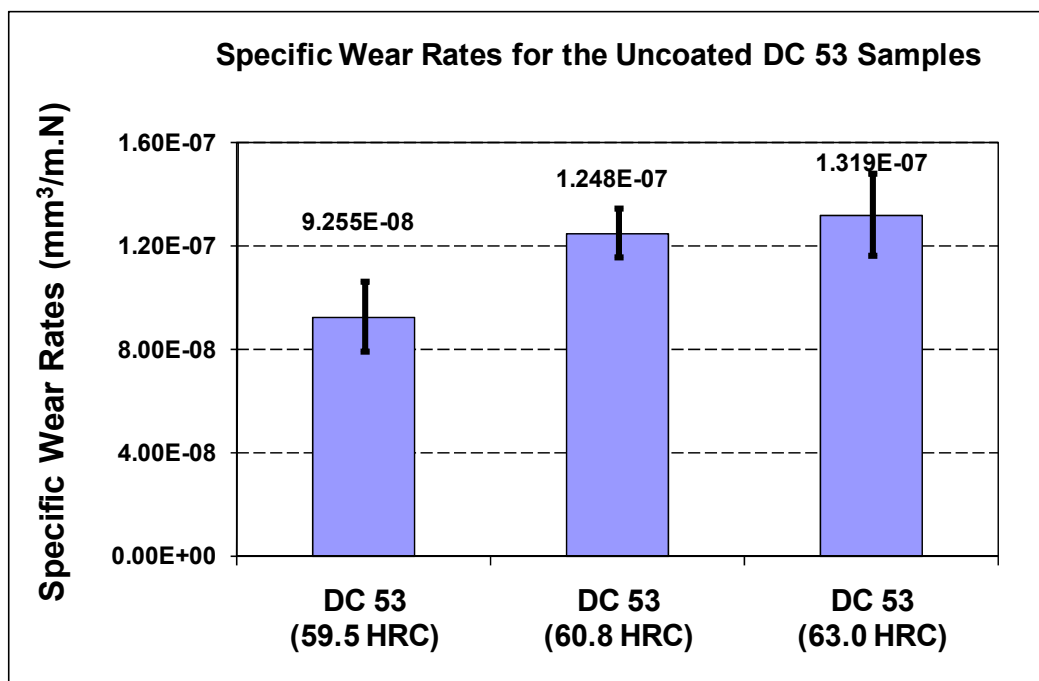
Figure 4.42 Specific wear rates for uncoated DC 53 die samples with 3 different substrate hardness values

Table 4.16 3D surface roughness values for Test Group IV samples

Roughness Parameter	Tested Die Samples					
	DC 53 #1-1	DC 53 #1-2	DC 53 #2-1	DC 53 #2-2	DC 53 #3-1	DC 53 #3-2
S_q (µm)	5.28	3.68	4.74	3.5	5.23	6.77
S_{sk}	-1.06	-0.664	0.0648	-0.0935	-0.574	-0.389
S_{ku}	10.9	12.1	9.58	6.47	22.6	6.55
S_p (µm)	21.5	13.7	23.3	12.5	22.4	22.3
S_v (µm)	47.8	39.2	46	29.2	71	49.3
S_z (µm)	69.3	52.8	69.3	41.7	93.4	71.5
S_a (µm)	3.62	2.56	3.29	2.33	3.05	4.86

4.8 Test Group V: Effect of Coating and Effect of Substrate Materials against DP600 from SSAB

After completing the first set of samples, second and third set of samples were tested with same test procedures, except small differences such as different sheet blank use, increased test duration or average contact normal load. The information about the die samples tested in this group is given in Table 4.17. As can be seen from the table that two different group of samples tested in this phase. First set of samples were from "Effect of coating type tests" group (samples numbered with 7, 8, and 9) while the other samples were from "Effect of substrate material tests" group (samples numbered with 10, 11, 12). Different from the first set of tests, these two groups did not include DC 53+ TD coated samples since all three samples tested in different test groups previously.

Table 4.17 Die sample configuration, and substrate hardness values for Test Group V

Sample #	Substrate material	Coating	Substrate Hardness Measured (HRC)	Sheet Blank	Test Length (km)
7-2	DC 53	Radical Nitriding+ TiCN (PVD)	61.3	DP 600 (SSAB)	2.5
7-3					
8-2	DC 53	TiCN (PVD)	61.2	DP 600 (SSAB)	2.5
8-3					
9-2	DC 53	TiC, TiCN, TiN (CVD)	63.1	DP 600 (SSAB)	2.5
9-3					
10-2	SKD 11	TD	58	DP 600 (SSAB)	4
10-3					
11-2	DRM 3	TD	64.3	DP 600 (SSAB)	4
11-3					
12-2	DRM 51	TD	63.8	DP 600 (SSAB)	4
12-3					

The sheet blanks used in this group of test was a commercially available cold reduced dual phase steels Docol DP 600 that is produced and was complimentarily provided by SSAB (Svenskt Stål AB, Sweden). Different from the formerly used DP 600 sheet blanks provided by US Steel, this sheet blank had no coating on them. Hardness measurements were performed on the sheet blanks and compared with the ones obtained for previously used US Steel DP 600 sheet blanks. There was no significant difference between the hardness values and this was confirmed with the t-test approach, too. The chemical composition of the Docol DP 600 sheet blanks is given in Table 4.18. Based on the first set of experimental results, the test length for "Effect of Coating Type" group of samples was

initially set as 2km, however; insignificant wear was obtained after 2 km tests and test length was extended to 2.5km. Similarly, since negligible amount of wear were experienced in testing of "Effect of Substrate Material" group of samples discussed in Section 4.6, the test length for the second and third set of samples was firstly set as 3 km. After 3 km of test length, immeasurable levels of wear was experienced for all tested samples, thereby the test length was extended to 4 km. In addition to lengthened tests, the average contact normal loads (220-245 N) were facilitated.

Table 4.18 Chemical composition of Docol DP 600 advanced high strength steel sheet blanks [*SSAB Docol DP/DL Datasheet, 2009*]

Material Grade	Chemical Composition						
	C	Mn	Si	Al	S	P	Nb
Docol DP 600	0.100	0.800	0.200	0.040	0.002	0.010	0.015

4.8.1 Experimental results and discussion for Test Group V

Surface examinations using optical and confocal microscopes given in Figure 4.43 through Figure 4.47 showed that negligibly small coating failures were experienced for "Effect of coating type" group of samples, although higher contact normal load and longer test distances were employed. Unlike from others, the coating was partly removed from the surface of one of the CVD coated samples surface (Sample # 9-3 given in Figure 4.47), without any sliding or polishing marks. It was concluded that coating failure mechanism might be fracture due to uncontrollable instantaneous peak forces during the tests rather than adhesive wear.
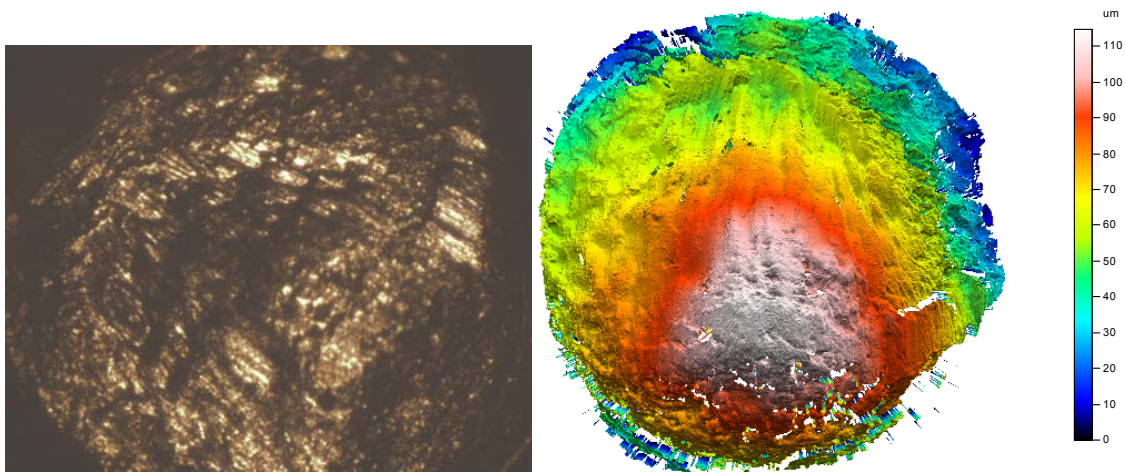
Figure 4.43 Optical (on the left) and confocal (on the right) microscope images for DC 53 sample with radical nitriding+ TiCN (PVD) coating (Sample # 7-2)
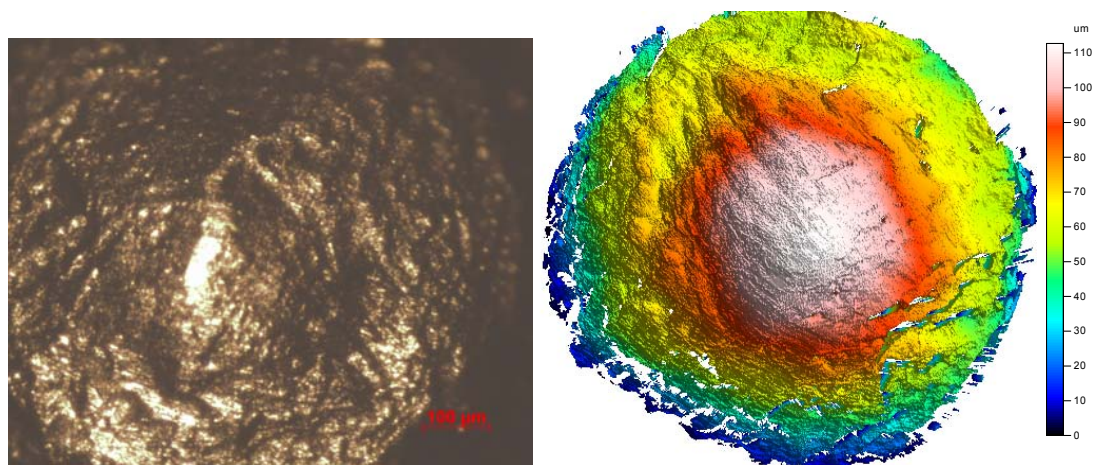
Figure 4.44 Optical (on the left) and confocal (on the right) microscope images for DC 53 sample with radical nitriding+TiCN (PVD) coating (Sample # 7-3)
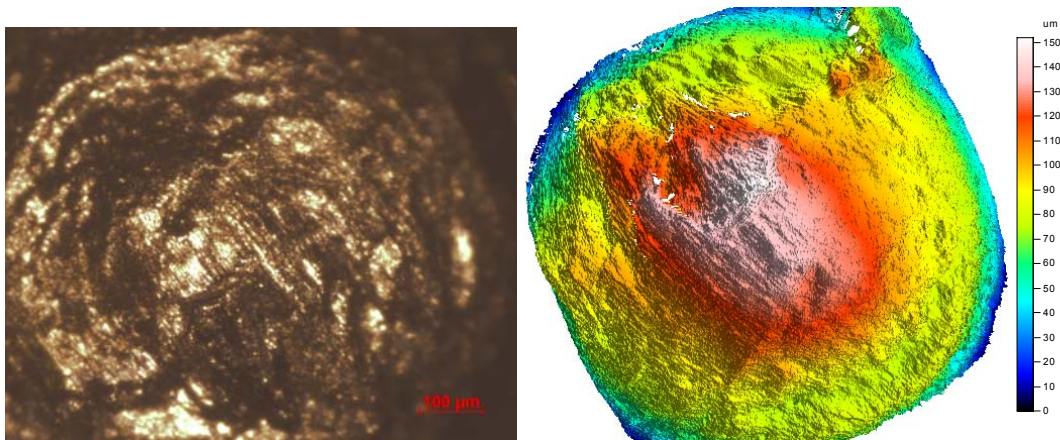
Figure 4.45 Optical (on the left) and confocal (on the right) microscope images for DC 53 sample with TiCN (PVD) (Sample # 8-2)
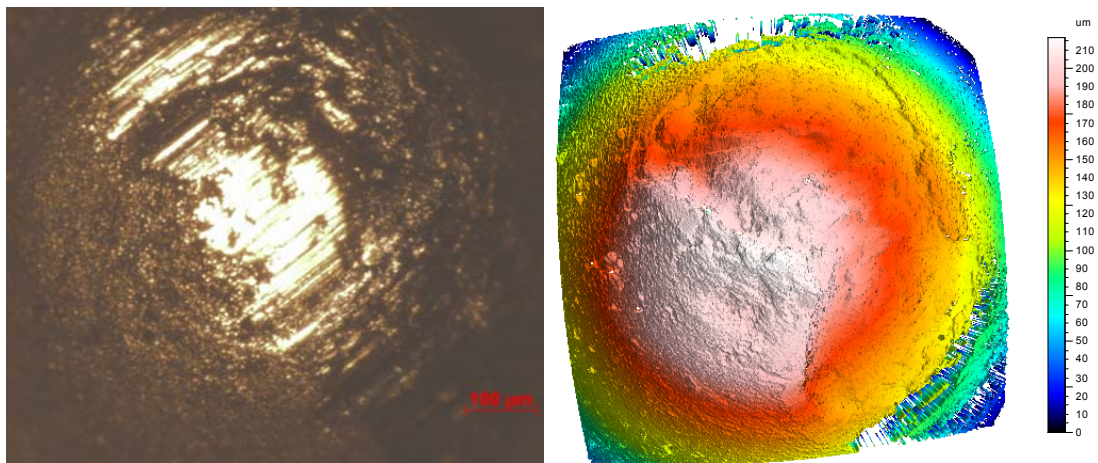
Figure 4.46 Optical (on the left) and confocal (on the right) microscope images for DC 53 sample with TiC+TiCN+TiN (CVD) coating (Sample # 9-2)
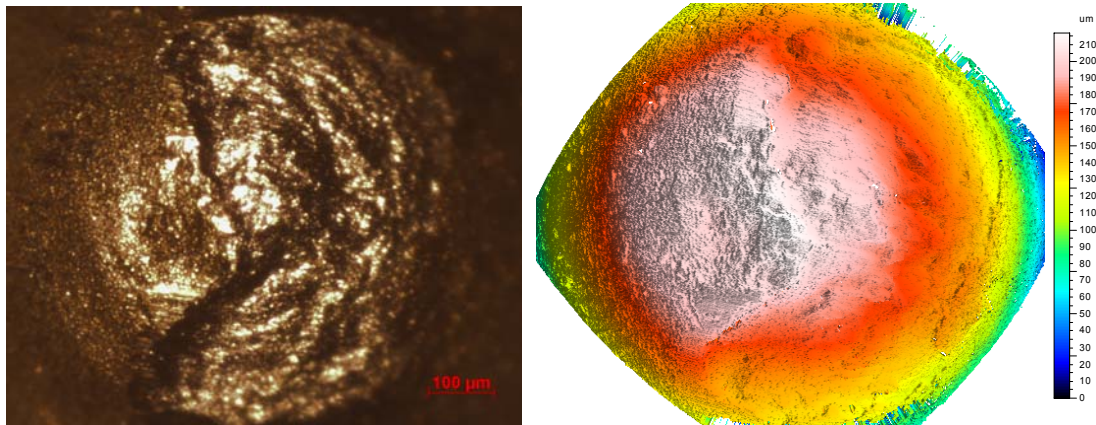
Figure 4.47 Optical (on the left) and confocal (on the right) microscope images for DC 53 sample with TiC+TiCN+TiN (CVD) coating (Sample # 9-3)

Representative SEM pictures of these samples are given in Figure 4.48 through Figure 4.50. In calculation of specific wear rates, since the mass losses were not quantifiable for some cases, the values shown in Figure 4.51 are based on one sample results from each die sample + coating configuration (samples numbered with 7-3, 8-2, 9-3 used). Based on this data, the performance of DC53 sample coated with radical nitriding and PVD was higher compared to PVD and CVD coated samples. This fact is in agreement with the optical and confocal microscope examinations of the surfaces. It is noted that the specific wear rate values considerably higher when related Test Group II and Test Group V samples are compared. 3D surface roughness measurements presented in Table 4.19 demonstrated that average and root-mean square roughnesses are relatively close to each other compared to other measured parameters. Skewness values were interpreted that the valleys dominates the measurement surface. Kurtosis values denoted the availability of high peaks and valleys which was confirmed with S_p and S_v values.
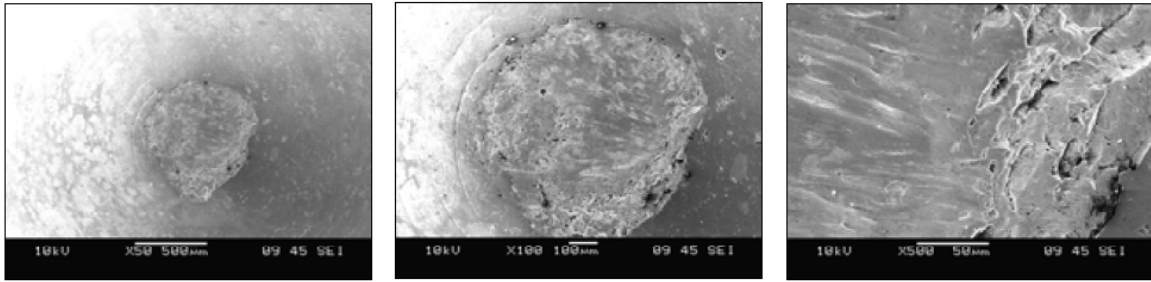
Figure 4.48 SEM picture at the tip of DC 53 die sample with radical nitriding + TiCN (PVD) coating (Sample # 7-2) with magnifications of a) 50X, b) 100X, c) 500X
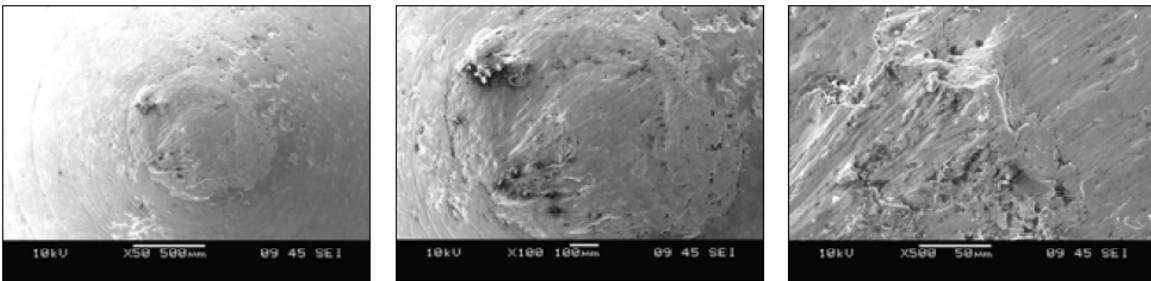
Figure 4.49 SEM picture at the tip of DC 53 die sample with TiCN (PVD) coating (Sample # 8-2) with magnifications of a) 50X, b) 100X, c) 500X
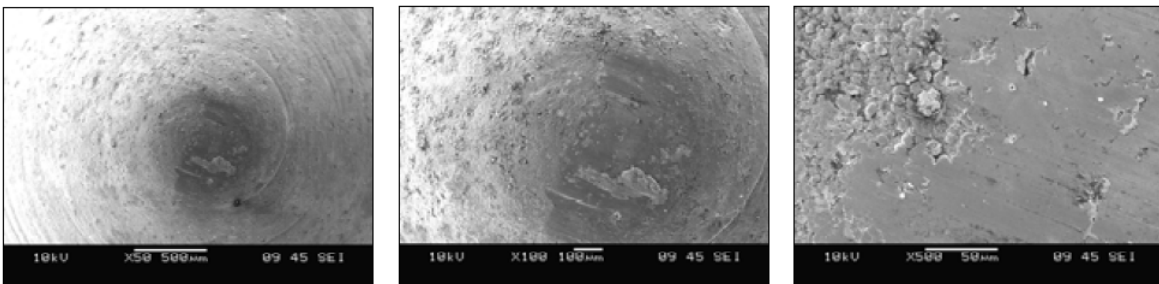
Figure 4.50 SEM picture at the tip of DC 53 die sample with TiC, TiCN, TiN (CVD) coating (Sample # 9-2) with magnifications of a) 50X, b) 100X, c) 500X
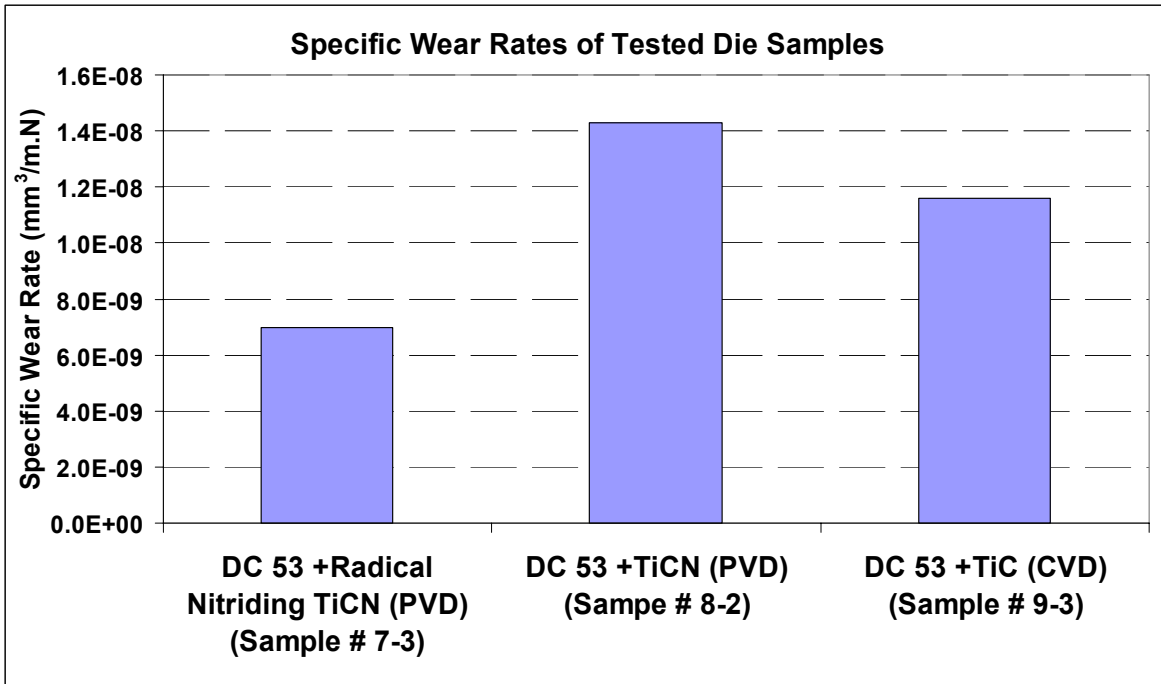
Figure 4.51 Specific wear rates of the "Effect of coating type" study samples tested in Group V

Table 4.19 Surface area roughness values for tested die samples

Roughness Parameter	Tested Die Samples				
	Sample # 7-2	Sample # 7_3	Sample # 8_2	Sample # 9_2	Sample # 9_3
S_q (µm)	6.05	5.11	5.02	2.95	3.64
S_{sk}	-4.05	-3.74	-2.6	-3.17	-13.4
S_{ku}	39.8	40.4	41.7	77.5	453
S_p (µm)	17.1	20.6	24.3	12.7	14.3
S_v (µm)	97.9	82.3	120	89.4	186
S_z (µm)	115	103	144	102	200
S_a (µm)	3.54	2.98	3.31	1.99	2.11

Microscope pictures for "Effect of substrate material" study die samples tested in Test Group V are presented in Figure 4.52 through Figure 4.57. As mentioned before, although higher contact normal loads and longer test distances were facilitated, the TD coatings were not fully failed nor removed from the substrate surfaces. Partial coating cracks were observed in some cases. SEM pictures for some of the tested die samples are shown in Figure 4.58 to Figure 4.60. Microscope and SEM pictures demonstrated that TD coatings were broken off fractionally with an unsymmetrical manner in some cases. It was also noticed from the comparison of SEM pictures that the damage level on coating layer for the current die samples (Figure 4.58 through Figure 4.60) were relatively higher compared to effect of coating type die samples tested in this group (Figure 4.48 through Figure 4.50).
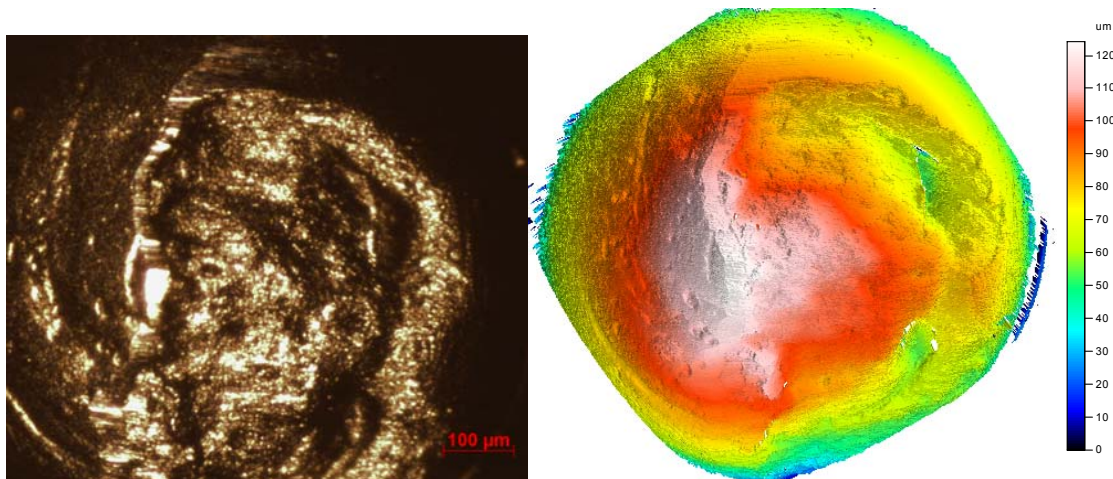
Figure 4.52 Optical (on the left) and confocal (on the right) microscope images for SKD 11 sample with TD coating (Sample # 10-2)
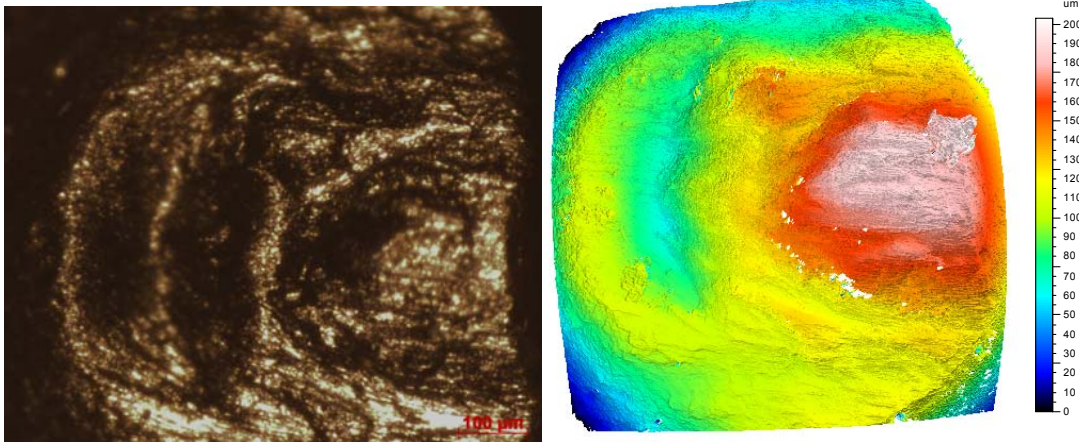
Figure 4.53 Optical (on the left) and confocal (on the right) microscope images for SKD 11 sample with TD coating (Sample # 10-3)
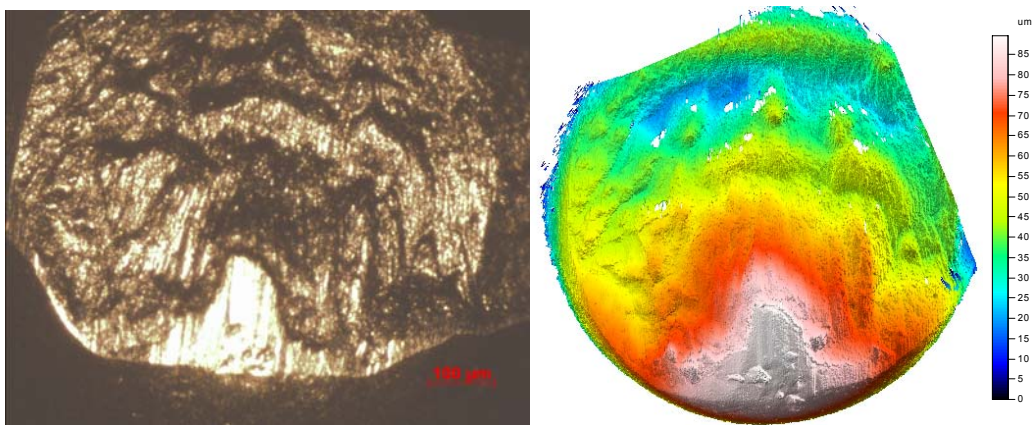
Figure 4.54 Optical (on the left) and confocal (on the right) microscope images for DRM 3 sample with TD coating (Sample # 11-2)
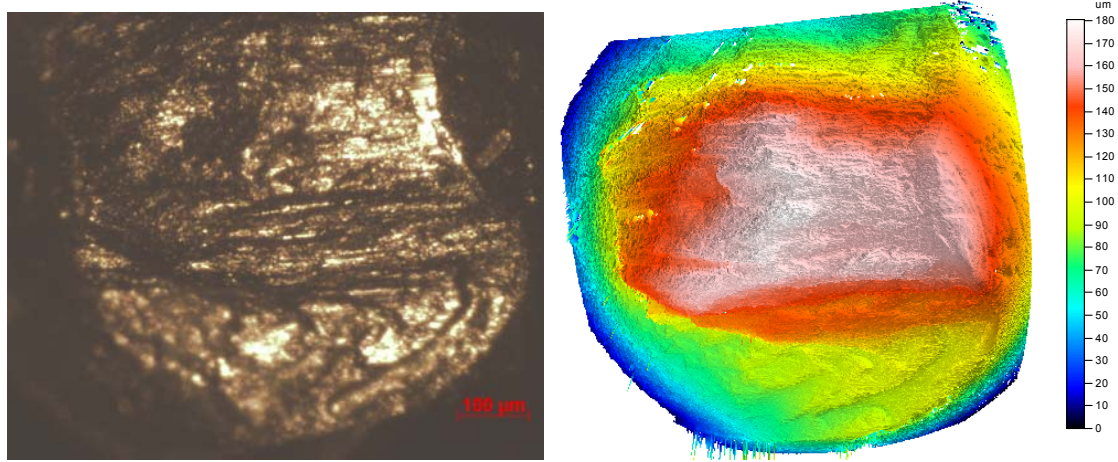
Figure 4.55 Optical (on the left) and confocal (on the right) microscope images for DRM 3 sample with TD coating (Sample # 11-3)
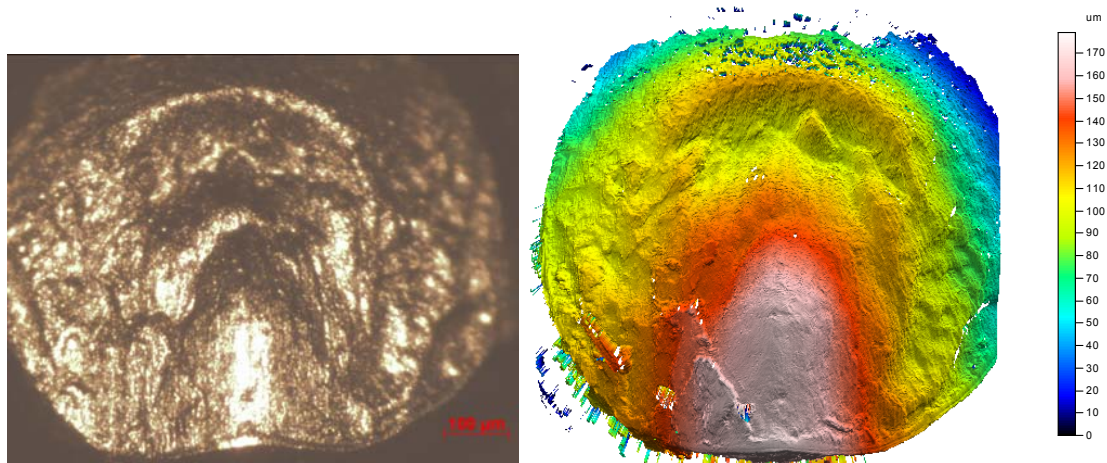
Figure 4.56 Optical (on the left) and confocal (on the right) microscope images for DRM 51 sample with TD coating (Sample # 12-2)
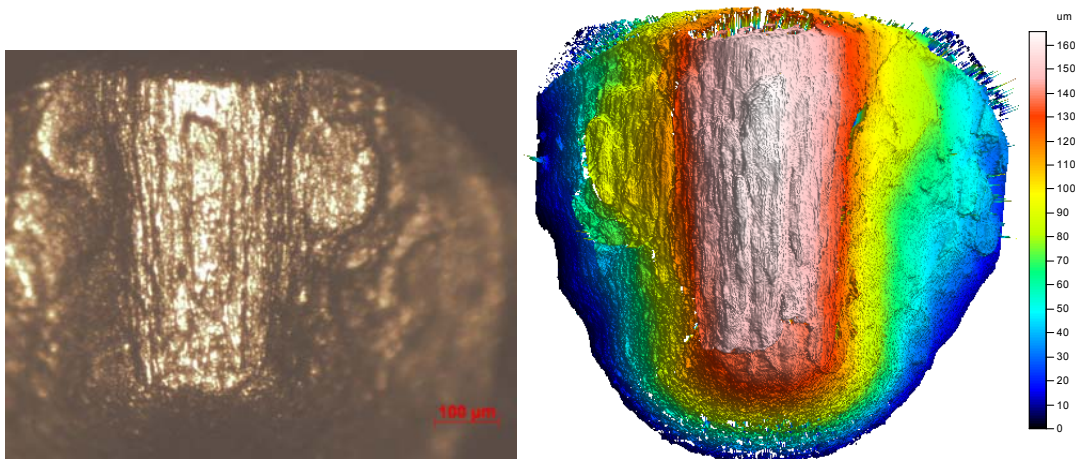
Figure 4.57 Optical (on the left) and confocal (on the right) microscope images for DRM 51 sample with TD coating (Sample # 12-3)
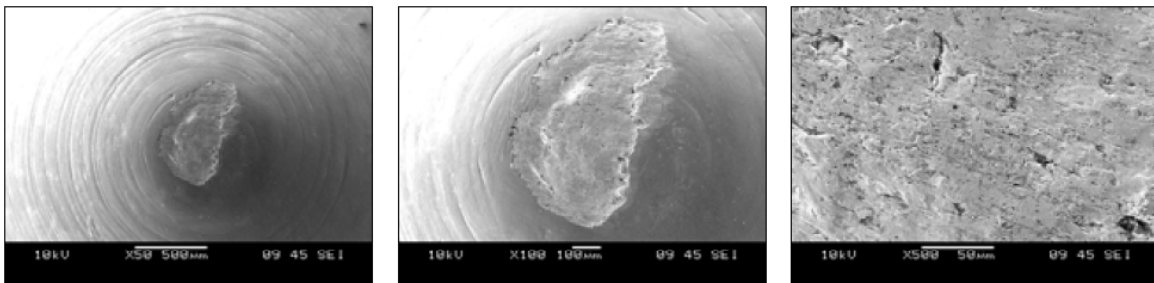
Figure 4.58 SEM picture at the tip of SKD 11 die sample with TD coating (Sample # 10-3) with magnifications of a) 50X, b) 100X, c) 500X
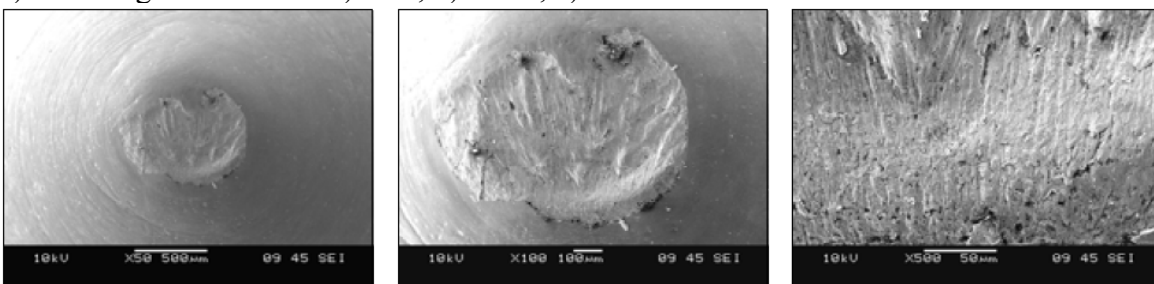
Figure 4.59 SEM picture at the tip of DRM 3 die sample with TD coating (Sample # 11-2) with magnifications of a) 50X, b) 100X, c) 500X
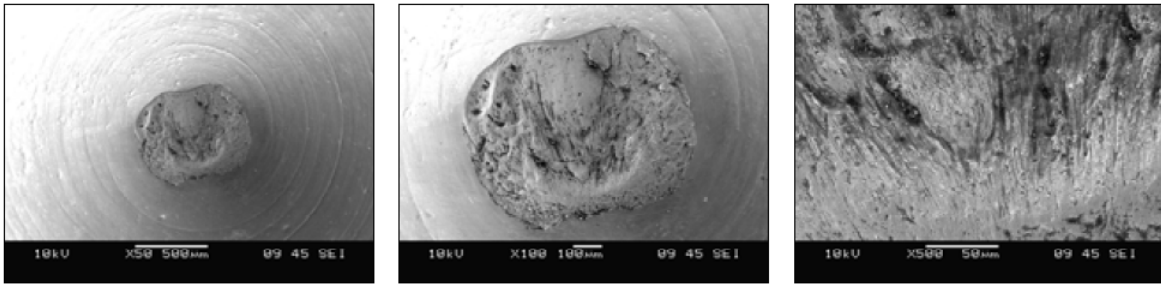
Figure 4.60 SEM picture at the tip of DRM 51 die sample with TD coating (Sample # 12-2) with magnifications of a) 50X, b) 100X, c) 500X

3D surface roughness measurements and specific wear rate values for the "Effect of substrate material" die samples tested in Test Group V are presented in Table 4.20, and Figure 4.61, respectively. Relatively low roughness, skewness, and kurtosis values were obtained for sample # 11-2. In particular, average surface area roughness value was obtained as lowest as 2.31 μm for die sample # 10-2 while highest values obtained for die sample # 10-3 as 5.45 μm. Comparatively higher values for maximum peak and deepest valley measurements were experienced probably due to large boundary area selection that not only covers contact points but also some points in lateral surface of the die sample tip that were not in contact with the sheet metal continuously. TD coating applied DRM 3 sample was the die sample that had lower mass loss, consequently specific wear rate that stands for higher wear resistance. The specific wear rate value could not be calculated for sample # 10-2 because of unquantifiable mass loss was encountered for this sample. Therefore, the specific wear rate values presented in Figure 4.61 are averages of two samples except the one for SKD 11 sample.

146

Table 4.20 Surface area roughness values for "Effect of substrate material" study die samples tested in Test Group V

Roughness Parameter	Tested Die Samples					
	Sample # 10-2	Sample # 10_3	Sample # 11_2	Sample # 11-3	Sample # 12-2	Sample # 12-3
S_q (µm)	3.64	7.65	3.43	6.85	9.17	8.4
S_{sk}	-4.25	-2.81	-0.476	-2.23	-3.97	-3.38
S_{ku}	64.8	32.6	6.25	31.8	51.3	37.3
S_p (µm)	14.6	33	14.1	41.3	31.2	37.4
S_v (µm)	84.3	142	43.8	121	151	124
S_z (µm)	99	175	57.9	163	182	161
S_a (µm)	2.31	5.45	2.71	4.5	5.33	5.33
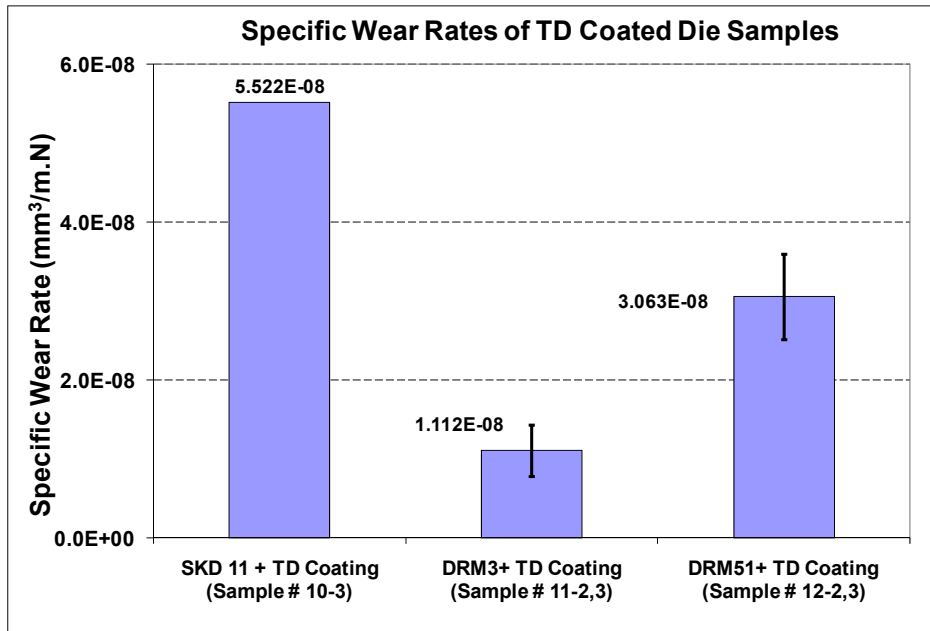
Figure 4.61 Specific wear rates for the "Effect of substrate material" study die samples tested in Group V

4.9 Test Group VI: Effect of Substrate Hardness, TD Coated DC53 against DP800

   from SSAB

   As final group of the tests, TD coated DC 53 samples with different substrate
hardness values were tested against Docol DP 800 (ultimate tensile strength of 800 MPa)
type sheet blanks provided by SSAB. Based on the first set test results for "Test Group I:
Effect of substrate hardness" study in which coatings did not failed at all in all cases,
increased test lengths (4 km), and relatively higher average contact normal loads (250–
290N) were employed in testing of second and third group of samples. As can be noticed
from Table 4.1 that the "Effect of substrate material" study consisted of three different
samples (samples numbered with 4, 5, and 6), however; since sample # 5 was included in
other studies too, and an extra sample was not available, it could not be exploited here.
Similarly, a different grade sheet blank was utilized since DP 600 blanks provided by
supplier were not enough to test current die sample test group, a whole new grade of sheets
were used to cover all the die samples. Table 4.21 and Table 4.22 presents the tested die
sample information, and chemical composition of sheet blanks used in this group of tests.
Hardness measurements, in Rockwell B and micro-Vicker hardness scales, performed on
Docol DP 800 sheet blanks demonstrated statistically significant differences compared to
hardness values of formerly used DP 600 sheet blanks. Hardness measurements for each
blank type were subjected to D'Agostino and Pearson omnibus normality test using Prism
software v.5 (GraphPad Software Inc, La Jolla, CA). Normality test is accepted as
prerequisite for performing t-tests. After confirming that the measurements had Gaussian
type distribution, t-tests for measurement groups were executed. It was found that means

between hardness values of two different DP 600 sheet blanks were not significant, while their means were significantly different when compared to ones for DP 800 sheet blanks. It was concluded that it is not appropriate to compare test results of group I samples where DP 600 sheet blanks used with the ones for group VI, (Samples # 4-1, 6-1 in Test Group I, vs. Samples # 4-2, 4-3, 6-2, 6-3), even though they were produced to have same properties. Figure 4.62 shows a typical micro-hardness measurement using Duramin-5 (Struers Inc. Westlake, OH, USA) Vickers micro-hardness tester while Figure 4.63 demonstrate the comparison of hardness values for sheet blanks used in this study obtained in Rockwell scale B.

Table 4.21 Die sample configuration, and substrate hardness values for Test Group VI

Sample #	Substrate material	Coating	Substrate Hardness Measured (HRC)	Sheet Blank	Test Length (km)
4-2	DC 53	TD	58.7	DP 800 (SSAB)	4
4-3					
6-2	DC 53	TD	62	DP 800 (SSAB)	4
6-3					

Table 4.22 Chemical composition of Docol DP 800 advanced high strength steel sheet blanks [*SSAB Docol DP/DL Datasheet, 2009*]

Material Grade	Chemical Composition						
	C	Mn	Si	Al	S	P	Nb
Docol DP 800	0.130	1.500	0.200	0.040	0.002	0.010	0.015
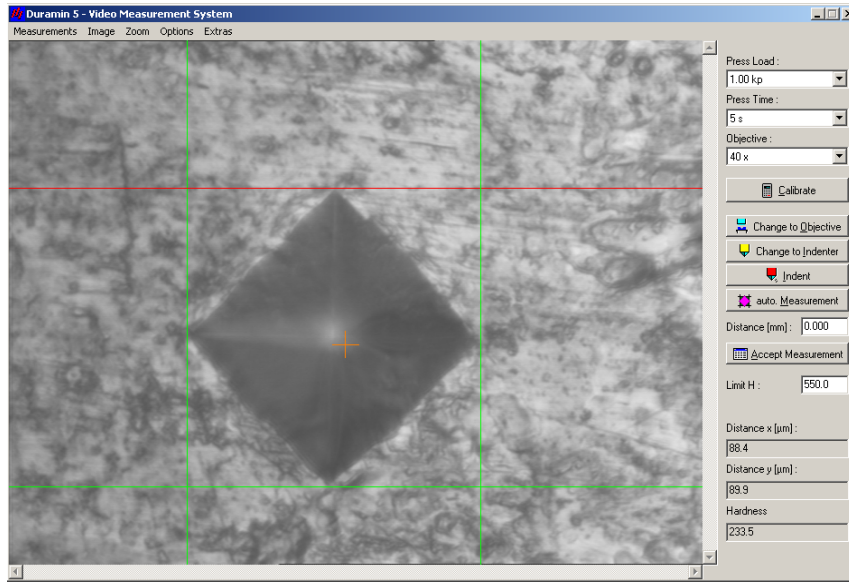
Figure 4.62 Typical micro-Vickers hardness measurement result from Duramin 5 (Struers) for SSAB Docol DP 800 sheet blank (HV$_1$: 233.5)
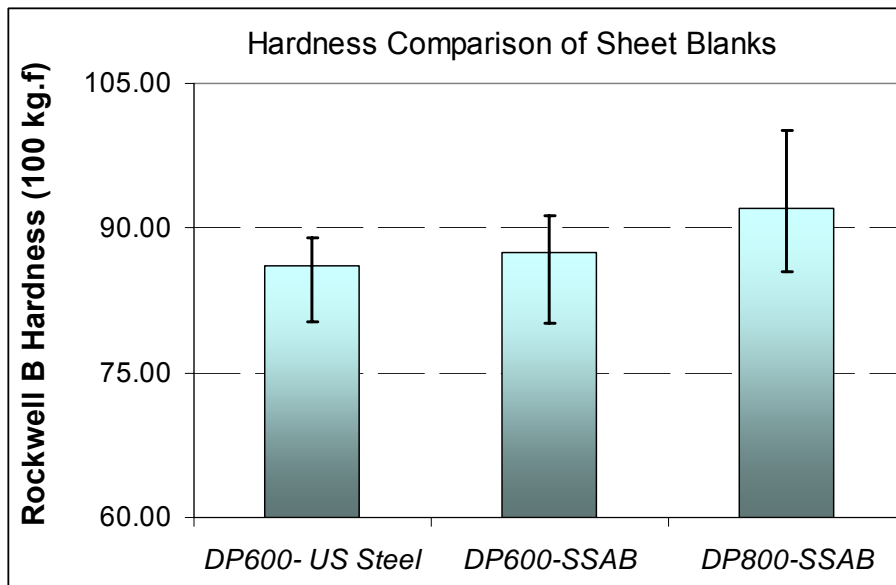
Figure 4.63: Rockwell B scale hardness measurements of the sheet blanks used in this study

4.9.1 Experimental results and discussion for Test Group VI

In testing last group of samples same measurement techniques were employed. Special to this group of samples confocal microscope examination of die samples were obtained both before and after tests. Figure 4.64 through Figure 4.67 demonstrates the optical microscope picture of before test sample, before and after test confocal microscope pictures of the samples, correspondingly. As can be noticed that surfaces were considerably smooth prior to tests, and symmetric height profile was observed at the tip. Interaction with sheet blank mainly occurs at red-light red area colored tip of the die sample, lateral surfaces contact with the sheet blank as the die sample indents to sheet blank, though. Careful examination of confocal microscope pictures obtained both before and after tests confirmed that both material removal from die sample and pile-up from sheet blank occurred.

(a)   *(b)*   *(c)*
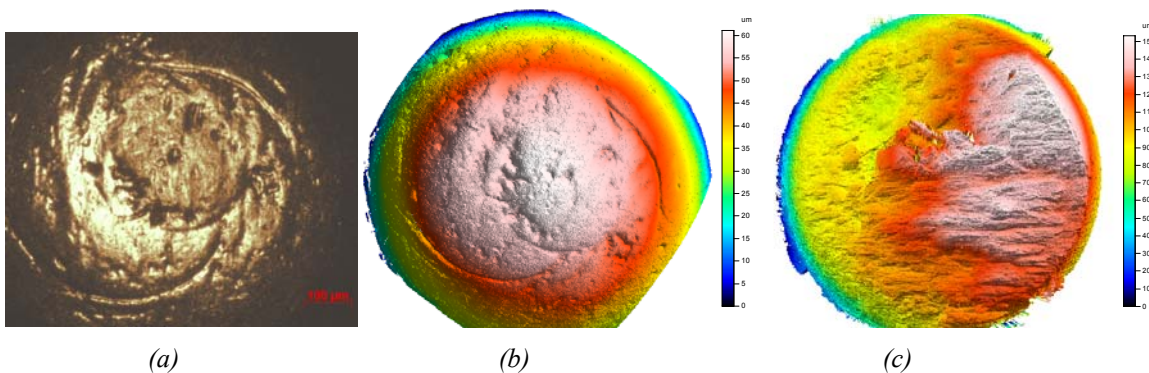
Figure 4.64 Contact surface pictures for DC 53 sample with TD coating (Sample # 4-2) before test obtained by (a) optical, (b) confocal microscope; (c) after test view of contact surface obtained by confocal microscope

(a)   *(b)*   *(c)*
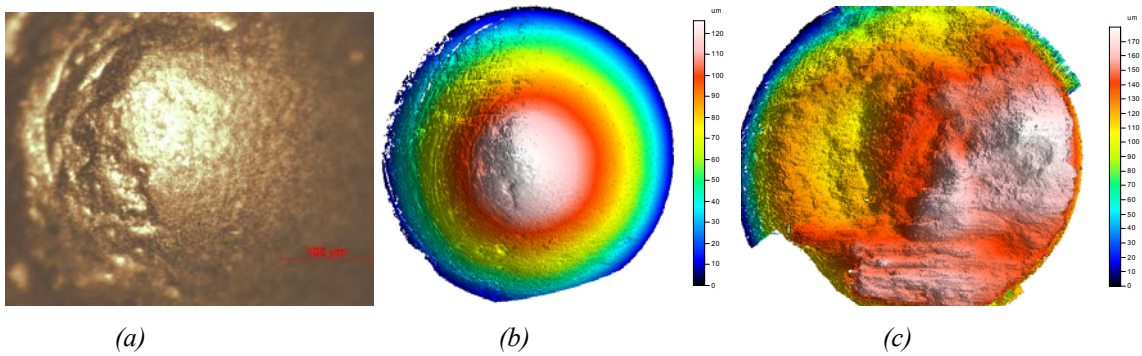
Figure 4.65 Contact surface pictures for DC 53 sample with TD coating (Sample # 4-3) before test obtained by (a) optical, (b) confocal microscope; (c) after test view of contact surface obtained by confocal microscope

(a)

(b)   *(c)*   *(d)*
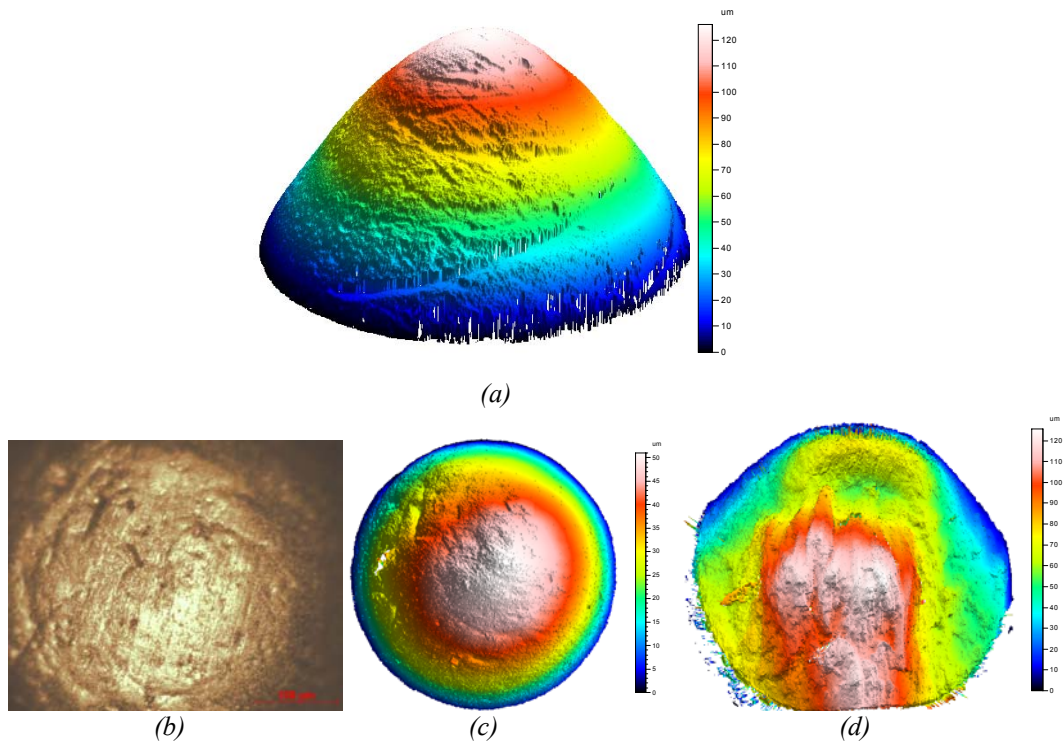
Figure 4.66 Contact surface pictures for DC 53 sample with TD coating (Sample # 6-2) before test obtained by (a) side view with confocal, (b) top view with optical, (c) top view with confocal microscope; (c) after test view of contact surface obtained by confocal microscope

(a)   *(b)*   *(c)*
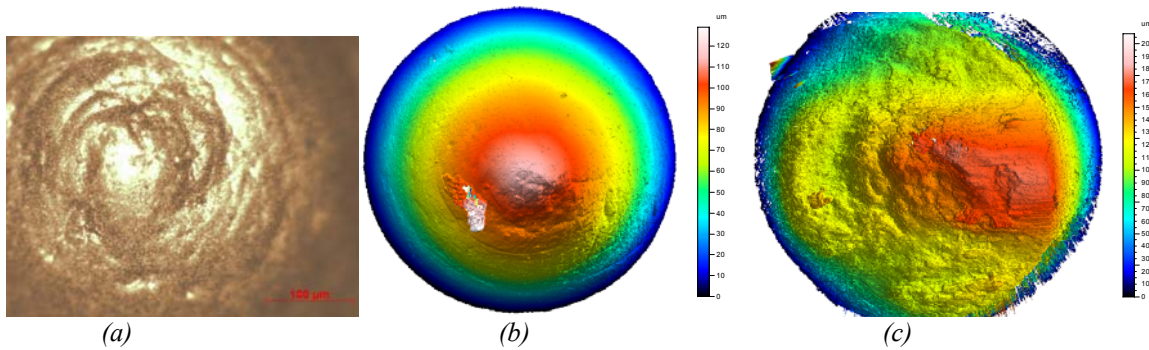
Figure 4.67 Contact surface pictures for DC 53 sample with TD coating (Sample # 6-3) before test obtained by (a) optical, (b) confocal microscope; (c) after test view of contact surface obtained by confocal microscope

The test group VI die samples were underwent higher forces for longer test distances compared to all the die samples tested so far, yet no significant wear elevation was observed. SEM investigations given in Figure 4.68 and Figure 4.69 revealed that the coating layer was damaged partly at the contact surface. Scars seen in Figure 4.69 along the periphery of die sample # 6-2 were thought to be the cracks on coating layer caused by instantaneous peak forces. When the SEM micrographs of current die samples are compared with the previous group samples given in Figure 4.58 through Figure 4.60, the coating failure were less noticeable for the current group of die samples. Specific wear rates given in Figure 4.70 was average of sample # 4-2 and 4-3, however; one data was shown for sample # 6-3 since the other data could not be calculated due to insignificant mass loss for sample # 6-2. On the other hand, Figure 4.71 shows the specific wear rates and substrate hardness values for all the tested die samples in "Effect of substrate hardness study" including Test Group I and current test group VI samples. As can be noticed, different sheet blanks were used in different groups as explained before. The results

showed that that increased substrate hardness led to increased wear resistance (lower specific wear rate values).

Figure 4.68 SEM picture at the tip of DC 53 die sample with TD coating (Sample # 4-2) with magnifications of a) 50X, b) 100X, c) 500X
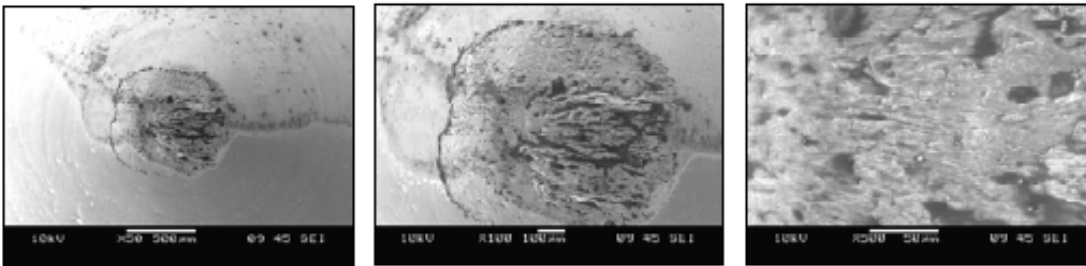
Figure 4.69 SEM picture at the tip of DC 53 die sample with TD coating (Sample # 6-2) with magnifications of a) 50X, b) 100X, c) 500X
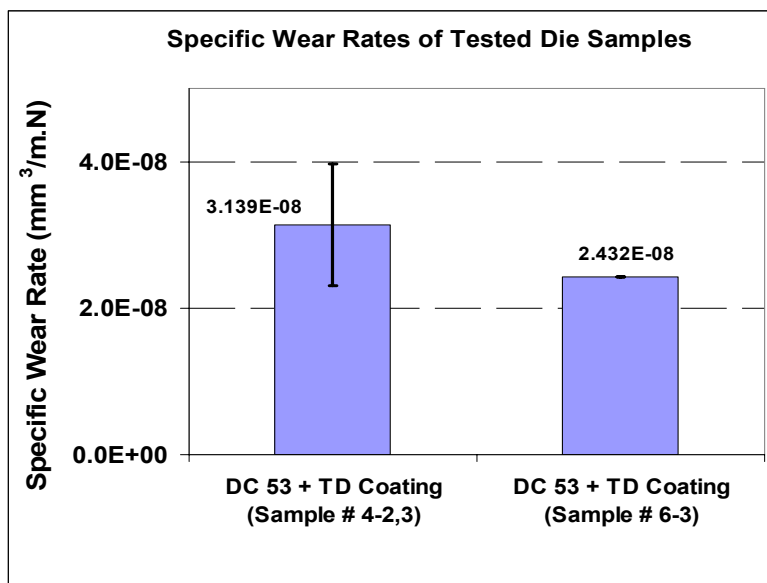
Figure 4.70 Specific wear rates for the die samples tested in Test Group VI
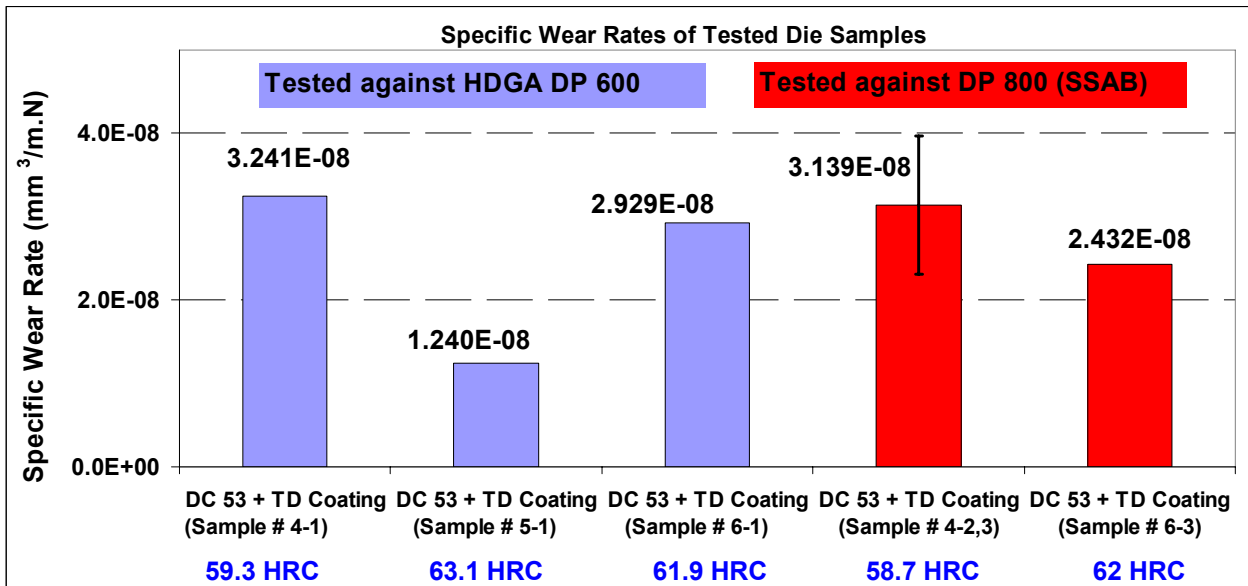
Figure 4.71 Specific wear rate comparisons for the samples in "Effect of substrate hardness" study

Confocal microscope analyses, given in Table 4.23, obtained after the tests showed elevated surface roughness values, as expected. Resultant average and root-mean square roughness values were in a narrow range for tested die samples.

Table 4.23 3-d surface roughness parameters for the Test Group VI samples

Roughness Parameter	Sample # 4-2 (Before Test)	Sample # 4-2 (After Test)	Sample # 4-3 (Before Test)	Sample # 4-3 (After Test)	Sample # 6-2 (Before Test)	Sample # 6-2 (After Test)	Sample # 6-3 Before Test)	Sample # 6-3 (After Test)
S_q (µm)	0.809	5.27	1.42	5.12	1.12	5.72	2.4	5.21
S_{sk}	-3.87	-5.91	-5.63	-6.4	-3.36	-2.57	-1.21	-3.62
S_{ku}	114	101	140	92.3	60	29.4	242	50.4
S_p (µm)	2.2	32.4	4.64	17.2	9.78	46	34.2	17.6
S_v (µm)	36	129	55.1	120	26.6	91.8	88.3	86.6
S_z (µm)	38.2	161	59.8	138	36.3	138	122	104
S_a (µm)	0.59	3.22	0.899	2.97	0.819	4.1	0.917	3.2

CHAPTER 5

Summary of Conclusions, and Recommended Future Work

This chapter aims to provide an overall evaluation and discussion on the development of a new die wear test system and the experimental results. Some common problems encountered in wear studies as well as pros and cons of developed test systems, possible improvements and future work will be discussed.

5.1 Overall Discussions

5.1.1 Discussions on first generation die wear test system and test results

As discussed in a detail in Chapter 3, seven different die materials without coating were tested against DP 600 advanced high strength steel sheet blanks using the 1st generation robot-based die wear test system. Since the contact normal force exertion of robot based test system capability was limited, this system was morphed to a more robust system with a CNC machine. Alternative die materials as well as conventional tool steel AISI D2 were tested in this phase. Results showed that the die materials developed to replace AISI D2 were performed better. Among the tested materials cast steel 0050A was an exception, since its primary use in industry is short-run or prototype production. It

should also be noted that the die materials showed better performances compared to AISI D2 are more expensive than the cost of D2, which is one of the main concerns for their prevalent use in metal forming industry.

5.1.2 Discussions on 2nd generation (CNC-based) die wear test system and results

A test plan that aimed to investigate the effect of important parameters on wear performance was prepared by Daido Steel Co. This plan included different substrate materials at different hardness values and different coating applications on them were tested against different AHSS sheet blank grades.

Effect of substrate hardness for uncoated DC 53 samples study showed that as the substrate hardness increased the wear resistance of DC 53 samples was slightly reduced. Figure 5.1 shows the substrate hardness – specific wear rate relation.
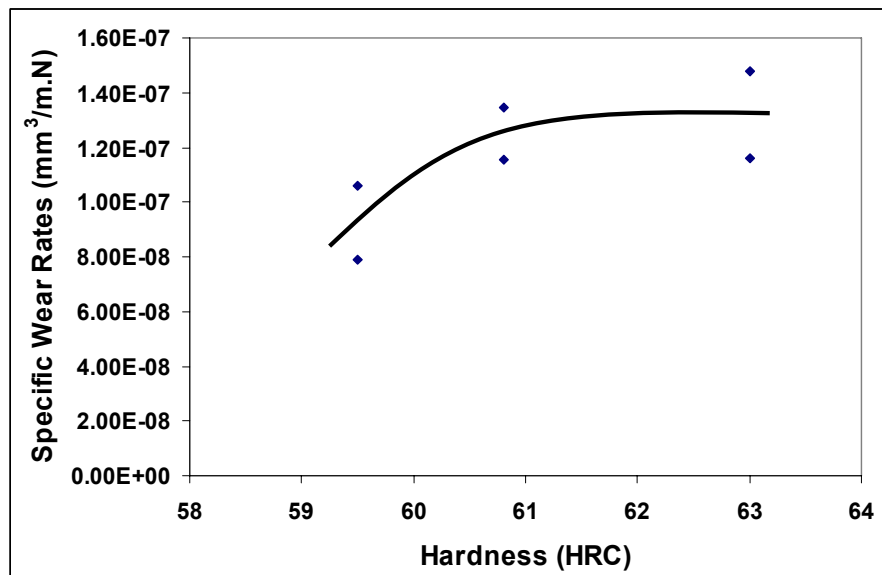
Figure 5.1 Variation of substrate hardness with specific wear rates calculated for uncoated DC 53 samples

TD and CVD coated samples performed considerably higher compared to PVD coating and radical nitriding+ PVD coated samples in the test of first set of samples, however it was concluded that the results were significantly affected by coating thickness differences. Second and third set of sample showed amplified wear resistance with partial coating failures at the contact interface. Figure 5.2 shows specific wear rates for test group I, II, and VI (Effect of substrate hardness, Effect of Coating Type) test samples which all have same substrate material DC 53. Since the different group of samples tested along different track lengths, specific wear rate values were normalized at 4 km sliding distance. In order to exhibit the relatively wide range values of specific wear rate, vertical axis is scaled logarithmically. It is noted that that there is an increasing specific wear rate trend with increasing substrate hardness. TD coated samples tested against DP 800 (SSAB) sheet blanks yielded higher wear resistance.
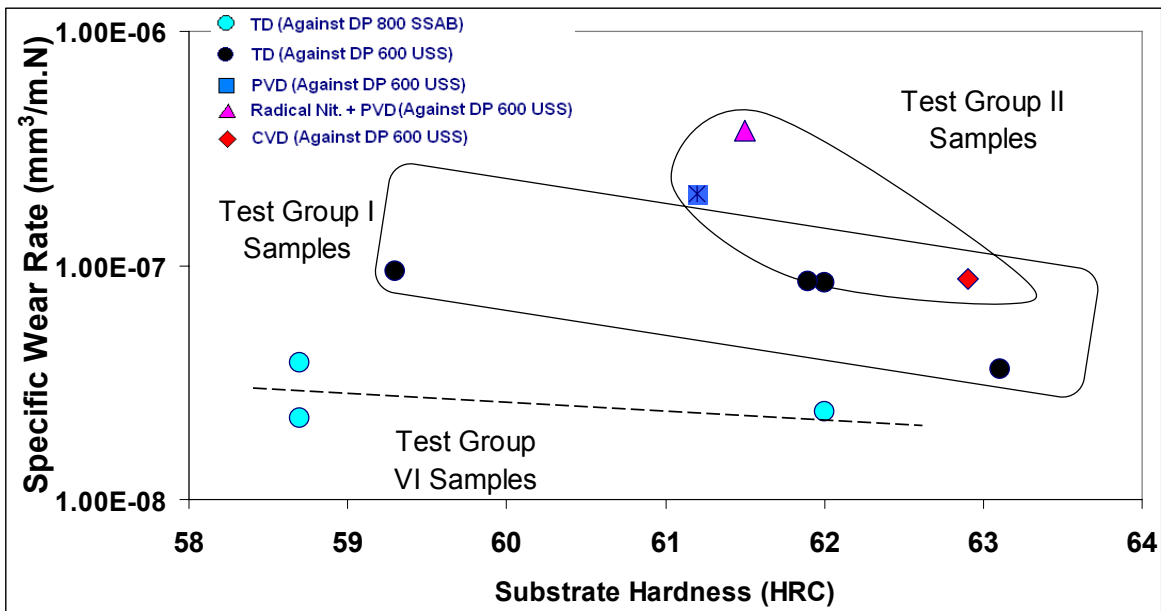
Figure 5.2 Variation of substrate hardness with specific wear rates calculated for "Effect of coating type" study die samples

Similar trends were encountered when the test group I,II,III,V samples (Effect of coating type, substrate hardness, and substrate material) are compared as presented in Figure 5.3. Vertical axis is logarithmically scaled to demonstrate scattered specific wear rates for tested samples.
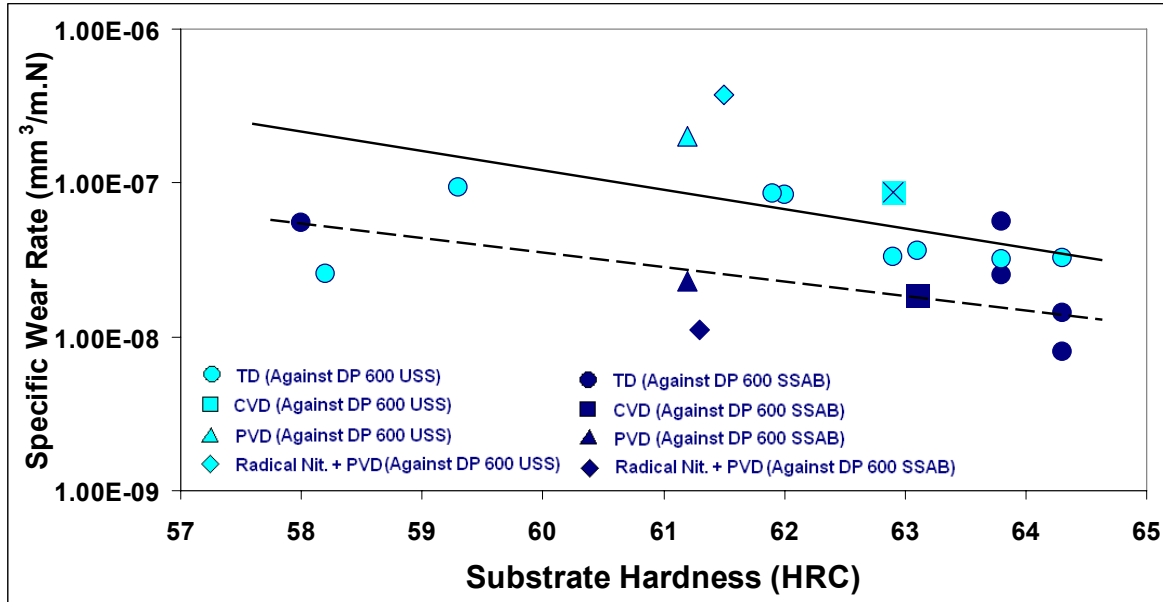
Figure 5.3 Specific wear rates for "Effect substrate material" study samples corresponding to their substrate hardness values

5.2 Concluding Remarks and Recommended Future Work

Wear is an inherently complex phenomenon that is affected by several parameters, and not understood completely. Die wear, in particular, is vitally important in terms of robustness of manufacturing processes that should be in acceptable and controllable levels to prevent from undesired production downtimes and inquality parts. Optimal and complete solutions for wear problems in manufacturing require design and selection of 1) substrate material (hardness, heat treatment, cost, machinability, reparability, etc.), 2) coating (type, thickness), and 3) surface enhancement strategies (texturing, hardening) for

a given set of manufacturing process conditions, sheet blank, temperature, etc. At this point, there is an absolute need to assess the effects of all possible combinations of cited parameters with a fast and reliable wear test system.

One of the main issues in wear related studies is the inability to model the wear process accurately. There are more than 300 friction and wear models reported in literature however; there is no single universal model that is capable of modeling wear accurately [Meng and Ludema, 1995]. Although Archard's Law is one of the most widely used wear models and highly cited in literature, the necessity of development of more comprehensive models are inevitable. A wear model that relates wear volume with dissipated friction energy for sliding contacts is a noteworthy approach since the wear is caused by frictional force rather than contact normal load as misrepresented in Archard's wear law [Ramalho and Miranda, 2000].

Quantification of wear (mass and volume loss measurements) in the case of material pile-up to the surface of interest is a drawback that limits the reliability of wear performance assessment. Therefore, mass or volume loss measurements should cautiously be handled, and these measurements should be verified with microscopic and/or SEM examinations.

Along with the theoretical model establishments, the numerical models that provide quite useful information about wear are also quite essential. Finite element analysis (FEA) is a powerful tool in simulating metal forming operations and offer invaluable information on process characteristics such as stress and strain levels experienced on both forming and formed part. Nevertheless, wear modeling is in its crawling stage and is not available in

most commercially available FEA softwares since it is an intrinsically complex matter yet. Different from the forming simulations, the wear process enforces material removal from the model. Although this problem has already been solved with different approaches such as element elimination, it is necessary to have relatively small sized finite elements at the contact surface for higher accuracy of material removal from surface of interest. Moreover, modeling issues are elevated when AHSS sheet blanks are concerned. Springback simulation of AHSS forming as well as die wear has not been solved satisfactorily enough yet. From tool material point of view, as the particle size decreased and uniformly distributed in chemical composition like in powder metallurgical tool steel case, which provides more isotropic properties, finite element models with higher accuracy can be established. The successful implementation of both springback and die wear modeling is estimated to be achieved in next 5-10 years.

To sum up, the developed test method and system demonstrated promising capability in assessment of various combinations of alternative solutions (substrate material, coating, surface conditioning), and effect of different parameters in an inexpensive, faster and reliable manner. Continuous fresh contact surface interaction between sheet blank and die sample as experienced in real stamping operation is one of the key features of the developed test system. Current study evaluated a fraction of those alternatives and further investigations are needed for broader understanding of effect of certain parameters on wear resistance. Wear test results should be correlated and confirmed with industrial practice and FEA models.

Literature Cited

1.   Advanced High Strength Steel (AHSS) Application Guidelines, Version 4.0, edited by Stuart Keeler, March 2009, web page address: www.autosteel.org , Last access date: 9/25/2009.

2.   Anderson, D., "Application and Repairability of Advanced High-Strength Steels – Use, growth and repair for AHSS", presented in I-CAR International Annual Meeting, July 24-26, 2008, Scottsdale, AR, USA. Web page address: http://www.autosteel.org/AM/Template.cfm?Section=PDFs&TEMPLATE=/CM/ContentDisplay.cfm&CONTENTID=24669, Last access date : 9/13/2009.

3.   Andreasen, J. L., Olsson, D. D., Chodnikiewicz, K., Bay, N., (2006), "Bending under tension test with direct friction measurement", *Proceedings of the Institution of Mechanical Engineers, Part B: Journal of Engineering Manufacture*, v. 220, pp. 73-80.

4.   Antunes, P.V., Ramalho, A., (2005), "Fretting behaviour of glass-fibre-reinforced polypropylene composite against 2024 Al alloy", *Tribology International*, v. 38, issue 4, pp. 363-379.

5.   ASM Metal Handbook, Volume 5: Surface Engineering, Second printing, ASM International, Materials Park, Ohio, 1996.

6.   ASTM G 40 standard in "Friction and Wear Testing: Source Book of Selected References from ASTM Standards and ASM Handbooks, p. 102, American Society for Testing and Materials, West Conshohocken, PA, 1997.

7.   Automotive Steel Design Manual, Revision 6.1, American Iron and Steel Institute & Auto/Steel Partnership, August 2002, web page address: http://www.a-sp.org/database/default.asp?doc=28 , Last access date: June 23th, 2009.

8.   Bernick, L.M., Hilsen, R.R., Wandrei, C.L., (1978), "Development of a quantitative sheet galling test", *Wear*, v.48, pp. 323-346.

9.   Bay, N., Olsson, D.D., Andreasen, J.L., (2008), "Lubricant test methods for sheet metal forming", *Tribology International*, v.41, pp. 844-853.

10. Bay Cast Inc. Web page address: www.baycastinc.com, Last access date: June 23th, 2009.

11. Bernquist J., "Safety Cage Design in the Volvo XC 90", *Great Design in Steel Seminar 2004*, February 18, 2004, Livonia, Michigan, USA.

12. Bhushan B., (1996), "Macro- and microtribology of magnetic rigid-disk storage devices", *Journal of Magnetism and Magnetic Materials*, v.155, issues 1-3, pp.318-322.

13. Boher, C., Attaf, D., Penazzi, L., Levaillant, C., (2005), "Wear behaviour on the radius portion of a die in deep-drawing: Identification, localisation and evolution of the surface damage", *Wear,* v.259, pp.1097–1108.

14. Boron and Ultra-high strength steel information web site, http://www.boronextrication.com/, Last access date 9/26/2009.

15. Böhler-Uddeholm Product Specification Sheets;

16. Böhler-Uddeholm product specification sheet for D2 tool steel, web page address: http://www.bucorp.com/files/aisi_d2.pdf, Last access date: June 23th, 2009.

17. Böhler-Uddeholm product specification sheet for Caldie tool steel, web page address: http://www.bucorp.com/files/caldie-english_061104-1.pdf, Last access date: June 23th, 2009.

18. Böhler-Uddeholm product specification for Vanadis 4 extra powder metallurgical tool steel, web page address: http://www.bucorp.com/files/Vanadis_4_Extra_Am.pdf, Last access date: June 23th, 2009.

19. Böhler-Uddeholm product specification sheet for K340 ISODUR cold work tool steel, web page address: http://www.bucorp.com/files/k340.pdf, Last access date: June 23th, 2009.

20. Böhler-Uddeholm product specification sheet for Vancron 40 cold work tool steel, Edition 5, web page address: http://www.uddeholm.com/files/vancron_40-english.pdf, Last access date: June 23th, 2009

21. Böhler-Uddeholm product specification sheet for Carmo tool steel, web page address:http://www.uddeholm.nl/dutch/files/Uddeholm_carmo_E.pdf, Last access date: June 23th, 2009.

22.	Carlsson, P., Olsson, M., (2006), "PVD coatings for sheet metal forming processes – a tribological evaluation", *Surface & Coatings Technology*, v.200, pp. 4654-4663.

23.	Carpenter, Jr., Joseph A.; "Automotive Lightweighting Materials", "Great Design in Steel Seminar 2004, Livonia, Michigan, February 18, 2004.

24.	Cao, J., Zhou, R., Wang, Q., Xia, Z.C., (2009), "Strip-on-cylinder test apparatus for die wear characterization", *CIRP Annals – Manufacturing Technology*, v. 58, pp. 251-254.

25.	Costello, M.T., Riff, I.I., (2005), "Study of hydroforming lubricants with overbased sulfonates and friction modifiers", *Tribology Letters*, v.20, Issue 3–4, pp. 201–208.

26.	Coughbrough, G.J., Alinger, M.J., Van Tyne, C.J., (2002), "Angle of contact between sheet and die during stretch-bend deformation as determined on the bending-under-tension friction test system", *Journal of Materials Processing Technology*, v. 130-131, pp. 69-75.

27.	Cuddy, V.K, Merkle, H., Richardson, A., Hudin, O., Hildenbrand, A., Richter, H., Nilsson,T., Larsson, J., "Manufacturing guidelines when using ultra high strength steels in automotive applications", European Commission – Technical Steel Research, Final Report, ISBN 92-79-00139-6, Luxembourg, 2005.

28.	Dalton, G., "Enhancing stamping performance of high strength steels with tribology - Report on phase 1 testing", prepared for the Auto/Steel partnership tribology project team, TribSys Inc. Ontario, Canada, December 31, 2002.

29.	Dalton, G., "Enhancing stamping performance of high strength steels with tribology - Report on phase 2: Effect of stroke length and penetration", prepared for the Auto/Steel partnership tribology project team, TribSys Inc., Ontario, Canada, March 26, 2003.

30.	Dalton, G., "Enhancing stamping performance of high strength steels with tribology - Report on phase 3 testing", prepared for the Auto/Steel partnership tribology project team, TribSys Inc. Ontario, Canada, May 11, 2004.

31.	Daniel, Edwards, J.; "FreedomCAR Partnership", Argonne National Laboratory, Energy Systems Divisions web site: http://www.es.anl.gov/Energy_Systems/Process_Engineering/Documentation/Presentations/FreedomCAR.pdf, Last access date: 08/31/2009

32.	Demeri, Mahmoud Y., "Forming of Advanced High-Strength Steels", ASM Handbook, Volume 14B: Metalworking: Sheet Forming, p. 530, ASM International, Materials Park, Ohio, USA, 1996.

33. Department of Transportation, "Number of U.S. Aircraft, Vehicles, Vessels, and Other Conveyances" in *National Transportation Statistics*, Research and Innovative Technology Administration, Bureau of Transportation Statistics, Edited by William H. Moore, 2009, Web page address: http://www.bts.gov/publications/national_transportation_statistics/pdf/entire.pdf , Last Access Date: 05/08/2009

34. Dubar, M., Dubois, A., Dubar, L., (2005), "Wear analysis of tools in cold forging: PVD versus CVD TiN coatings", *Wear*, v. 259, pp. 1109–1116.

35. Emanuelsson, P., "Award winning problem solvers – Uddeholm's steels for powder compacting", Uddeholm Automotive Tooling Seminar, 6-9 February 2008, Sweden.

36. Energy Information Administration, "Annual Energy Review 2006", Department of Energy Report No. DOE/EIA-0384(2006), Posted: June 27, 2007, http://www.eia.doe.gov/emeu/aer/petro.html, Last Access Date: 05/21/2008

37. Eriksen, M., (1997), "The influence of die geometry on tool wear in deep drawing", *Wear*, v.207, pp.10-15.

38. Farahani, A., "Future Generation Passenger Compartment (FGPC)", Great Design in Steel Seminar 2004, Livonia, Michigan, February 18, 2004.

39. Firat, M., (2008), "An analysis of sheet drawing characteristics with drawbead elements", *Computational Materials Science*, v.41, pp. 267-274.

40. FreedomCAR & Fuel Partnership Materials Technical Team, 2006, "FreedomCAR and Fuel Partnership – Materials Technology Roadmap", Department of Energy, Energy Efficiency and Renewable Energy Web Site: http://www1.eere.energy.gov/vehiclesandfuels/pdfs/program/materials_team_technical roadmap.pdfLast Access Date: 09/01/2009

41. Gåård, A., Krakhmalev, P.V., Bergström, J., Hallbäck, N., (2007), "Galling resistance and wear mechanisms – cold work tool material sliding against carbon steel sheets", *Tribology Letters*, v.26, pp. 67-72.

42. Gåård, A., Krakhmalev, P.V., Bergström, J., (2008) "Wear mechanisms in deep drawing of carbon steel – correlation to laboratory testing", *Tribotest*, v.14, pp. 1-9.

43. Gåård, A., Krakhmalev, P.V., Bergström, J., (2009), "Wear mechanisms in galling: Cold work tool materials sliding against high-strength carbon steel sheets, *Tribology Letters*, v. 33, pp. 45-53.

44.   Geyer, R., "CO_2 equivalent with Advanced High-Strength Steels", Great Designs in Steel Seminar 2006, Livonia, Michigan, March 8, 2006.

45.   Hall, J.N., "50 year perspective of automotive engineering body materials and an analysis of the future", Great Designs in Steel Seminar 2008, April 9th, 2008, Livonia, Michigan, USA.

46.   Hao, S., Klamecki, B.E., Ramalingam, S., (1999) "Friction measurement apparatus for sheet metal forming", *Wear*, v. 224, pp. 1-7.

47.   Hardell, J., E. Kassfeldt, B. Prakash, (2008), "Friction and wear behaviour of high strength boron steel at elevated temperatures of up to 800 °C" ,*Wear*, v. 264, issues 9-10, pp. 788-799.

48.   Hardell J., "High temperature tribology of high strength boron steel and tool steels", Licentiate Thesis, Luleå University of Technology, Luleå, Sweden, June 2007.

49.   Holleck, H., (1986), "Material selection for hard coatings", *Journal of Vacuum Science and Technology A*, v.4, issue 6, pp.2661-2669

50.   Hortig, D., Schmoeckel, D., (2001), "Analysis of local loads on the draw die profile with regard to wear using the FEM and experimental investigations", *Journal of Materials Processing Technology*, v.115, pp. 153-158.

51.   Holmberg, K., Laukkanen, A., Ronkainen, H., Wallin, K., (2009),"Surface stresses in coated steel surfaces- influence of a bond layer on surface fracture", *Tribology International*, v. 42, pp. 137-148.

52.   Horvath, C.D., "The future revolution in automotive high strength steel usage", Great Designs in Steel Seminar 2004, February 18, 2004, Livonia, Michigan, USA.

53.   Huang, L. "Application of advanced high-strength strength steels in roof strength design steels in roof strength design", Great Designs in Steel Seminars 2007, March 7, 2007, Livonia, Michigan.

54.   Janoss, B. J., "Selecting, using tool coatings to stamp AHSS", *The Fabricator* journal, web page address: http://www.thefabricator.com/ToolandDie/ToolandDie_Article.cfm?ID=1976,   Last access date: 10/05/2009.

55.   Johansonn, B., Olsson, K., "Tooling solutions for advanced high strength steels", Uddeholm Automotive Tooling Seminar, February 9-11, 2005, Sweden.

56.   Jonasson, M., Pulkinen,T., Gunnarsson, L., Schedin, E., 1997, "Comparative study of shotblasted and electrical-discharge-textured rolls ", *Wear*, v.207, pp. 34-40.

57.   Kim, H., Altan, T., Yan, Q., (2009) "Evaluation of stamping lubricants in forming advanced high strength steels (AHSS) using deep drawing and ironing tests", *Journal of Materials Processing Technology*, v. 209, pp. 4122-4133.

58.   Kim, H., Sung, J., Goodwin F. E., Altan, T., (2008), "Investigation of galling in forming galvanized advanced high strength steels (AHSSs) using the twist compression test (TCT)", *Journal of Materials Processing Technology*, v. 205, issues 1-3, pp. 459-468.

59.   Koç, M., Mahabunphachai, S., (2007), *"*Feasibility investigations on a novel micro-manufacturing process for fabrication of fuel cell bipolar plates: Internal pressure-assisted embossing of micro-channels with in-die mechanical bonding", *Journal of Power Sources*, v. 172, pp. 725–733.

60.   Kleiner, M., Geiger, M., Klaus A., (2003), "Manufacturing of lightweight components by metal forming", *CIRP Annals - Manufacturing Technology*, v. 52, issue 2, pp. 521-542.

61.   Klocke, F., Maßmann, T., Bobzin, K., Lugscheider E., Bagcivan N., (2006), "Carbon based tool coatings as an approach for environmentally friendly metal forming processes", *Wear*, v. 260, issue 3, pp. 287-295.

62.   Kuvin, B. F., "Ford's New DP 600 Die Standards", Metal Forming Magazine, February 2006, pp.20-22.

63.   Lebau T., "*CVD - Chemical Vapour Deposition*", Desing inSite, http://www.designinsite.dk/htmsider/p1144.htm, Last Access Date : 10/26/2009

64.   Lee, I., Park, I., (2007), "Microstructures and mechanical properties of surface-hardened layer produced on SKD 61 steel by plasma radical nitriding", *Materials Science and Engineering A*, v. 449–451, pp. 890–893.

65.   Lenard, J.G., Medley, J.B., Schey, J.A., (1996), "Laboratories at work: Tribology at the University of Waterloo", *Tribotest Journal*, v.2, pp. 383–394.

66.   Lee, M. J., "Advanced High Strength Steel Technology in the Ford 500 and Freestyle", Great Designs in Steel Seminar 2005, March 9, 2005, Livonia, Michigan, USA.

67.   Mallen, R.Z., Tarr, S., "Applications of high strength steels in North American Honda production", Great Designs in Steel Seminar 2008, April 9, 2008, Livonia, Michigan, USA.

68.   Matthes, B., Herr, W., Broszeit, E., Kloos, K.H., Nürnberger, G., Schmoeckel, D., Höhl, F., Stock, H.-R., Mayr, P., (1991), "Tribological properties and wear behaviour of sputtered titanium-based hard coatings under sheet-metal-forming conditions", *Materials Science and Engineering: A*, v.140, pp. 593-601.

69.   Meng, H.C., Ludema, K.C., (1995) "Wear models and predictive equations: their form and content", *Wear*, v.181, pp. 443-457.

70. Metalforming magazine, "Stamper replaces carbide tooling with coated DC 53", April 2008 issue, p. 41, Metalforming magazine, Independence, OH, USA. Online version: http://archive.metalformingmagazine.com/2008/04/Carbide_Tooling.pdf, Last access date: 10/24/2009.

71.   Metals Handbook, Volume 1 Properties and Selection: Irons and Steels, Fifth edition, p.378, American Society for Metals, 1990.

72.   Michler, J.R., Weinmann, K.J., Kashani, A.R., Majlessi, S.A., (1994), "A strip-drawing simulator with computer-controlled drawbead penetration and blankholder pressure", *Journal of Materials Processing Technology*, v. 43, pp. 177-194.

73.   Miller, P., from Böhler-Uddeholm USA, Personal communication, June 2009.

74.   Nakahama, S-S., Matsuda, Y., Namiki, K., Ozaki, K., (2005), "The development of high hard and tough matrix type high speed tool steels", *Steel Grips*, v.3, no.4, pp. 268-275.

75.   Nanofocus AG, μsoft analysis software v. 5.0.4, user's guide, Oberhausen, Germany 2009.

76.   National Highway Traffic Safety Administration, "Average Fuel Economy Standards, Passenger Cars and Light Trucks, MY 2011-2015", report, Docket No. NHTSA-2008 -0089.

77.   Nine, H.D., "Draw bead forces in sheet metal forming", in D. Koistinen and N.M. Wang (Editors), Proceedings of a Symposium on Mechanics of Sheet Metal Forming: Behaviour and Deformation Analysis, 1978. Warren, Michigan, Plenum Press, pp. 179-211.

78.   Nilsson, A., Gabrielson, P., Stahl, J., (2002), "Zinc-alloys as tool materials in short-run sheet metal forming processes, Experimental analysis of three different zinc-alloys", *Journal of Materials Processing Technology*, v. 125-126, pp.806-813.

79.   Oliver, S., Jones, T.B., Fourlaris, G., (2007) "Dual phase versus TRIP strip steels: Microstructural changes as a consequence of quasi-static and dynamic tensile testing", *Materials Characterization*, v. 58, pp. 390–400.

80.   Pafumi, M., "Advanced High Strength Steel Technology in the 2006 Honda Civic, Creating Special Appeal with Steel", Great Designs in Steel Seminar 2007, March 7, 2007, Livonia, Michigan, USA.

81.   Pearson, A.D., Dalton, G., "Improving the Life of High-Strength Steel Stamping Dies – Report on A/SP Tribology Team Die Wear Study", Great Designs in Steel Seminar 2007, March 7, 2007, Livonia, Michigan, USA.

82.   Pereira, M. P., Yan, W., Rolfe, B. F., (2008), "Contact pressure evolution and its relation to wear in sheet metal forming", *Wear*, (265), issues 11-12, pp. 1687-1699.

83.   Podgornik B, Hogmark, S., Pezdirnik, J., (2004), "Comparison between different test methods for evaluation of galling properties of surface engineered tool surfaces", *Wear*, v. 257, issues 7–8, pp. 843–851.

84.   Porsche Engineering, "Advanced high strength steel technology in the Porsche Cayenne", Great Designs in Steel Seminar 2004, February 18, 2004, Livonia, Michigan, USA.

85.   Powers; Willliam F., (2000) "Automotive Materials in the 21st Century", *Advanced Materials & Processes*, v. 157, issue 5, pp. 38-41.

86.   Ramalho, A., Miranda, J.C., (2006), "The relation between wear and dissipated energy in sliding systems", *Wear*, v.260, pp. 361-367.

87.   Ramalho, A., Miranda, J.C., (2007), "Tribological characterization of electroless NiP coatings lubricated with biolubricants", *Wear*, v. 263, issues 1-6, pp. 592-597.

88.   Rivard, J.D.K., Blue, C.A., Harper, D.C., Kiggans, J.O., Menchhofer, P.A., Mayotte, J.R., Jacobsen, L., Kogut, D., (2005), "The thermomechanical processing of titanium and Ti-6Al-4V thin gage sheet and plate", *JOM Journal of the Minerals, Metals and Materials Society*, v. 57, number 11, pp. 58-61.

89.   Russias, J., Cardinal,S., Esnouf, C., Fantozzi, G., Bienvenu, K., (2007), "Hot pressed titanium nitride obtained from SHS starting powders: Influence of a pre-sintering heat-treatment of the starting powders on the densification process", *Journal of the European Ceramic Society*, v. 27, pp.327–335.

90.   Sakamotoa, Y., Takayaa, M., Ishiib, Y., Igarashi, S., (2001), "Surface modified tool fabricated by radical nitriding", *Surface and Coatings Technology*, v.142-144, pp. 152-155.

91.   Sanchez, L.R., (1999), "Characterization of a measurement system for reproducible friction testing on sheet metal under plane strain", *Tribology International*, v. 32, pp. 575-586.

92.   Sato, T., Besshi, T., (1998), "Anti-galling evaluation in aluminum sheet forming", *Journal of Materials Processing Technology*, v.83, pp. 185–191.

93.   Schaeffler, D.J., "Introduction to Advanced High Strength Steels, Part 1: Grade Overview", Fabricator online journal, August 9, 2005, Web page address: http://www.thefabricator.com/MetalsMaterials/MetalsMaterials_Article.cfm?ID=1139 , Last access date: 9/25/2009.

94.   Schedin, E., Lehtinen, B., (1993), "Galling mechanisms in lubricated systems: A study of sheet metal forming", *Wear*, v. 170, Issue 1, pp. 119-130.

95.   Schedin, E., (1994), "Galling mechanisms in sheet forming operations", *Wear*, (179), pp.123-128.

96.   Schmoeckel, D., Frontzek, H., (1986), "Reduction of wear on sheet metal forming tools", *CIRP annals, Manufacturing Technology*, v. 35, issue 1, pp. 195-198.

97.   Schultz, R.A., "Metallic material trends for North American light vehicles", Great Designs in Steel Seminars 2007, March 7, 2007, Livonia, Michigan, USA.

98.   Shaw, J., "ULSAB-AVC – on the road today", Great Designs in Steel Seminar 2009, May 13th, 2009, Livonia, Michigan, USA.

99.   Shih, H-C, Shi, M.F., "Evaluation of Friction Behavior of Automotive Steels with Different Test Methods", Proceedings of MSEC 2006, International Conference on Manufacturing Science & Engineering (MSEC), October 8-11, 2006, Ypsilanti, Michigan, USA.

100.   Singh, H., "Future steel vehicle – Advanced powertrains and the influence on material selection", Great Designs in Steel Seminar 2009, May 13th, 2009, Livonia, Michigan, USA.

101.   Sniekers, R.J.M.M., Smits, H.A.A, (1997), "Experimental set-up and data processing of the radial strip-drawing friction test", *Journal of Materials Processing Technology*, v. 66, pp. 216-223.

102.   Sohmshetty, R., "Future of the Steel in the Automobile of 21st Century", Great Designs in Steel Seminar 2009, Livonia, Michigan, May 13th, 2009.

103.   SSAB Docol DP/DL Cold reduced dual phase steels, product datasheet, Document#:   GB8201Docol,   09-05-20,   web   page   address: http://www.ssab.com/Global/DOCOL/datasheets_docol/en/224_Docol%20DP,%20DL.pdf, Last Access date: 9/20/200

104.   Steel Castings Handbook, Supplement 2, and 1999 Summary of Standard Specification for Steel Castings, Steel Founder's Society of America, Prepared by the Specifications Committee Steel Founders' Society of America, Revised by David Poweleit, 1999.

105.   TeikuroTRD Corp. web site address: http://www.teikurotrd.com/products/TRD-process/default.html#principle , Last access date 10/08/2009.

106.   Tsuchiya, Y., Kubota, H., Dohda, K., Kitamura, K., "Damage Behavior and Tribo-characteristics of DLC-Si Coating for Forming", ASME, 2007 International Manufacturing Science and Engineering Conference (MSEC), October 15-17,2007, Atlanta, GA, USA.

107.   ULSAB-AVC, Advanced Vehicle Concepts, Technical Transfer Dispatch # 6, ULSAB-AVC Body Structure Materials,ULSAB-AVC Consortium, May 2001. Web page address:http://www.autosteel.org/AM/Template.cfm?Section=Technical_Documents6&CONTENTID=33452&TEMPLATE=/CM/ContentDisplay.cfm , Last Access Date: 9/25/2009.

108.   ULSAB-AVC Overview Report, Automotive Applications Committee, American Iron and Steel Institute, January 2002.

109.   U.S. Steel Corporation web sites

        http://www.ussteel.com/corp/auto/tech/grades/advanced/dual-ten.asp ,
        http://www.ussteel.com/corp/auto/tech/grades/advanced/trip.asp, Last Access Date: 09/01/2009.

110. United Nations Framework Convention on Climate Change Web Site, http://unfccc.int/kyoto_protocol/status_of_ratification/items/2613.php, Last Access Date: August, 30th, 2009.

111. van der Heide, E.; "Lubricant failure in sheet metal forming processes", Ph.D dissertation, University Twente, Netherlands, 2002.

112. van der Heide, E., E.D. Stam, H. Giraud, G. Lovato, N. Akdut, F. Clarysse, P. Caenen, and I. Heikillä, (2006), "Wear of aluminum bronze in sliding contact with lubricated stainless steel sheet material.", *Wear*, v. 261, pp. 68–73.

113. van der Heide, E., Burlat M., Bolt, P.J., Schipper, D.J., (2003), "Wear of soft materials in sliding contact with zinc-coated steel sheet", Journal of Materials Processing Technology, v.141, pp. 197-201.

114. Wan, Y., Xue, Q., (1995), "Effect of antiwear and extreme pressure additives on the wear of aluminium alloy in lubricated aluminium-on-steel contact", *Tribology International*, v. 28, Issue 8, pp. 553–557.

115. Weist, C., Westheide, H., Lange, K., (1986), "Application of chemical and physical methods for the reduction of tool wear in bulk metal forming processes", *CIRP Annals - Manufacturing Technology*, v. 35, issue 1, pp. 199-204.

116. Westeneng, J. D., "Modelling of contact and friction in deep drawing processes", Ph.D dissertation, University Twente, Netherlands, 2001.

117. Wichern, C. M., Van Tyne, C. J., (1999), "Frictional behavior of the sliding interface between and a2 steel die and zinc-coated steel sheet*", Journal of Materials Engineering and Performance*, v. 8, issue 5, pp. 571-576.

118. Williams, J. A., (1999), "Wear modelling: analytical, computational and mapping: a continuum mechanics approach", *Wear*, v. 225-229, part 1, pp. 1-17.

119. Wohlecker; R., Johannaber M., Espig M., "Mass Sensitivity", Great Designs in Steel Seminar 2006, Livonia, Michigan, March 8th 2006.

120. Wojtowicz, W. J., (1955), "Sliding friction test for metalworking lubricants", *Lubrication Engineering*, v. 11, issue 3, pp. 174-177.

121. Yan, W., (2006), "Theoretical investigation of wear-resistance mechanism of superelastic shape memory alloy NiTi", *Materials Science and Engineering A*, v. 427, pp. 349-355.

APPENDIX A

Calculation of the contact pressure and dimensions of a nominal line contact.

Contact pressure calculation a cylinder and a flat
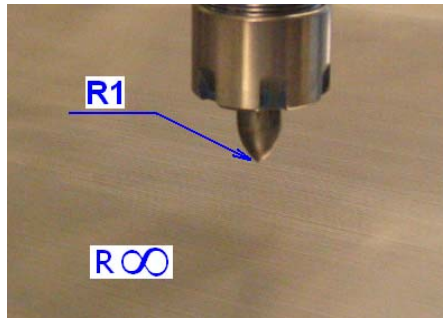
Notation : $GPa := 10^9 \cdot Pa$ $MPa := 10^6 \cdot Pa$ $kN := 1000 \, N$

Input : $D_1 := 2 \cdot mm$ $E_1 := 210 \cdot GPa$ $\nu_1 := 0.3$

$D_2 := \infty \cdot mm$ $E_2 := 210 \cdot GPa$ $\nu_2 := 0.3$

$F := 110 \dfrac{N}{mm}$

1) Calculate R' (Effective Curvature) and E' (Contact Modulus)

$$R_1 := \frac{D_1}{2} \qquad R_2 := \frac{D_2}{2}$$

$$E' := \frac{1}{\dfrac{1 - \nu_1^2}{2 \cdot E_1} + \dfrac{1 - \nu_2^2}{2 \cdot E_2}} \qquad E' = 230.769\,GPa \qquad R' := \frac{1}{\dfrac{1}{R_1} + \dfrac{1}{R_2}}$$

2) Calculate the semi-contact width b
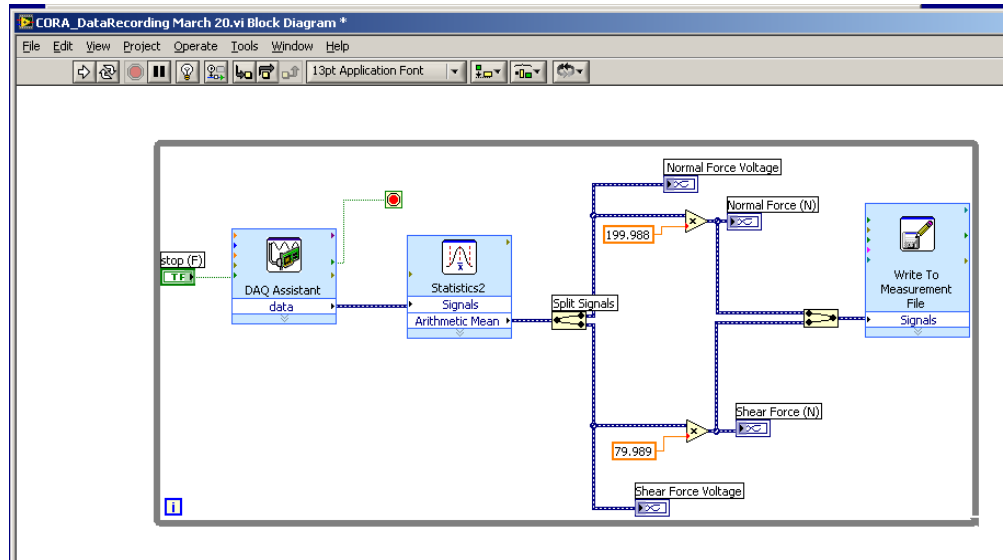
$$b := 2 \cdot \left(\frac{2}{\pi} \cdot F \cdot \frac{R'}{E'} \right)^{\frac{1}{2}} \qquad b = 0.035\,mm$$

3) Calculate the contact pressure (eq.2.23) and (eq.2.24)

$$p_m := \frac{F}{2 \cdot b} \qquad \boxed{p_m = 1.579\,GPa} \qquad p_{max} := \frac{4}{\pi} \cdot p_m \qquad p_{max} = 2.01\,GPa$$

173

APPENDIX B

Labview flow-chart to store the data load sensor data

Matlab code to average the stored normal load data

```matlab
%% starter
clear all
clc
close all
%% change directory
% Change the folder names for each seperate data
cd('C:\DIE_WEAR\PHASE2\CORA_DAQ\PHASE2\REPETITION_CALDIE\CALDIE2-
DP600\xls_converted\')   % change directory

dlist=dir('C:\DIE_WEAR\PHASE2\CORA_DAQ\PHASE2\REPETITION_CALDIE\CALDIE2-
DP600\xls_converted\');   % read file names in the directory
dlist=dlist(3:end);

stind=1;
for ind=1:length(dlist) %
force(ind).fname=dlist(ind).name; % pass file name to variable
force(ind).data=xlsread(dlist(ind).name,'A23:C19000');  % read data from
excel
end

con=cat(1,force(1:length(dlist)).data);     % Concatenate the all the in
one column, delete the voltage data
indis=find(con(:,2)>0.15);                  % less than 0.15,
cp=con(indis,2);                            %
mean(cp)                                    % Average
```

VITA

Personal Information

Date/Place of Birth: 11.24.1978 / Bristol, England

          Nationality: Turkish

Educational Background

- Ph.D Student *&* **Graduate Research Assistant**, **(August 2007- December 2009)**, *Department of Mechanical Engineering, Virginia Commonwealth University, Richmond, VA, USA*

- Visiting Scholar, (September 2006 –August 2007), *Department of Mechanical Engineering Virginia Commonwealth University, Richmond, VA, USA*

- Ph.D student, Mechanical Engineering (February 2005- September 2006), *Middle East Technical University- Ankara, TURKEY. (Classes were completed prior to visiting scholarship)*

- **M. S. in Mechanical Engineering (December 2004)** *Middle East Technical University- Ankara, TURKEY,* **Thesis title: "Friction Analysis in Cold Forging"**

- Department of Basic English, Middle East Technical University (2000-2001)

- **B.S. in Mechanical Engineering (1996-2000)** *Karadeniz Technical University- Trabzon, TURKEY, "Sensors in Automotive Industry" graduation study*

Research Interests:

Metal Forming, FEA, Tribology in Metal Forming, Die Wear Testing, Powder Metallurgy

Work Experience

- **Graduate Research Assistant,** NSF I/UCR Center for Precision Forming, Department of Mechanical Engineering, Virginia Commonwealth University, *Richmond, VA, USA* **(September 2006 – December 2009)**

- **Research & Teaching Assistant,** *Middle East Technical University, Department of Mechanical Engineering* **(October 2002-September 2006)**
*Teaching assistant of the courses***:** ME-202 Manufacturing Technologies, ME-205 Statics, ME-206 Strength of Materials, ME-212 Principles of Production Engineering, ME-307 Machine Elements I, ME-308 Machine Elements II   in various semesters.

- **Mechanical Engineer;** *MİTAŞ Bolt Ltd.*, Ankara, TURKEY **(March-July 2002)**
Research & development activities for the bolts produced by cold forging; finding new suppliers of trimming, thread rolling dies, Die-shop responsibility.

PUBLICATIONS:
Books & Chapters:
1- M. Koç, **O.N. Cora** *"Chapter 1: Introduction and state of the art of hydroforming"* in **"**Hydroforming for advanced manufacturing**",** Woodhead Publishing Limited, Cambridge, ENGLAND, 2008.

Journal Papers:
2- Ömer Necati Cora, Muammer Koç, (2009), *"Experimental investigations on wear resistance characteristics of alternative die materials for stamping of advanced high-strength steels (AHSS)"*, International Journal of Machine Tool and Manufacture, v.49, pp.897-905.

3- **Ö. N. Cora**, M. Koç , (2009), *"Influence of substrate material on wear performance of stamping dies utilizing a new die wear test system",* Transactions of the North American Manufacturing Research Institute of SME, v.37, pp. 325-331.

4- **Ö.N. Cora**, K. Namiki, M. Koç, (2009), *"Wear performance assessment of alternative stamping die materials utilizing a novel test system"*, Wear, Volume 267, Issues 5-8, 15 June 2009, pp. 1123-1129

5- D.H. Min, G.S. Hwang, Y. Usta, **O.N. Cora**, M. Koç, M. Kaviany, (2009), *"2-D and 3-D Modulated Porous Coatings for Enhanced Pool Boiling"*, International Journal of Heat and Mass Transfer, v52, pp.2607-2613

6- **Ö.N. Cora**, Y. Usta, M. Koç, (2009), *"Micro-Manufacturing of Micro-Scale Porous Surface Structures for Enhanced Heat Transfer Applications – An Experimental Process Optimization Study"*, Journal of Micromechanics and Microengineering, v.19, 045011.

7- **Ö. N. Cora**, Metin Akkök, H. Darendeliler, (2008), *"Modeling of Variable Friction in Cold Forging",* Proceedings of the Institution of Mechanical Engineers, Part J, Journal of Engineering Tribology, Volume 222 (No:7), pp. 899-908, DOI: 10.1243/13506501JET419.

Journal Papers Under Review / in Preparation:

- **Ömer Necati Cora,** Dahye Min, Muammer Koç and Massoud Kaviany**,** "Microscale Modulated Porous Coatings: Fabrication and Pool-Boiling Heat Transfer Performance", Submitted to Journal of Micromechanics and Microengineering, December 2009, Under Review.

- Sasawat Mahabunphachai, **Ömer Necati Cora**, Muammer Koç, *"Effect of Manufacturing Processes on Formability and Surface Topology of PEMFC Metallic Bipolar Plates",* in preparation.

Conference Proceedings & Oral/Poster Presentations:

- Irfan Kaya, **Ömer Necati Cora**, Muammer Koç, Chris Fitzgerald, John Sheridan, Lee Ann Schwope, "Mechanical Behavior of UAM-Fabricated Al-Ti LMC Blanks", 2nd Ultrasonic Additive Manufacturing Technology Symposium, October 20-21, 2009, Columbus, OH, USA.

- Ömer Necati Cora, and Muammer Koç, (2009), "Manufacturing of Micro-engineered Surfaces for Fuel Cell, Heat and Mass Transfer Applications by Powder Compaction Process", NSF CMMI Grantee Conference (poster presentation session), June 22-25, 2009, Honolulu, Hawaii, USA.

- Ö. N. Cora, M. Koç , (2009), "Influence of substrate material on wear performance of stamping dies utilizing a new die wear test system", 37th The North American Manufacturing Research Conference (NAMRC 2009), May 19-22, 2009, Clemson, SC, USA.

- Ö.N. Cora, K. Namiki, M. Koç, "Wear performance assessment of alternative stamping die materials utilizing a novel test system", 17th International Conference on Wear of Materials, 19-23 April 2009, Las Vegas, Nevada, USA.

- Ömer N. Cora, and Muammer Koç, "Micro-engineered Surfaces for Fuel Cell, Heat and Mass Transfer Applications by Powder Compaction", Proceeedings of the 5th JSTP

International Seminar on Precision Forging, pp.167-170, (in poster presentation session also), March 16-19, 2009, Kyoto, JAPAN.

- Yusuf Usta, **Ömer N. Cora**, Muammer Koç, "Hot Compaction of Micro/Mesoscale Porous Surface Features For Enhanced Heat Transfer Applications - Investigations on the Effect of Powder Size on Porosity Control", Proceedings of 5th International Powder Metallurgy Conference, October 08-12, Ankara, TURKEY.

- **Ömer N. Cora**, and Muammer Koç, "Micro-scale porous surface structures for integrated compact heat and mass transfer applications: *Compact heat exchangers, fuel cells, and e-cooling",* (in poster presentation session) NSF CMMI Grantee Conference, January, 7-10, 2008, Knoxville, TN, USA.

- **Ömer N. Cora**, and Muammer Koç, *"*Experimental investigations on wear resistance characteristics of alternative die materials for stamping of advanced high strength steels (AHSS)", Proceedings of International Manufacturing Science And Engineering Conference, (MSEC 2008), October 7-10, 2008, Evanston, Illinois, USA.

- **Ömer N. Cora**, and Muammer Koç, "Effect of substrate hardness on wear performance of alternative die materials for stamping of advanced high strength steels", Proceedings of the Material Science and Technology Conference (MS&T 2008), October 5-9, 2008, Pittsburgh, PA, USA.

- Yusuf Usta, **Ömer N. Cora**, and Muammer Koç, "Micro-manufacturing of porous and modulated surface structures for enhanced heat transfer applications- Experimental investigations on process parameters", The 3rd International Conference on MicroManufacturing (ICOMM 2008), September 9-11, 2008, Pittsburgh, PA, USA.

- **Ömer N. Cora**, Yusuf Usta, Muammer Koç, (2007), *"Experimental investigations on development of rapid die wear tests for stamping of advanced high strength steels"*, Proceedings of the 2007 International Manufacturing Science And Engineering Conference (MSEC 2007), October 15-18, 2007, Atlanta, Georgia, USA.

- **Ömer Necati Cora,** *"Nanotechnology in Defence Industry"* , International German Summer School 2006 on Aviation, Weather and Atmosphere, August, 30th, 2006, Braunschweig, GERMANY.

- **Ö. N. Cora**, M. Akkök, and H. Darendeliler, (2006), *"Modification of friction coefficient in simulation of metal forming operations via user-subroutines", (in Turkish),* Proceedings of MSC Software Users Conference 2006, June 1-2, 2006, İstanbul, TURKEY.

Memberships:

- *ASM International, The Materials Information Society*
- *Society of Tribologists and Lubrication Engineers, (Student Member, 2009)*
- *Turkish Chambers of Mechanical Engineers (since 2000)*

Awards and Grants:

- VCU Graduate School research assistantship
- VCU School of Engineering Dean's scholarship
- Travel grant by NSF CMMI (Civil, Mechanical and Manufacturing Innovation) for attending NSF CMMI Grantee Conference, June 22-25, 2009, Honolulu, Hawaii, USA (not used).

181